AD-A181 890 A COMPARISON OF TRIPPING BEHAVIOR OF WIDE AND NARROW 1/2
FLANGED 'T' AND 'Z' STIFFENED PANELS(U) NAVAL
POSTGRADUATE SCHOOL MONTEREY CA R B MILLER MAR 87
UNCLASSIFIED F/G 13/10 1 NL

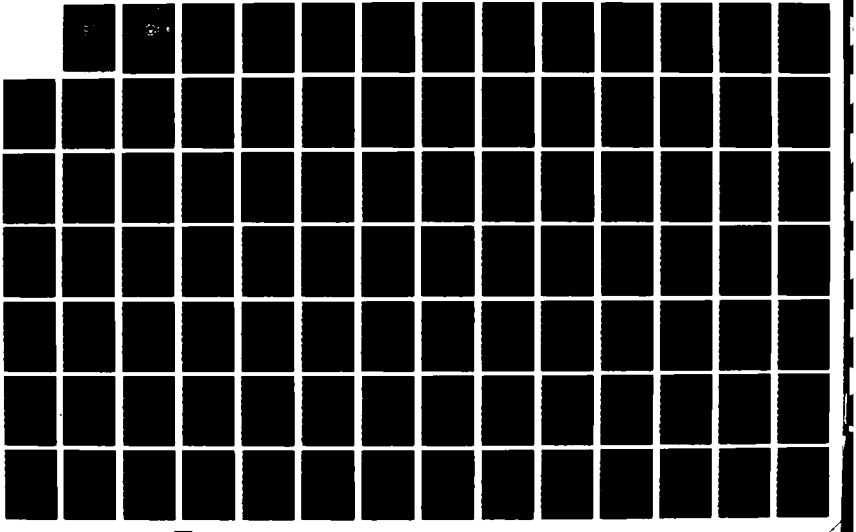

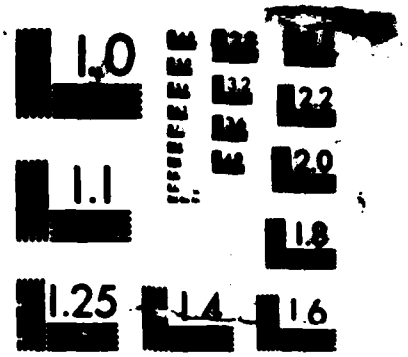

MICROCOPY RESOLUTION TEST CHART

(2)

NAVAL POSTGRADUATE SCHOOL
Monterey, California

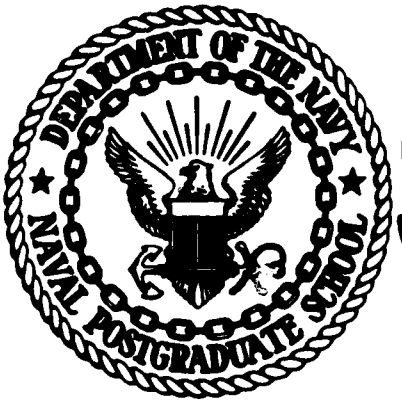

THESIS

A COMPARISON OF TRIPPING BEHAVIOR OF WIDE AND NARROW FLANGED "T" AND "Z" STIFFENED PANELS

by

Robert Bruce Miller

March 1987

Thesis Advisor: Y. S. Shin

A181 890

SECURITY CLASSIFICATION OF THIS PAGE

REPORT DOCUMENTATION PAGE

1a REPORT SECURITY CLASSIFICATION Unclassified	1b RESTRICTIVE MARKINGS
2a SECURITY CLASSIFICATION AUTHORITY	3 DISTRIBUTION/AVAILABILITY OF REPORT Approved for public release; distribution is unlimited.
2b DECLASSIFICATION/DOWNGRADING SCHEDULE	
4 PERFORMING ORGANIZATION REPORT NUMBER(S)	5 MONITORING ORGANIZATION REPORT NUMBER(S)
6a NAME OF PERFORMING ORGANIZATION Naval Postgraduate School 6b OFFICE SYMBOL (If applicable) Code 69	7a NAME OF MONITORING ORGANIZATION Naval Postgraduate School
6c ADDRESS (City, State, and ZIP Code) Monterey, California 93943-5000	7b ADDRESS (City, State, and ZIP Code) Monterey, California 93943-5000
8a NAME OF FUNDING/SPONSORING ORGANIZATION 8b OFFICE SYMBOL (If applicable)	9 PROCUREMENT INSTRUMENT IDENTIFICATION NUMBER
8c ADDRESS (City, State, and ZIP Code)	10 SOURCE OF FUNDING NUMBERS PROGRAM ELEMENT NO / PROJECT NO / TASK NO / WORK UNIT ACCESSION NO

11 TITLE (Include Security Classification)
A COMPARISON OF TRIPPING BEHAVIOR OF WIDE AND NARROW FLANGED "T" AND "Z" STIFFENED PANELS

12 PERSONAL AUTHOR(S)
Miller, Robert Bruce

13a TYPE OF REPORT	13b TIME COVERED	14 DATE OF REPORT (Year, Month, Day)	15 PAGE COUNT
Master's thesis	FROM _____ TO _____	1987 March	141

16 SUPPLEMENTARY NOTATION

17 COSATI CODES			18 SUBJECT TERMS (Continue on reverse if necessary and identify by block number)
FIELD	GROUP	SUB-GROUP	stiffener tripping; static/impulsive loads; narrow/wide flanged T stiffeners; Z stiffener

19 ABSTRACT (Continue on reverse if necessary and identify by block number)

An experimental investigation was conducted to study the dynamic instability and tripping characteristics of a specific stiffened rectangular flat plate design due to hydrostatic and impulsive loading. The air backed test panels were constructed of 6061-T6 aluminum with externally machined longitudinally, wide flanged "T" or "Z" stiffeners and were tested under clamped boundary conditions. Test panel loading was provided by a manual hydropump for static testing and by the underwater detonation of an eight pound, cylindrical TNT charge for the dynamic test. The static test panel was instrumented to measure pressure, strain and plate deflection. The dynamic test panel was instrumented to measure transient strains and free-field pressure. The data obtained from these tests was

20 DISTRIBUTION/AVAILABILITY OF ABSTRACT ☒ UNCLASSIFIED/UNLIMITED ☐ SAME AS RPT ☐ DTIC USERS	21 ABSTRACT SECURITY CLASSIFICATION Unclassified
22a NAME OF RESPONSIBLE INDIVIDUAL Y. S. Shin	22b TELEPHONE (Include Area Code) (408) 646-2568 22c OFFICE SYMBOL Code 69Sg

DD FORM 1473, 84 MAR 83 APR edition may be used until exhausted
All other editions are obsolete

SECURITY CLASSIFICATION OF THIS PAGE

19. ABSTRACT (cont'd)

qualitatively analyzed and compared to the results of geometrically similar narrow flanged "T" stiffened panel results currently available in the literature.

Approved for public release; distribution is unlimited.

A Comparison of Tripping Behavior of Wide and Narrow Flanged "T" and "Z" Stiffened Panels

by

Robert Bruce Miller
Lieutenant, United States Navy
B.S.O.E., Florida Institute of Technology, 1978

Submitted in partial fulfillment of the requirements for the degree of

MASTER OF SCIENCE IN MECHANICAL ENGINEERING

from the

NAVAL POSTGRADUATE SCHOOL
March 1987

Author: _____
Robert Bruce Miller

Approved by: _____
Y. S. Shin, Thesis Advisor

_____
R. E. Newton, Second Reader

_____
Anthony J. Healey, Chairman,
Department of Mechanical Engineering

_____
Gordon E. Schacher,
Dean of Science and Engineering

ABSTRACT

An experimental investigation was conducted to study the dynamic instability and tripping characteristics of a specific stiffened rectangular flat plate design due to hydrostatic and impulsive loading. The air backed test panels were constructed of 6061-T6 aluminum with externally machined longitudinally, wide flanged "T" or "Z" stiffeners and were tested under clamped boundary conditions. Test panel loading was provided by a manual hydropump for static testing and by the underwater detonation of an eight pound, cylindrical TNT charge for the dynamic test. The static test panel was instrumented to measure pressure, strain and plate deflection. The dynamic test panel was instrumented to measure transient strains and free-field pressure. The data obtained from these tests was qualitatively analyzed and compared to the results of geometrically similar narrow flanged "T" stiffened panel results currently available in the literature.

TABLE OF CONTENTS

LIST OF TABLES

LIST OF FIGURES

ACKNOWLEDGEMENTS

I would like to thank Professor Young S. Shin for his encouragement and support, Professor R. E. Newton for his careful and objective review of this paper and especially LCDR. Howard L. Budweg, USN, for his interest and patience in intimating the various fine points and subtleties inherent in undex testing. In addition, I would thank Mr. Tom McCord and his army of skilled technicians; specifically Mr. Charles Crow, Mr. Tom Christian (the resident black box wizard), and Mr. Jim Scholfield, without whose timely and energetic support the hectic schedule devised for this project would have long ago been abandoned. Finally, I would like to express my great appreciation to my wife, Suzanne, whose love, understanding and patience made the all too frequent long nights of preparation more bearable and those nights in between more fun.

I. INTRODUCTION

A. BACKGROUND

The process of submersible hull design is largely a function of its proposed mission. Mission design requirements can be categorized as vehicle performance, human considerations, emergency procedures, environmental constraints and support requirements. These categories can be further reduced to items such as pressure limits, size and weight constrains and, in the case of military submersible hulls, acceptable hull deflection due to battle damage [Ref. 1:p. 13]. High hydrostatic pressures are best withstood by axisymmetric structures, hence, pressure hulls are usually a series of connected cylinders spheres and hemi-heads [Ref. 2:Sect. 1]. In an effort to improve the ability of a pressure hull to resist collapse without increasing its thickness and thereby significantly increasing its weight, stiffeners are generally added [Ref. 3:p. 9-3]. The addition of stiffeners improves the load bearing efficiency and renders a thin cylindrical hull suitable for use at moderate depths [Ref. 3:p. 9-15]. The use of stiffeners in the production of pressure hulls is common, however the accurate prediction of the structural failure of the shell-stiffener system is sometimes quite difficult. Work in the area of prediction of critical loading has been done but cannot be

validated due to an extreme lack of experimental data available [Ref. 4:p. 66].

Hydrostatic failure of the pressure hull generally occurs in one of the following modes [Ref. 3:p. 9-7]:

(1) Axisymmetric collapse of the shell between adjacent stiffeners.

(2) Asymmetric collapse of the shell between adjacent stiffeners.

(3) Overall asymmetric collapse of the shell and stiffeners together.

The third of these failure modes is usually initiated at a point of local instability on the stiffener allowing the stiffener to deform laterally by a buckling of its web. This deformation of the stiffener and its associated loss of load support is called tripping and represents total strucutral failure [Ref. 5:p. 732]. In view of the fact that no satisfactory ultimate load design exists [Ref. 6: p. 255] and that experimental results in this area are scarce, design of this type of structure has been based on avoidance of structural collapse rather than its prediction [Ref. 1:Sect. 2.1]. This entails using larger safety factors and heavier framing, to ensure that collapse could not possibly occur, as opposed to more accurately determining the stiffener size required (thereby minimizing the weight penalty).

The over-design of stiffener framing in an attempt to avoid the possibility of collapse may in itself pose a detriment to the strength of the overall hull structure. If

the ring stiffeners of a thin shell, cylindrical pressure hull are over-designed, as is the case in collapse avoidance design, then the stiffener will be excessively rigid. At high loads the circumferential stress in the shell in the vicinity of the toe of the rigid stiffener would be excessive and failure would occur [Ref. 7:p. 120]. It follows that the lightest, strongest and most resilient hull construction would be one where the relative strengths and strain responses of the framing and shell are equivalent. This would ideally result in a structure where the framing and shell would react as a unit over the entire range of load and deflection expected in the vessel's service life.

Current submarine hull design makes use of the strength levels available in high-strength alloys. This allows a reduction in both the shell thickness and the cross sections of the associated system of stiffeners required for operation in a given pressure range. In addition, the use of high-strength alloys has the additional benefit of an increased toughness. Toughness is not only required for the standard low temperature operational requirements, but also to resist the effect of the incidence of high dynamic loads such as from a depth charge attack. [Ref. 1:Sect. 1]

B. STATIC TRIPPING

In marine usage the stiffener-plating system serves several functions such as contouring and sealing as well as supporting the incident environmental loading experienced

as the vessel performs its designed mission. The bending stresses developed in the stiffener are a result of the interaction between the plate and stiffener caused by the loading incurred as the system fulfills the aforementioned functions [Ref. 8:p. 104]. It is when these stresses become excessive that tripping occurs.

In the case of a T-stiffener the web can be considered as a flat plate whose edge conditions are clamped (restrained against rotation) on the plate side and free and elastically supported by the flange on the other side. In addition, the flange can be represented as a plate which is simply supported by the web on one side and free on the other [Ref. 9:p. 342]. In actuality, a stiffener is welded to the plate which results in a higher flexural rigidity than that which results from the above approximation. This is because adjacent portions of the supported plate take part in the bending of the stiffener. In effect the stiffener carries a portion of the load and subdivides the plate into smaller panels. This subdivision increases the critical stress at which the plate will fail. As loading of the stiffener-plate system grows the longitudinal strain in both the web and flange also grows. Because of the various boundary conditions, as previously described, and their physical geometry these components have specific, favored modes of failure. In the absence of the flange, the web would tend to fail in a mode producing numerous small buckling waves,

conversely, under similar loading the flange tends to buckle in a mode producing fewer waves. This incompatibility in failure modes produces an inherent competition which tends to make the overall buckling load requirement higher than it would be for either the web or flange by itself [Ref. 10:p. 2]. Because of these considerations various combinations of these components allow the plate to support ultimate loads far above the ultimate buckling load of the plate alone. When the load finally does exceed the buckling load for the system the fact that the toe of the stiffener is welded to the plate, thereby being laterally constrained, dictates the form of the stiffener deformation. This deformation consists of a twisting of the stiffener about its line of attachment to the plate as shown in Figure 1.1. [Ref. 2: p. 732]

The failure of Z-stiffeners under compressive load occurs by a rolling over of the stringers. Due to the profile of the Z-stiffener the centroid of the flange is not in the plane of the web, because of this the impressed strains of loading cause a downward deflection of the flange. The downward movement of the flange causes additional bending stresses in the web resulting in general stiffener instability. Once instability is reached the load supporting capability of the stiffener is lost with the only exceptions being the resistance to bending remaining in the web of the

stiffener or the effect of the base flange (if present) on the plate. [Ref. 5:p. 259]

C. DYNAMIC TRIPPING

During the dynamic loading of a structure due to an incident shock wave the amount of initial kinetic energy considerably exceeds the maximum amount of strain energy which could be absorbed by that structure in a wholly elastic manner [Ref. 11:p. 17]. The result of this incident energy is that as the shock front contacts a part of the structure that portion goes plastic in nature or, in the presence of exceedingly high instantaneous strain levels, it may even act fluid in nature [Refs. 12, 13:p. 123, 321]. Due to this behavior of high, instantaneous, localized loading the stresses and associated strains throughout the system during the loading are extremely transient. These transient stresses and strains are representative of the attempt of the structure to distribute the loading both macroscopically and microstructurally (in the form of inelastic deformations). The deformation of the system due to the distribution of load is referred to as the plastic flow and its amount, location and direction is largely a function of the geometry of the structure as well as the direction in which the shock propagates. In addition, in the presence of the high transient strains produced, the metal in certain localized regions may undergo significant changes in its mechanical

properties (e.g., an increase in hardness and tensil strength and a decrease in flow characteristics due to dislocation saturation). The combination of the above effects, material flow and the alteration of mechanical properties, enable the system to deform and retain its stability under loads which would be many times greater than the static critical buckling load. This is why the dynamic critical load occurs in the plastic range and results in what is referred to as dynamic plastic buckling. [Ref. 11:p. 6]

D. OBJECTIVE

In order to develop an appropriate analytical model the system behavior must be understood to the point of rendering key events, such as the point of inelastic tripping, reliably predictable. Unfortunately, no satisfactory method exists even for this key event and a need clearly exists for additional test data for further development of the underlying theory [Refs. 14, 15:p. 42, 333].

The objective of this paper is two fold. First, to present much needed experimental data obtained while testing longitudinally stiffened panels under hydrostatic and dynamic conditions. Second, it is hoped that a better understanding of the tripping mechanism (under hydrostatic and dynamic conditions) is obtained by qualitative analysis of this data.

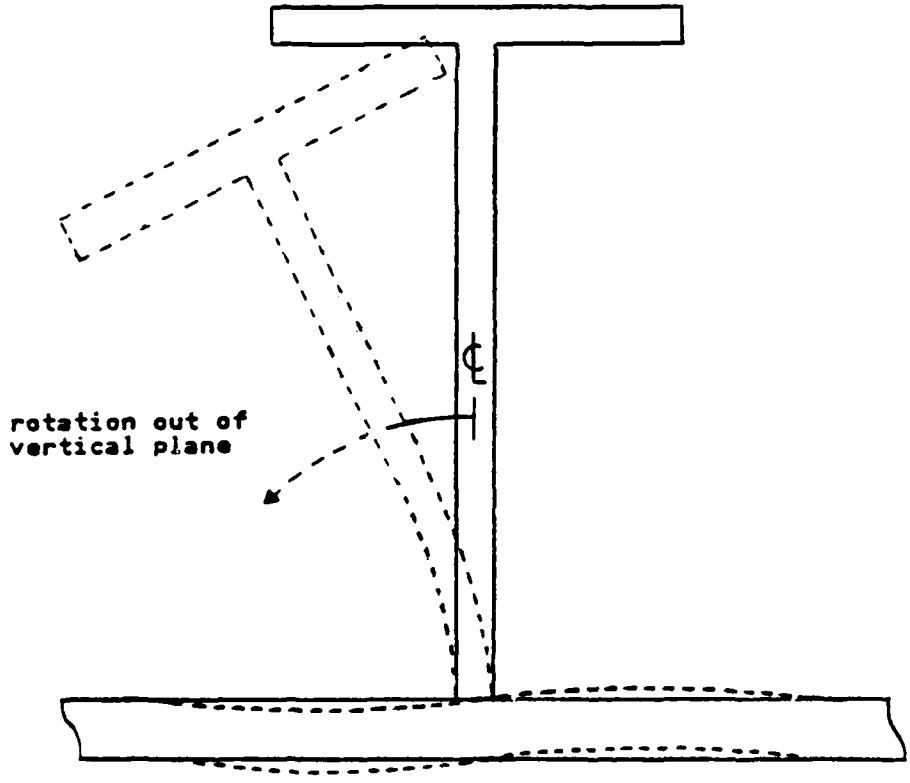

Figure 1.1 Stiffener Tripping

II. EXPERIMENT AND MODEL DESIGN

A. BASIC MODEL

The intent of this investigation was similar to that of reference 16 in that it was to perform static and dynamic loading tests on a rectangular flat plate model with various types of longitudinal stiffeners. The purpose of these tests was to provide data for the qualitative analysis and comparison of stiffener-plate system behaviors exhibited by the different stiffener geometries considered. Early investigations conducted in this area [Refs. 17-19] were unable to produce measureable structural instability in the form of tripping, but could by no means be considered failures overall. These earlier investigations provided a great amount of insight into what combinations of plate-stiffener geometry, charge size and instrumentation would be most appropriate for the development of a model which would generate usable data.

The first productive model design was realized by LT Budweg [Ref. 16:p. 17] by combining the stiffener geometry as used in the Langan investigation [Ref. 19:p. 51] with the plate thickness and instrumentation used by Rentz [Ref. 17: pp. 75, 132], as well as incorporating modifications to the stiffener end boundary conditions (based on his observations of previous test results). Based on these considerations,

the model was established as a .1875 inch test plate, 18 inches in length by 12 inches in width machined out of the center of a blank panel of 6061-T6 aluminum measuring 27 by 33 inches. Previous results were obtained with the stiffener being integrally machined into the plate cavity; under dynamic testing this raised a question of mutual constructive interference of reflected pressure waves during the test. As a result the location of the stiffener for the dynamic test was changed to be on the flush side of the panel as shown in Figure 2.1. The location of the stiffener and plate geometry of the hydrostatic test remained similar to reference 16, page 18 as shown in Figure 2.2.

B. STATIC TEST ARRANGEMENT

The test panel configuration used in this investigation is shown schematically in Figure 2.2. The cross section of the narrow flanged "T" stiffener, whose data [Ref. 16] is considered the baseline for comparison with the results of this investigation, is shown in Figure 2.3. The cross sections of the wide flanged "T" and "Z" stiffeners to be tested in this investigation are shown in Figures 2.4 and 2.5, respectively.

Generally, this test was accomplished by instrumenting the test panel for both deflection and strain measurement, mating the panel with a high-strength steel strongback, filling the cavity formed thereby with water, increasing the

pressure in 25 psi increments from zero to 400 psi and recording the associated data. Specifically, the strongback was constructed from one inch thick steel sheeting, was drilled and tapped for standard three-quarter inch pipe fittings for low point fill and high point vent connections, and was drilled for a 28 x 1 inch bolt pattern for mating with the test panel. Mating was accomplished by using a pre-cut gasket (high-pressure graphite coated one-sixteenth inch oil paper for the "Z" stiffener test and one-eighth inch oil paper for the wide flanged "T" stiffener test), supplemented by a coating of silicone sealant and secured by 28, one inch diameter A325 high-strength steel bolts torqued to 500 ft. lbs. Potable water was the pressurized medium and load pressure was provided by a manually operated, single piston, reciprocating hydropump. Test panel load pressure was determined from a zero to 400 psig Ashcroft pressure gauge located between the inlet valve and the strongback. The vent seal was provided by a standard three-quarter inch gate valve. During the accomplishment of the tests a few minutes (1+ to 3 minutes) were required, at each pressure increment, to record the resultant plate deflections. Associated plate and stiffener strain readings were continuously recorded by a Honeywell MD-101 magnetic tape unit. Positioning of the static test plate deflection dial indicators was based on an assumption of symmetric deflection existing in both the longitudinal and transverse

directions. These positions and the hydrostatic test configuration are represented schematically in Figure 2.6.

C. DYNAMIC TEST ARRANGEMENT

A structure loaded by an underwater explosion experiences not only the effect of the initial pressure pulse emanating from the explosion, but a series of effects resulting from the interacttion between the charge and the water as well as the water and the test panel. These other effects take the form of bulk cavitation, cavitation closure, reloading from the explosive gas bubble, bubble pulse, bubble migration, surface cutoff and bottom reflection [Ref. 20]. By considering the proper test configuration, consisting of a specified test charge depth, standoff distance and data sampling timeframe, the effects of those interface interactions other than the initial incident shock wave can be neglected.

As previously determined [Refs. 16, 17, 18, 19:p. 23, 80, 116, 59], shock waves produced by the eight pound TNT charges supplied were of a magnitude equivalent to those produced by a standard TNT charge approximately 30% larger (about 10.4 pounds). This is because the contractor who originally prepares the charge does so such that the charge would react as an eight pound charge even if charge deterioration occurs during the charge's shelf life. Based on the assumption that all eight pound charges supplied would

react in this manner [Ref. 16] a test configuration was determined using the larger apparent charge size in the calculations of charge depth and standoff distance. In view of that test's success in obtaining meaningful data and in order to achieve as similar a test panel loading as possible, the same configuration was adopted (with only minor modifications) for use in this investigation. The schematic of the test configuration is shown in Figure 2.7. The minor modifications to the previous test's configuration entailed: exchanging the pneumatic fender support floats in favor of styrofoam blocks (to avoid their subsequent rupture during the test), orienting the plate-stiffener flush to the outer surface of the panel (as previously discussed and shown in Figure 2.1), and securing a counter weight opposite to the instrumentation box mounted on the test chamber as well as redirecting the cable such that it was suspended directly below the chamber (this ensured that the chamber would present the panel as nearly level as possible).

The air-backed test chamber made use of in this investigation was designed and built by Rentz [Ref. 17:p. 105] and used in all subsequent tests [Refs. 16-19]. The test panel was secured to the test chamber by 60, one inch diameter, A325 high-strength steel bolts torqued to 500 ft.-lbs. each. The seal between the mated surfaces was formed by use of an "O" ring supplemented by silicone sealant. Instrumentation for the measurement of induced plate and stiffener strains

was accomplished with the use of 12 strain gauges oriented on the test panel as shown in Figure 2.8. The free field pressure was measured at a ten foot radius for use as the baseline data of the incident pressure pulse. The twelve strain gauges used were mounted as described in reference 17, page 132 and were sealed with silicone sealant to ensure their watertight integrity. These gauges were connected, by way of a set of amplifiers, to two Honeywell MD-101 wideband II (direct record) tape units. Channels recorded consisted of two trigger channels (directly from the charge to provide the initiation), twelve strain gauge channels, and two free-field pressure channels. Recording was accomplished at a tape speed of 120 inches-per-second. Post shot data processing was accomplished on the NPS vibration laboratory's HP-5451 C Fourier Analyzer. Equipment identification is provided in Table 1.

TABLE 1

IDENTIFICATION OF EQUIPMENT

EQUIPMENT	TYPE	RANGE
strain gauges	CEA-350 ohms	$\pm$50k microstrain
pressure transducers	.25" Tourmaline	10 ksi, 97% response ratio
amplifiers	Ektron 563F J	----------

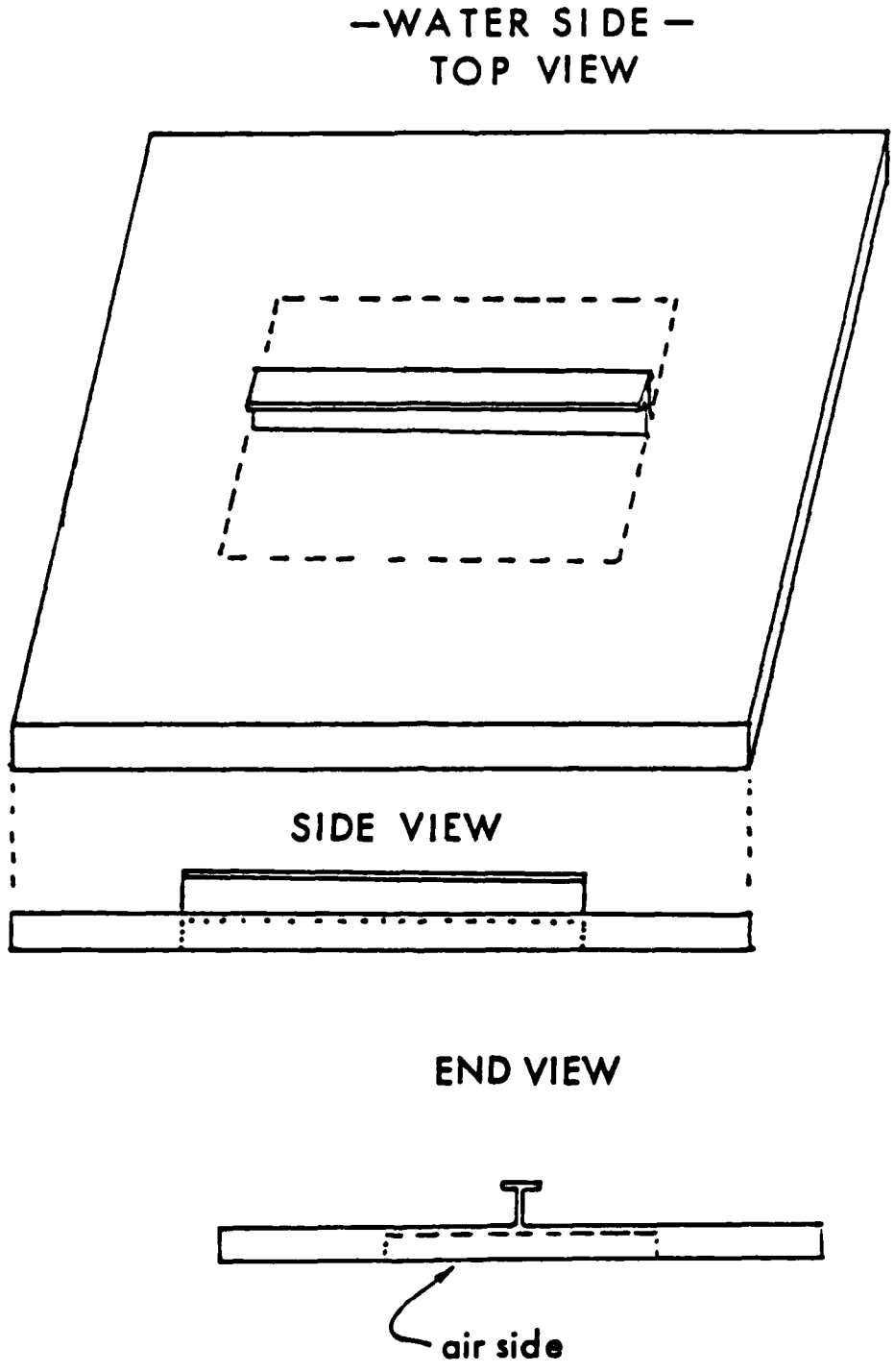

Figure 2.1 Dynamic Test Panel Configuration

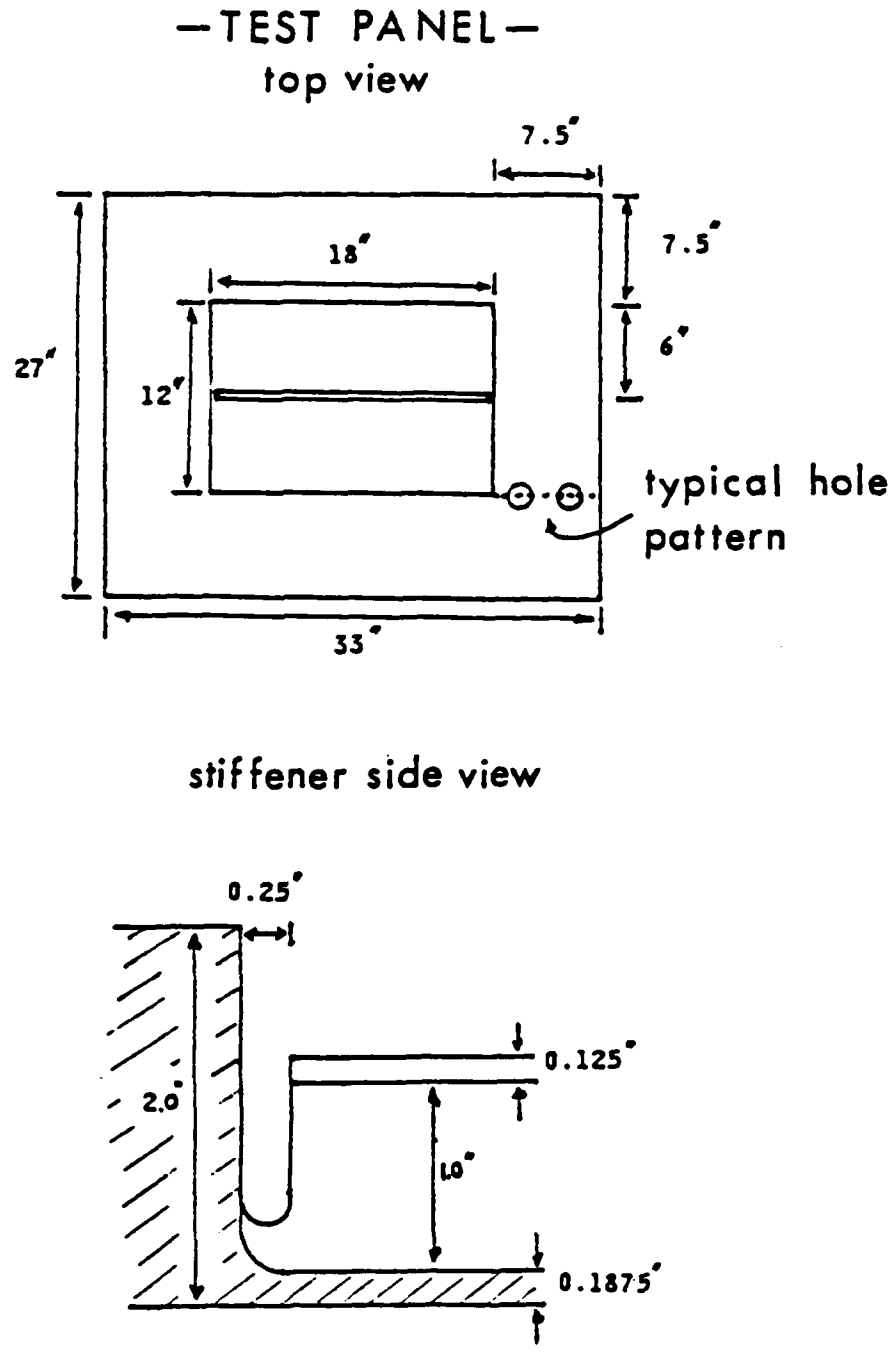

Figure 2.2 Hydrostatic Test Panel Configuration

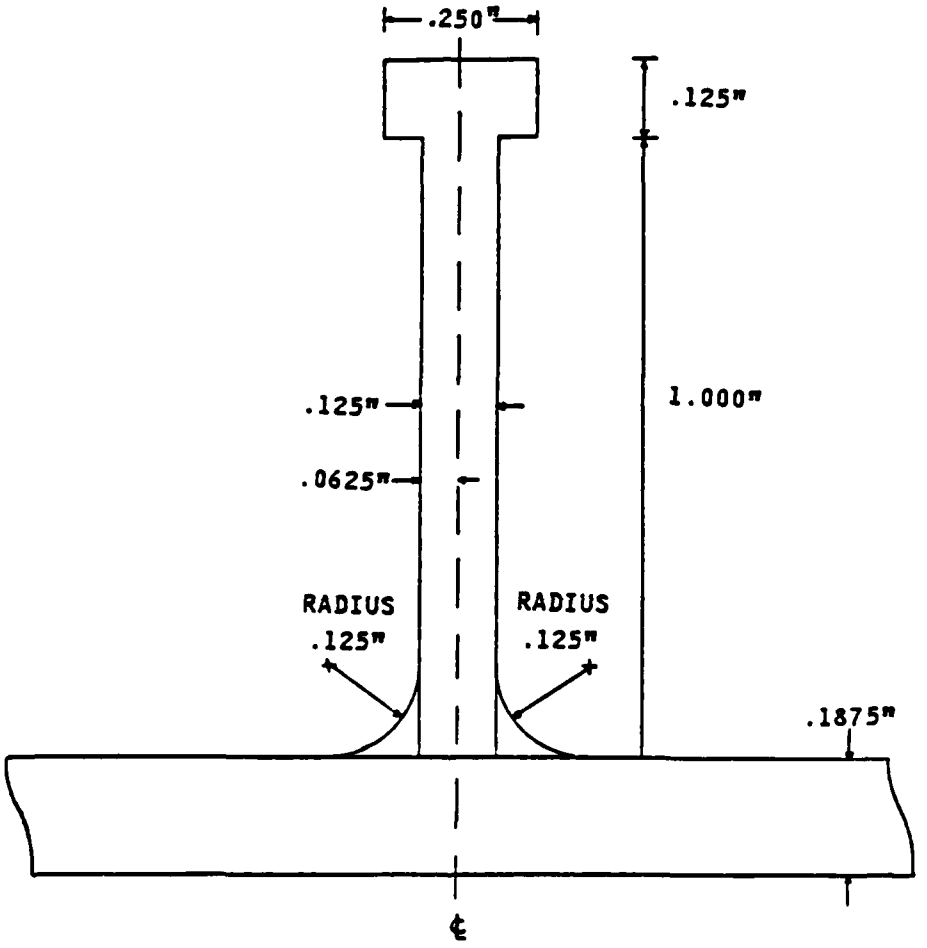

Figure 2.3 Narrow Flanged "T" Stiffener Cross-Section

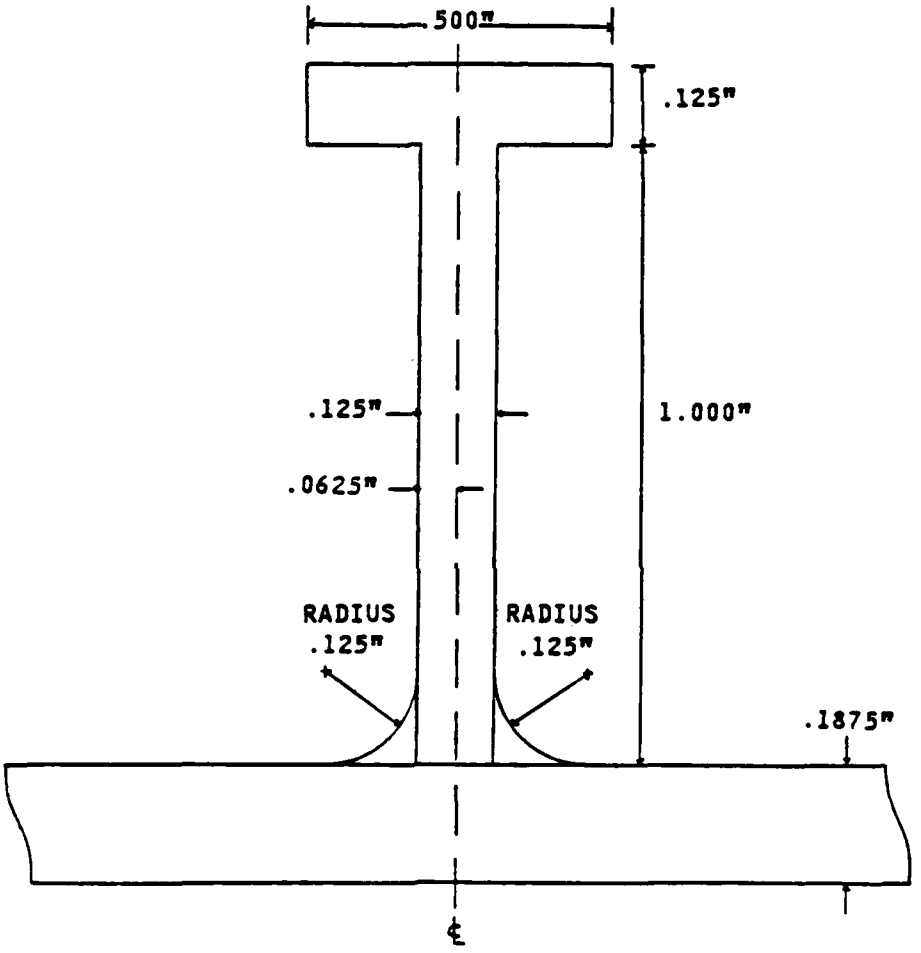

Figure 2.4 Wide Flanged "T" Stiffener Cross-Section

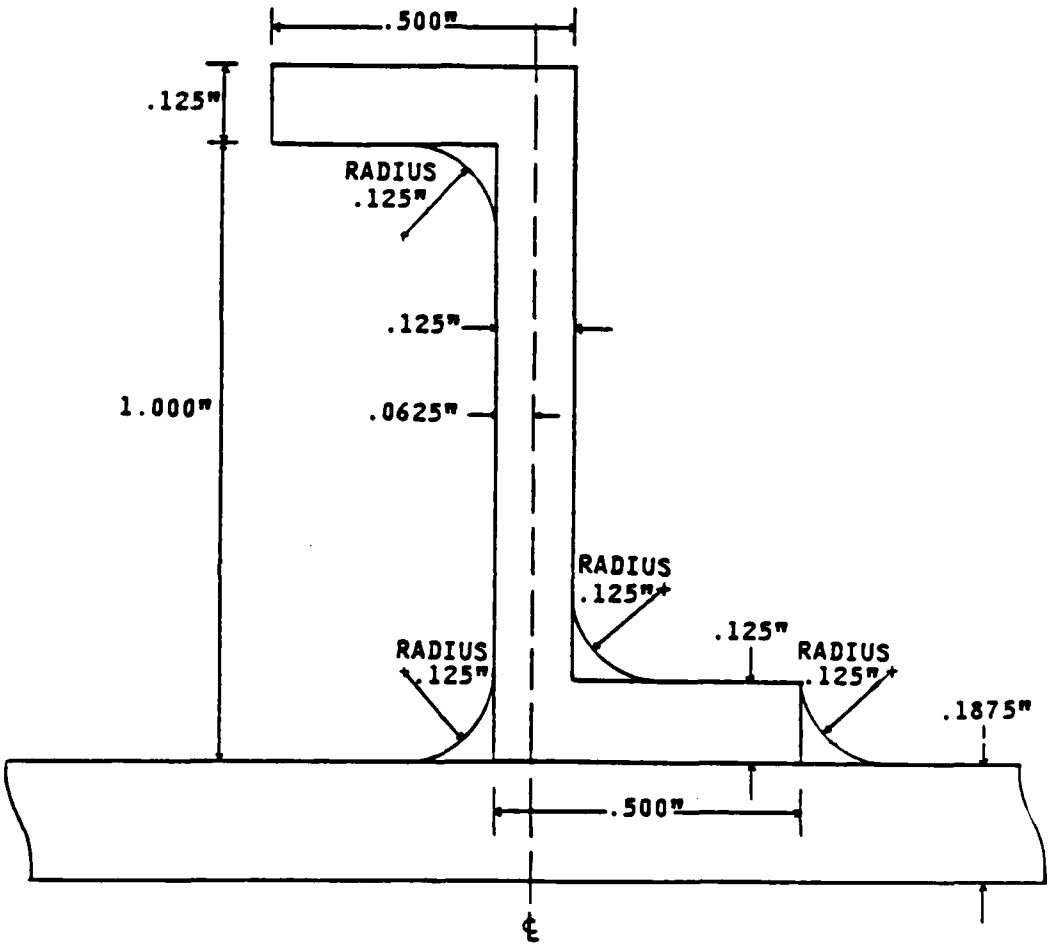

Figure 2.5 "Z" Stiffener Cross-Section

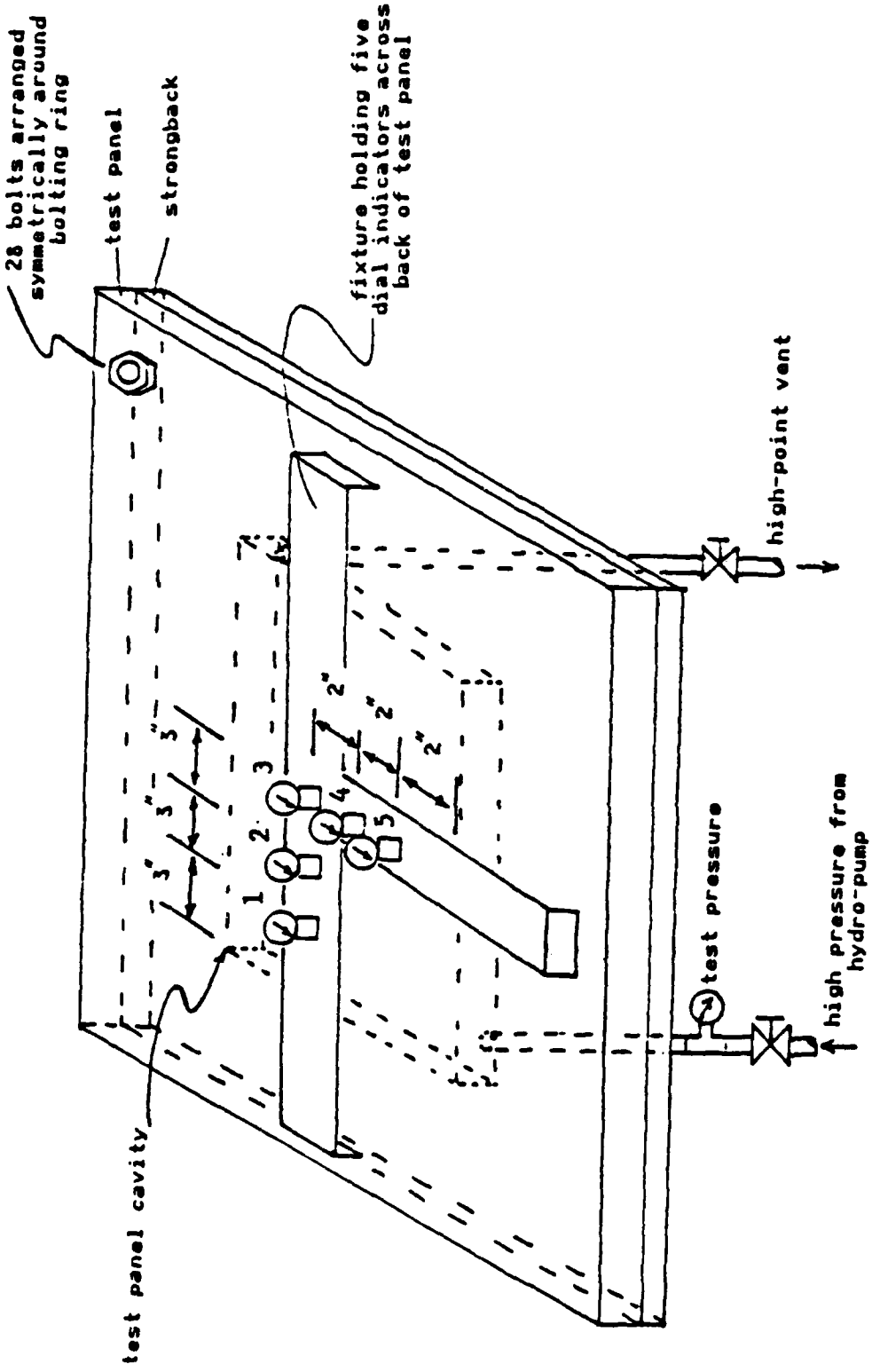

Figure 2.6 Hydrostatic Test Configuration

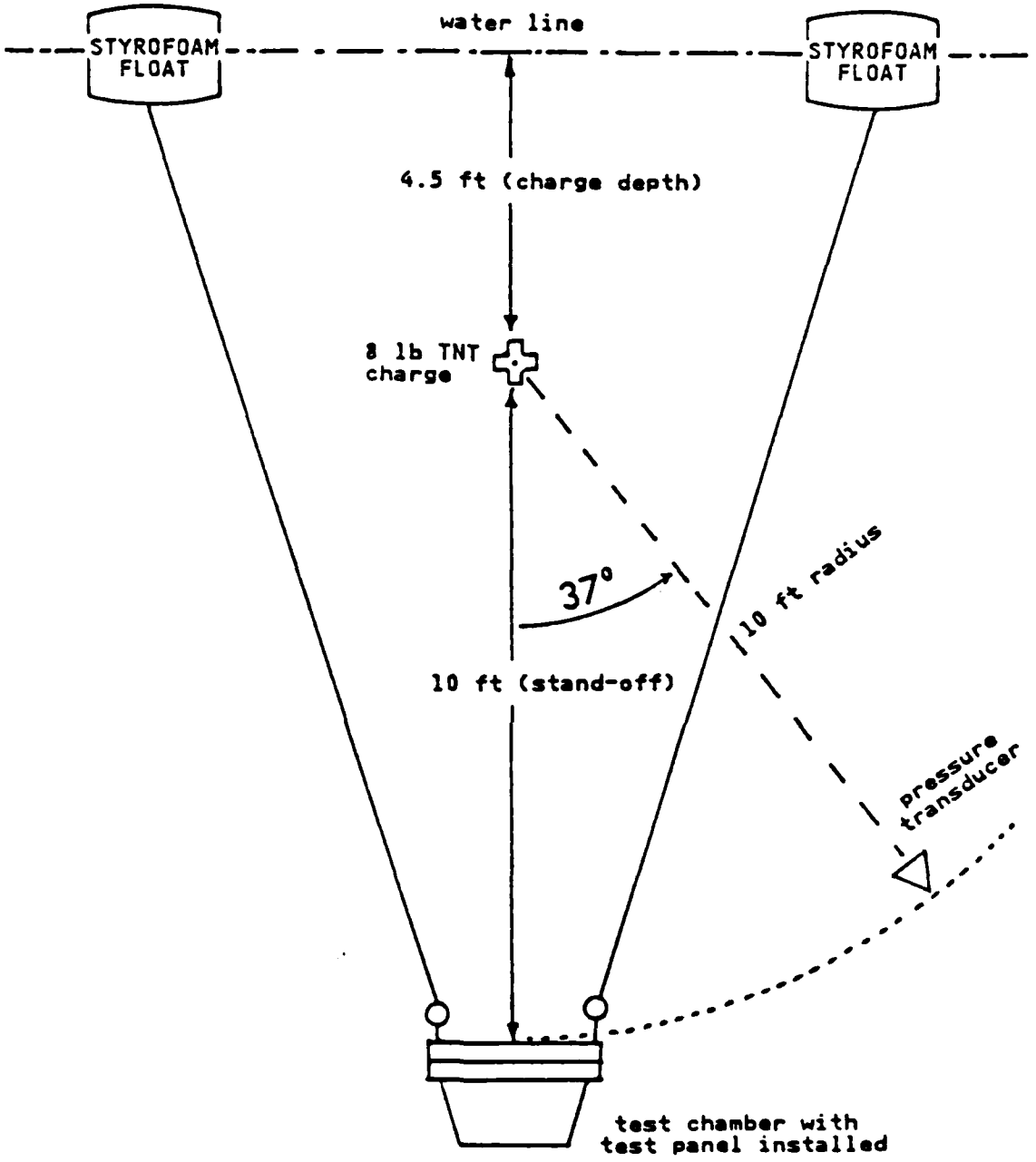

Figure 2.7 Schematic of the Dynamic Test Geometry

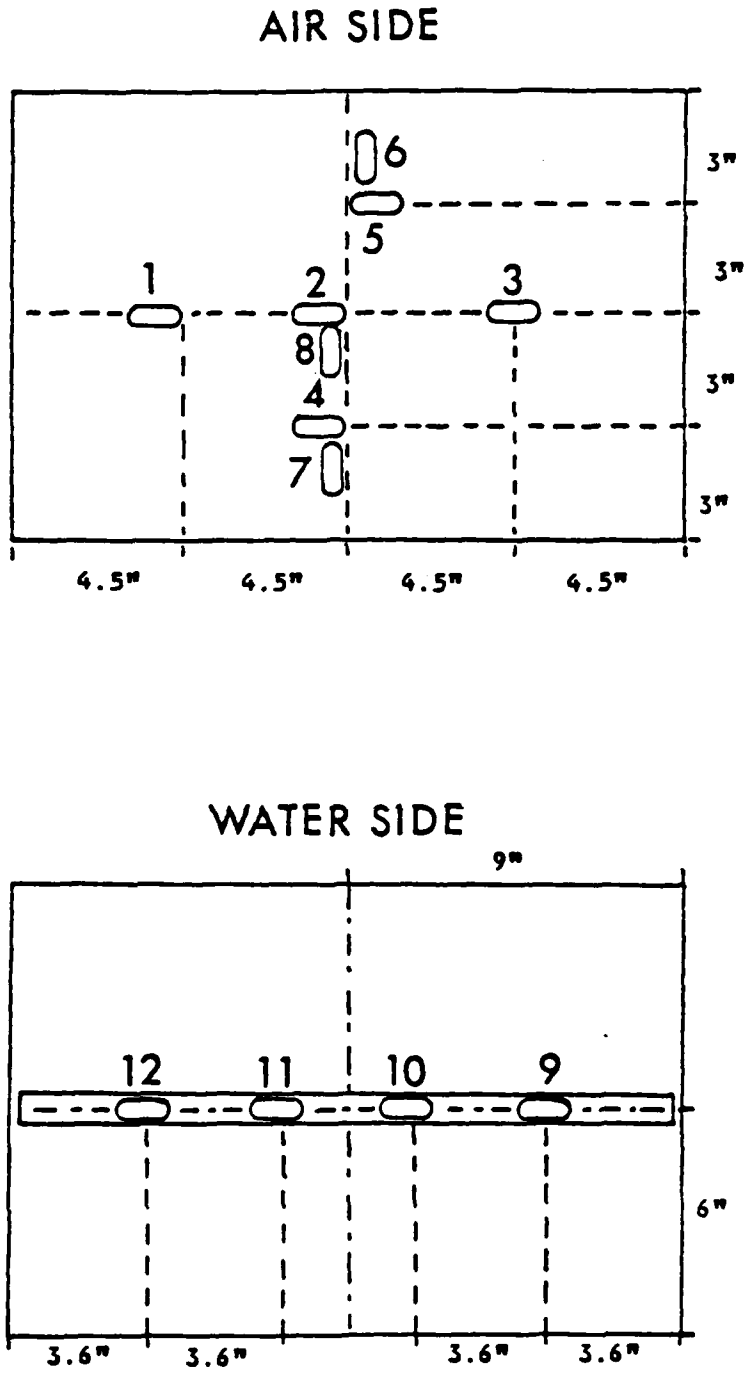

Figure 2.8 Diagram of Strain Gauge Placement

III. RESULTS AND DISCUSSION OF DATA

A. STATIC TEST RESULTS

The analysis and discussion of the results of the static pressure tests will be presented in four sections. The first two sections will discuss individually the results of the wide flanged "T" and "Z" stiffener tests respectively, the third section will briefly review the results of the narrow flanged "T" stiffener as presented in reference 16, page 33; the fourth and final section will discuss similarities, differences and trends noted in the comparison of the results of the three tests.

1. Wide Flanged "T" Stiffened Panel Static Test Results

In order to analyze the deflection data obtained during this test and compare it with data collected in previous experiments, the location scheme used by Budweg [Ref. 16:p. 33] was adopted. To accomplish this, a series of point nodes were designated by a "one-half symmetrical section" method. This method assumes that symmetry exists about the plate's transverse centerline. By using this method the plate could be represented in half-section, by 416 nodes; 26 nodes along the full section transverse direction, and 16 nodes along the half section longitudinal direction. Figure 3.1 shows the segmentation of the half plate section. Dial indicators were positioned as described

in the previous section, these locations corresponded to nodes (5,13), (10,13), (16,13), (16,8), (16,4) for indicator positions 1 through 5 respectively. Table 2 contains the results of the deflection measurements taken during the test. Figure 3.2 provides the graphical representation of the transverse plate profile at the longitudinal midpoint (longitudinal node 16).

Strain data was recorded as described in the previous section and was output by strip chart for detailed analysis. The recorded strain data traces are shown in Figures 3.3 through 3.8. The values of strain at each strain gauge position throughout the test can be seen in Table 3. A graphical representation was made of the ratio of the magnitude of the incremental change in strain to the incremental pressure versus the test pressure; this is shown in Figure 3.9. The incremental strain per incremental pressure is a useful quantity to identify the progressive plate/stiffener behavior through the elastic, plastic plate behavior and elastic stiffener tripping regions.

In reviewing Figure 3.9 as well as the actual strain and deflection data, specific regions of elastic plate reaction, plastic plate reaction, and elastic stiffener tripping can be observed. From the deflection data a permanent set of .350 inches existed in the center of the plate (node (16,13) after venting from a deflection of

TABLE 2

WIDE FLANGED "T" STIFFENER
STATIC TEST DEFLECTION AND PRESSURE DATA

PLATE DEFLECTION (INCHES)

-NODES-

PRESSURE (PSI)	(5,13)	(10,13)	(16,13)	(16,8)	(16,4)
0	0	0	0	0	0
25	.043	.081	.094	.084	.040
50	.066	.126	.150	.131	.060
75	.096	.183	.219	.189	.088
100	.125	.238	.286	.245	.118
125	.151	.287	.342	.296	.148
150	.178	.335	.398	.343	.178
175	.203	.379	.446	.385	.202
200*	.225	.415	.482	.412	.224
225	.246	.450	.525	.450	.248
250	.266	.480	.555	.480	.265
275	.288	.512	.592	.512	.288
300	.310	.542	.620	.540	.310
VENTED+	.196	.325	.350	.320	.202

*At this point leaking starts, pressure maintained by constant operation of the manual hydrostatic test pump.

+Permanent set measurements taken after pressure was vented off.

TABLE 3

WIDE FLANGED "T" STIFFENER
STATIC TEST STRAIN AND PRESSURE DATA

STRAIN GAUGE DATA (MICROSTRAIN)

- STRAIN GAUGE POSITIONS -

PRESSURE (PSI)	1	2	3	4	5	6	7	8	9	10	11	12
0	0	0		0	0	0	0	0	0	0	0	0
25	450	600	F	300	300	625	625	500	-1725	-2950	-2925	-1600
50	775	1000		425	425	1000	1000	1000	-2450	-4625	-4500	-2275
75	1025	1550	A	625	650	1575	1500	1850	-2975	-7000	-6950	-2775
100	1325	2000		850	875	2200	2125	2700	-3375	-9050	-9250	-3150
125	1700	2350	I	1000	1000	2825	2750	3450	-3800	-10700	-11100	-3600
150	2100	2675		1175	1175	3400	3325	4325	-4275	-12225	-12825	-4200
175	2500	3000	L	1325	1275	4000	3850	5175	-4900	-13325	-14125	-5050
200	2850	3200		1400	1375	4550	4350	5825	-5500	-13950	-14900	-6050
225	3200	3400	E	1600	1500	5300	5100	6500	-6350	-14550	-15625	-7225
250	3600	3650	D	1700	1600	6100	5900	7200	-7200	-15050	-16225	-8400
275	4100	FAILED		1900	1775	7000	6800	625	-8225	-15400	-16700	-9800
300	4600	FAILED		2025	1900	7700	7600	500	-9300	-15700	-17000	-11025

.620 inches at 300 psi. This indicates an elastic recovery of a deflection of .270 inches which corresponds to the deflection at a pressure of about 94 psi. Thus 94 psi can be considered the upper limit of the elastic range. In addition to the elastic recovery observed, the elastic upper limit can be determined by observing radical changes in the behavior of the plot of incremental strain. In Figure 3.9 a significant change occurs between 75 psi and 100 psi corresponding to the shift from elastic to plastic behavior. A close review of the histories of strain gauges 9-12 (Figures 3.7 and 3.8) provides the test pressure range associated with the shift from plastic behavior to elastic stiffener tripping behavior. Both of the histories for gauges 10 and 11 show a marked decrease in the increase of strain for each pressure increment starting at 200 psi. That is, the amount of strain the center of the stiffener will accept with each increment of pressure lessens with each successive increase in pressure starting at 200 psi. Conversely, strain gauges 9 and 12 show a marked increase in the amount of strain they accept with each successive pressure increment staring at 200 psi. Both of these observations indicate that elastic tripping at the center of the stiffener is occurring and a portion of the load is accepted by those poritons of the stiffener not yet tripped out of the vertical plane. In addition, the fact that gauges 10 and 11 indicate the center of the stiffener

continues to accept additional strain past the onset of tripping shows that the flange and web continue to resist rotation out of the vertical plane even though stability is lost. Both of these effects can be clearly seen in the incremental strain graph, Figure 3.9. At 200 psi the slope of strain gauges 10 and 11 flatten out at a low level while gauges 9 and 12 continue to increase. As the stiffener tripping continues the load continues to be redistributed on the stiffener until at some point the portion of the plate at the toe of the web must unload as the stiffener above it unloads. Strain gauges 2 and 8 were in the location which should expect the earliest indication of this phenomenon. In fact gauge 8 shows unloading at the beginning of the 250 psi plateau followed by gauge 2 at the beginning of the 275 increment; unfortunately as gauge 2 was tapering to its unloaded state the gauge failed.

For the execution of this test a one-sixteenth inch graphite coated high pressure gasket material was used in an attempt to extend the pressure range of the test. This was an unfortunate choice in that the graphite debonded from the gasket material in the presence of the silicone sealant used. Because of the aforementioned debonding the test apparatus started to leak at about 200 psi. It was for this reason that the strain plateaus above that value are jagged in nature. By the time the pressure had reached 300 psi the leak was such that the small hydropump used could not maintain

that value, the double peak values shown in all strain histories are indicative of the two attempts made at maintaining 300 psi. The strain history for strain gauge 3 has been ommitted due to the gauge's failure at the beginning of the test.

In spite of the gauge failures and gasket leakage problems described, this test provided very useful data which allowed the determination of the general ranges for elastic behavior (0-94 psi), plastic behavior (94-200 psi) and the onset of the elastic stiffener tripping range (200 psi +).

2. "Z" Stiffened Panel Static Test Results

Analysis of the defleciton data for this test was conducted by methods similar to those used on the wide flanged "T" stiffener. Graphical representations of the transverse plate profiles are provided in Figure 3.10. Strain history traces resulting from data obtained throughout the test are provided in Figures 3.11 through 3.16. In addition, the numerical values for deflection and strain at their associated positions throughout the test can be found in Tables 4 and 5. The plotted behavior of the strain increment to pressure increment ratio is shown in Figure 3.17.

In determining the upper limit of the elastic plate reaction zone; the center node had a deflection of .772 inches at 400 psi and a permanent set deflection of .494

TABLE 4

"Z"STIFFENER
STATIC TEST DEFLECTION AND PRESSURE DATA

PLATE DEFLECTION (INCHES)

-NODES-

PRESSURE (PSI)	(5,13)	(10,13)	(16,13)	(16,8)	(16,4)
0	0	0	0	0	0
25	.044	.078	.090	.081	.041
50	,074	.135	.160	.143	.070
75	.106	.195	.232	.205	.102
100	.132	.244	.290	.257	.132
125	.162	.304	.358	.319	.169
150	.192	.352	.412	.366	.199
175	.218	.398	.462	.410	.228
200	.241	.435	.502	.447	.250
225	.266	.473	.543	.482	.275
250	.289	.505	.576	.513	.294
275	.312	.542	.615	.549	.319
300	.332	.570	.644	.575	.339
325	.349	.594	.669	.598	.354
350	.376	.628	.702	.630	.378
375	.401	.665	.739	.666	.402
400	.422	.692	.772	.692	.422
VENTED	.253	.462	.494	.406	.279

TABLE 5

"Z" STIFFENER

STATIC TEST STRAIN AND PRESSURE DATA

STRAIN GAUGE DATA (MICROSTRAIN)

- STRAIN GAUGE POSITIONS -

PRESSURE (PSI)	1	2	3	4	5	6	7	8	9	10	11	12
0	0	0	0	0	0	0	0	0	0	0	0	0
25	325	600	425	300	225	350	600	650	-1700	-2975	-2800	-1725
50	625	1050	800	500	425	600	1075	1350	-1675	-4975	-4800	-2725
75	1000	1600	1100	750	625	1000	1550	2175	-3300	-7500	-7250	-3300
100	1300	2000	1375	950	800	1500	2100	2850	-3825	-9625	-9125	-3750
125	1725	2400	1800	1150	1000	2200	2700	3725	-4650	-11800	-11075	-4400
150	2200	2750	2275	1300	1175	1750	3250	4575	-5650	-13300	-12400	-5250
175	2600	3000	2700	1425	1275	3200	3700	5250	-6850	-14350	-13400	-6325
200	3100	3300	3050	1600	1400	3600	4215	6000	-8075	-15000	-14550	-7425
225	3600	3600	3600	1750	1525	4150	4900	6650	-9400	-15575	-14850	-8675
250	4025	3800	4100	1850	1625	4675	5500	7125	-10700	-15950	-15100	-9900
275	4600	4100	4700	2025	1800	5425	5900	7700	-12200	-16250	-15300	-11250
300	5000	4300	5175	2200	1950	6100	6150	6400	-13650	-16400	-15400	-12400
325	5350	4500	5600	2300	2025	6675	6450	1075	-14350	-16525	-15475	-13225
350	5950	4825	6300	2525	2200	7575	6700	1000	-15700	-16700	-15500	-14800
375	6500	4800	7025	2800	2425	8350	7100	900	-17200	-17200	-25700	-16150
400	6925	2450	7600	2900	2600	8800	7400	775	-18100	-17000	-15800	-17000

inches. These indicate an elastic recovery deflection of .278 inches which corresponds to the deflection at a pressure of about 95 psi. As in the wide flanged "T" results, this pressure corresponds to a point of radical change in slope or general curve behavior in the incremental strain plot. Hence 95 psi is considered to be the elastic limit for the "Z" stiffened case. In observing the trace histories of strain gauges 9 through 12 (Figures 3.15 and 3.16) and the incremental strain plot (Figure 3.17) the lower limit of elastic stiffener tripping can be readily determined using the same method utilized in the previous test case. A value for the lower limit of elastic stiffener tripping of 220 psi was determined for the "Z" stiffened test case.

In scrutinizing the individual strain histories several interesting points concerning the mechanism of the stiffener tripping could be seen. At about 200 psi the central portion of the stiffener begins the characteristic acceptance of lesser amounts of strain with increasing load as the outer edges of the stiffener, gauges 9 and 12, accept larger amounts. This effect, as discussed in the previous test case, is representative of the stiffener elastically rotating out of its vertical plane. Essentially, for a "Z" stiffener this is effected by the web of the stiffener buckling and the flange rotating. At about 250 psi changes in the strain histories of gauges 6 and 7 (Figure 3.14) indicate

that another mechanism is contributing to the stiffener tripping. These changes are the asymmetric increase in the strain accepted at gauge 6 and decrease in the amount of strain accepted at gauge 7. The mechanism which would account for these changes is a wholesale rotation of the stiffener about its base. Both of the above mechanisms are schematically shown in Figure 3.18. In this case, the rotation is toward gauge 6 causing larger increases in tension in that region and smaller increases in the vicinity of gauge 7. After considering the upper pressure ranges of strain gauges 9 and 12 (Figure 3.15) it was found that those outer portions of the stiffener started to show the decrease in additional strain accepted with increasing load which was seen in the central portion at the onset of tripping. This observation indicates that the tripping which had started elastically in the center of the stiffener had progressed outward and at a test pressure of 375 psi included the outermost gauges. At this point the stiffener is essentially totally involved in the tripping process and it could be expected that plastic tripping of the stiffener is occurring. As was discussed in reference 16, page 35, more than 4 plate thicknesses of central deflection would be required to produce plastic stiffener tripping. The required 4 plate thickness deflection was reached at about 380 psi and a maximum deflection of 4.11 plate thicknesses was realized at 400 psi. Upon completion of the test and dismantling the test apparatus

measurement of the stiffener showed a permanent plastic set of .06 inches toward strain gauge 6. The configuration of the plastic tripping of the stiffener was as shown in Figure 3.19. At the extreme ends the stiffener remained in the vertical plane. Progressing towards the center, the tripping quickly increased to the maximum of .06 inches at a point .5 inches to the outside of gauges 9 and 12. At that point the deflection remained constant at .06 inches across the entire central portion of the stiffener.

From the analysis of the deflection data for nodes (10,13), (16,13) and (16,8), after the onset of stiffener tripping, it can be seen that these points deflect very nearly the same amount with each succesive test pressure increment. This means that after the stiffener has started to trip the central portion of the plate remains essentially unchanged and moves more or less as a rigid body. This observation is supported by the fact that the incremental strain values of gauges 10 and 11 as shown in Figure 3.17 have bottomed out at an extremely low value indicating very little or no change in shape of the central longitudinal region over the elastic and plastic stiffener tripping range. One problem with this description is that the locations of the dial indicators only included one half of the transverse data section which assumes that symmetry exists about the longitudinal centerline which, from the previous discussion of gauges 6 and 7 is known not to be the case.

So, in actuality, the plate can only be said to be moving rigidly with respect to the longitudinal profile.

At about 275 psi the expected decrease in strain associated with the unloading of the tripped stiffener becomes evident in the transverse direction as seen in Figure 3.12 (Strain Gauge 8). At about 350 psi the evidence of longitudinal unloading is also seen in Figure 3.12 (Strain Gauge 2). During this test all gauges and equipment performed extremely well, providing the necessary data to determine all ranges; elastic behavior (0-95 psi), plastic behavior (95-220 psi), elastic stiffener tripping (220-375 psi), and plastic stiffener tripping (375 + psi).

3. Narrow Flanged "T" Stiffened Panel Static Test Results

In order to provide continuity in the progress of research conducted in this subject area, comparisons of recently compiled data should be made with data collected from past successful tests. To fulfill this requirement the appropriate necessary graphical plots, data traces and tables from reference 15, pages 38 through 55 are provided in Figures 3.20 through 3.25 and Tables 6 and 7. Detailed analysis and discussion of this data is contained in reference 16, page 33. However, for the purpose of the forthcoming comparison it is noted here that the upper limit of the elastic range was determined to be 100 psi and the lower

TABLE 6

NARROW FLANGED "T"
STATIC TEST DEFLECTION AND PRESSURE DATA

PLATE DEFLECTION (INCHES)

-NODES-

PRESSURE (PSI)	(5,13)	(10,13)	(16,13)	(16,8)	(16,4)
25	.043	.079	.095	.080	.040
50	.080	.148	.180	.154	.075
75	.110	.204	.247	.211	.103
100	.139	.255	.304	.260	.131
125	.180	.308	.361	.311	.165
150	.197	.352	.407	.352	.190
175	.223	.394	.451	.392	.217
200	.248	.434	.492	.430	.242
225	.275	.473	.532	.466	.267
250	.297	.506	.566	.497	.288
275	.321	.540	.601	.529	.311
300	.342	.570	.632	.557	.333
325	.364	.601	.664	.586	.354
350	.387	.632	.695	.615	.376

NOTE: After pressure was vented off, a permanent set of 0.408 inches remained at node (16,13).

TABLE 7

NARROW FLANGED "T" STIFFENER
STATIC TEST STRAIN AND PRESSURE DATA

STRAIN GAUGE DATA (MICROSTRAIN)

- STRAIN GAUGE POSITIONS -

PRESSURE (PSI)	1	2	3	4	6	7	8	9	10	12
25	403	616	373	242	622	579	745	-1156	-2655	-1236
50	781	1243	741	509	1271	1186	1697	-2015	-4348	-1988
75	1140	1716	1083	694	1846	1763	2595	-2681	-5132	-2608
100	1522	2026	1451	841	2448	2340	3314	-3253	-7644	-3155
125	1995	2297	1882	997	3098	3030	4025	-4018	-9720	-3907
150	2440	2537	1100	1100	3654	3572	4769	-4781	-11122	-4789
175	2922	2802	2802	1231	4334	4274	5550	-5669	-12074	-5992
200	3408	3053	3281	1359	5014	5031	6183	-7081	-12948	-7323
225	3975	3330	3833	1515	5830	5942	6778	-8613	-13458	-9014
250	4456	2633	4340	1542	6548	6708	7351	-9911	-13877	-10574
275	5070	1261	4938	1258	6288	7512	7901	-11552	-14132	-12359
300	5637	871	5490	1073	2754	2686	5401	-13078	-14314	-14181
325	6223	760	6089	1030	1873	2462	3091	-14910	-14496	-15985
350	6913	734	6779	996	1743	2377	2964	-16742	-14678	-17770
VENT	3266	284	3189	485	1048	691	1236	-10102	-8190	-11137

NOTE: STRAIN GAUGES SG-5 AND SG-11 FAILED PRIOR TO TEST, ALSO STRAIN VALUES IN THE VENT ROW INDICATE STRAIN REMAINING AFTER PRESSURE WAS VENTED OFF (i.e., AT ATMOSPHERIC PRESSURE.

limit of the elastic stiffener tripping region was located at 225 psi. That is, the region of elastic plate behavior is from 0-100 psi, plastic plate behavior is from 100-225 psi and the elastic stiffener tripping proceeds from 225 psi on.

4. Comparisons of Wide Flanged "T", "Z" and Narrow Flanged "T"

The cross sections of the three stiffeners chosen for these tests were selected in order to compare the effects on tripping behavior of varying both the stiffener slenderness ratio and the plastic section modulus. For the purpose of these comparisons, the measurement of the stiffener slenderness is taken as the ratio of the stiffener length to the effective radius of gyration and the plastic section modulus is the area moment of the effective cross section about the section's neutral axis. Both the radius of gyration and plastic section modulus were determined using the cross sectional area of the stiffener and the plating (based on its associated effective plate width). Using the existing data available for the narrow flanged "T" stiffener as the baseline, cross sections of the other two stiffeners were selected such that their plastic section moduli and slenderness ratios were as presented in Table 8. These cross sections would allow a comparison of the effects of a large change in the slenderness ratio and small and large changes in the plastic section modulus on the hydrostatic panel behavior.

TABLE 8

SUMMARY OF STIFFENER SLANDERNESS RATIOS
AND PLASTIC MODULI

STIFFENER CROSS SECTION	SLENDERNESS RATIO		PLASTIC SECTION MODULUS	
	$\frac{L}{K}$	PERCENTAGE DIFFERENCE IN L/K	Z_3 (IN^3)	PERCENTAGE DIFFERENCE IN Z
NARROW FLANGED "T"	56.00	*	.1860	*
WIDE FLANGED "T"	46.02	-18%	.1985	7%
"Z"	47.62	-15%	.2404	29%

NOTE: 1. L IS DEFINED AS THE STIFFENER LENGTH.

2. K IS DEFINED AS THE STIFFENER EFFECTIVE RADIUS OF GYRATION.

3. Z IS DEFINED AS THE PLASTIC SECTION MODULUS.

* DENOTES THE BASELINE CASE.

In comparing the results from these three different test cases one fact becomes immediately obvious: the regions of elastic plate behavior, plastic plate behavior, and elastic stiffener tripping coincide for all three tests. These ranges are from 0-100 psi, 100-225 psi and 225 + respectively. It appears that this indicates that these ranges are mostly functions of plate geometry and stiffener location; which remained constant throughout the tests, rather than stiffener cross sectional geometry or plastic section moduli, both of which were varied with each test.

It would be generally expected that increasing the slenderness of a stiffener would increase the strain experienced in the plate portion of a stiffened panel under increasing load. Conversely, one would also expect that strain to decrease if a larger or more rigid (and hence less slender) stiffener were to replace the existing one. Using the narrow flanged "T" stiffener with a slenderness ratio of 56.00 as the baseline, the other two cases were compared to determine what additional support the larger stiffeners provided to the panel. This was done by comparing the incremental strain plots of strain gauges 1 and 3 (as shown in Figures 3.9, 3.17 and 3.25) over all three behavioral ranges. The "Z" stiffener, with a slenderness ratio of 47.62, showed an 8% decrease in strain in the plate over the elastic range, a 9% decrease over the plastic range and a 10% decrease over the elastic stiffener tripping range. As compared to the strain

in the narrow flanged "T" stiffener in the same regions. The wide flanged "T" stiffener, with a slenderness ratio of 46.02, showed an 8% decrease in strain over the elastic range, a 30% decrease over the plastic range and a 25% decrease over the elastic tripping range. Clearly, the results of this comparison agree with the original premise that increasing the slenderness of a stiffener increases the amount of strain experienced by the plate.

Concentrating on the incremental strain plots for strain gauges 9, 10, 11, and 12 (stiffener gauges), as shown in Figures 3.9, 3.17 and 3.25, a comparison of the redistribution of load along the stiffener may be made. As both the "Z" and narrow flanged "T" stiffeners proceed into the elastic stiffener tripping zone the central portions of the stiffeners (gauges 10 and 11) quickly approach low levels of strain indicating that these areas of the stiffeners are providing little increased support to the plate. In this same behavioral region the wide flanged "T" stiffener starts at a higher level of strain and exhibits a continuous gentle decline in the additional amount of strain accepted in the center of the stiffener. Similarly, in the plot of the outer stiffener gauges (gauges 9 and 12) both the "Z" and narrow flanged "T" stiffeners show the strain reaching a plateau at the point where gauges 10 and 11 reach their low levels. The outer gauges on the wide flanged "T" show a constant increase in the amount of additional strain accepted with

increasing pressure in the same region where gauges 10 and 11 show a marked decrease in the amount of additional strain they accept. These effects can be explained by a combination of the stiffener geometry and the tripping mechanism. As described in the discussion of the results of the "Z" stiffener, the stiffener first initiates tripping by a buckling of the web and the resulting rotation of the flange. This mode of tripping is the equivalent of hinging the uppermost portion of the stiffener and effectively removes any support it may have provided. In the case of the narrow flanged "T" stiffener the flange is so narrow in relation to the length of the web that the stiffener can be nearly approximated as a bar stiffener which trips by buckling of the web as did the "Z" stiffener, thus the similarity which exists between the two. By contrast the wide flange, on the wide flanged "T" stiffener, provides a resistance to rotation from the vertical plane even after the stiffener has lost its stability, although it is to a lesser degree with increasing deviation from the vertical. Because of the support provided by the web, the amount of strain which must be redistributed both to the outer portions of the stiffener and the plate itself is less. This not only accounts for gauges 9 and 12 not reaching a maximum; but also why the wide flanged "T" stiffener provided a 25% improvement in the amount of strain developed in the free plate area, over the narrow flanged

"T" in the elastic tripping range when the "Z" stiffener only offered a 10% improvement.

From the comparisons presented above it appears that it would be practical to use a more slender (less rigid) "Z" stiffener rather than a more rigid wide flanged "T" stiffener if the improvement in the strength (hydrostatically) is to be realized only up to the point of elastic tripping. If structural survivability or residual post-tripping hydrostatic strength are to be major considerations in design then it would be more appropriate to concentrate on the wide flanged "T" stiffener. However, one advantage of the "Z" stiffener as noted in the previous discussion is that, as the tripping of the stiffener continues by its rotation, its asymmetry causes a decrease in strain on the side opposite the direction of its rotation.

B. UNDERWATER SHOCK TEST RESULTS

The analysis and discussion of the results of the dynamic pressure (shock) tests will be presented in a format similar to that of the hydrostatic test results. The results of the wide flanged "T" stiffener and the "Z" stiffener respectively will be discussed in the first two of the subsequent sections. The third section will briefly review the results obtained for the narrow flanged "T" stiffener as presented and discussed in reference 16, page 35. The fourth and final section will discuss similarities and

differences noted in the comparison of the results of the three tests.

1. Wide Flanged "T" Stiffened Panel Shock Test Results

As was discussed in the section concerning the test apparatus design several changes were incorporated into the test platform based on the recommendations made by LT Budweg [Ref. 16:p. 92]. The Undex test was successfully conducted and as in previous tests the 8 lb. cylindrical charge reacted as a larger charge. In the case of this test, post-shot calculations indicated that the charge produced a peak pressure of 3772 psi (Figure 3.26) which at a stand-off distance of 10 feet equates to the reaction expected of a charge of 10.66 lb. During this shot the styrofoam support floats, which were used instead of pneumatic fenders as in reference 16, page 24, suffered no collapse as in previous tests. The average of the shock front arrival times as presented in Table 9 is 3.5 msec after detonation at the plate gauge and 3.085 msec after detonation at the stiffener mounted gauges. The actual values obtained from the strain history plots (Figures 3.27 thorugh 3.32) vary much less than 1% from these average values which indicates that the pressure wave approached as a parallel wave front. Hence it is clear that the counter weight added to offset the instrumentation box performed its function admirably. One of the recommendations made by LT Budweg was to construct the stiffened portion of the plate flush with the bolted face of the test panel such that the

TABLE 9

WIDE FLANGED "T" STIFFENER
SUMMARY OF SHOCK WAVE ARRIVAL TIMES AND VALUES
OF MAXIMUM STRAIN PEAKS

SENSOR	ARRIVAL TIME (MILLISECONDS)	RECORDED PEAK (MICROSTRAIN)
SG-1	3.15	25.3 K
SG-2	3.16	38.1 K
SG-3	3.15	37.1 K
SG-4	3.14	40.0 K
SG-5	3.16	34.2 K
SG-6	3.16	33.0 K
SG-7	3.15	33.0 K
SG-8	3.15	37.7 K
SG-9	3.08	-40.0 K
SG-10	3.09	-37.7 K
SG-11	3.08	-40.0 K
SG-12	3.09	-40.0 K
P-XDCR	3.00	37.72 PSI

corner amplification of the incident pressure wave would be eliminated. In previous tests it was thought that the failure of the plate at the clamped edges was due to the effect of this amplification [Ref. 16:p. 88]. The end result of this test was similar to the Budweg test in that the plate was blown free of the test panel and was found in the bottom of the test chamber. Close observation of the failed plate shows that the failure started with a clean shear in the center area of the long sides. Near the corners of the long sides the plate failure changes to a ductile tearing which progressed around the corners where the tears from both sides met and completed the failure.

The recorded strain gauge histories were transferred from high speed magnetic tape to hard disk on the HP-5451C Fourier Analyzer where they were reviewed and graphical representations were prepared. Table 10 contains a summary of the various strain peak magnitudes and their associated appearance times. It is by comparing the data in Table 10 and Figures 3.27 through 3.32 that comments on the mechanism of dynamic tripping might be made. The general, or characteristic, form described by every strain gauge history was an eventual rise to a peak value of strain followed quickly by a drop to a negative value. This is representative of the plate separating from the water due to cavitation at the plate's surface. This allows the plate to come to rest or

TABLE 10

WIDE FLANGED "T" STIFFENER
SUMMARY OF OBSERVED PEAK STRAIN ACTIVITY

SENSOR	PEAK (MICROSTRAIN)	OCCURRENCE TIME (MILLISECONDS)
SG-1	9.3 K	3.46
	25.3 K *	3.64
SG-2 +	6.8 K	3.46
	26.1 K	3.58
	38.1 K *	3.74
SG-3 +	37.1 K *	3.46
	29.1 K	3.63
SG-4	40.0 K *	3.34
	36.1 K	3.46
SG-5	34.2 K	3.34
	32.9 K	3.46
SG-6	22.7 K	3.22
	13.1 K	3.35
	33.0 K *	3.46
SG-7	20.5 K	3.22
	25.3 K	3.36
	33.0 K	3.46
SG-8	5.5 K	3.22
	37.7 K	3.46
SG-9	-11.1 K	3.23
	-16.0 K	3.36
	-40.0 K *	3.45
	-30.1 K	3.62
	-40.0 K	3.73
SG-10	-3.6 K	3.23
	-7.1 K	3.34
	-37.7 K *	3.45

TABLE 10 (continued)

SENSOR	PEAK (MICROSTRAIN	OCCURRENCE TIME (MILLISECONDS)
	-10.6 K	3.51
	-11.9 K	3.62
	-18.1 K	3.72
SG-11	-10.3 K	3.19
	-6.0 K	3.22
	-10.0 K	3.36
	-40.0 K	3.45
	-13.5 K	3.25
	-12.9 K	3.62
	-22.8 K	3.72
SG-12	-11.2 K	3.23
	-16.1 K	3.30
	-18.7 K	3.36
	-40.0 K *	3.46
	-35.5 K	3.52
	-26.5 K	3.62
	-40.0 K	3.73

* INDICATES MAXIMUM PEAK VALUE.

+ CONTAIN MINOR STRAIN ACTION PRIOR TO 3.46 MSEC BUT PEAK VALUES 3 K STRAIN.

to approach a rest state until reloading occurs from water rushing in when the cavitation collapses [Ref. 12:p. 84-9].

In observing and comparing the strain history traces and data tables of the different gauges several points of interest become evident. First is that there is a high degree of symmetry throughout the test, both in the strain peak occurrence time and the relative strain magnitudes at these peaks. In addition, close scrutiny of the stiffener mounted gauge histories appears to provide insight concerning panel loading, initial stiffener tripping, reloading and continued tripping. Concerning symmetry, all histories of gauges in similar orientation but opposite positions relative to the transverse or longitudinal centerline exhibit nearly identical traces (e.g., pair 9 and 12, pair 10 and 11, pair 1 and 5, pair 1 and 3). Concentrating on strain gauges 9, 10, 11, and 12, which are mounted along the stiffener, it appears that from the time of arrival of the shockwave at 3.09 msec after detonation until about 3.45 msec the strain present in all portions of the stiffener builds to a peak. At the point just after 3.46 msec the central portion of the stiffener appears to lose stability and begins to rotate out of the vertical plane. At this point the central portion of the stiffener redistributes its load over the rest of the plate. Most of the other plate mounted gauges exhibit corresponding peaks at this time with magnitudes representing the maximum strain encountered during their history (in all

cases except gauges 2 and 5). Gauge 2 (Figure 3.29 shows a peak, however it is nowhere near the maximum peak for its history. This may be explained in that gauge 2 is directly beneath the stiffener as it trips. The additional loading it accepts as a result of the stiffener unloading is only slightly larger than the strain which is relieved as the stiffener no longer forces the plate downward. The end result is a small peak for gauge 2. After this initial or primary tripping, the center portion of the stiffener might still retain a small resistance to rotation from the vertical which effectively supports the outer portion of the stiffener. This additional support to those, as yet untripped, outer portions of the stiffener, together with the fact that the plate near the ends of the stiffener has less deflection (and hence a larger radius of curvature of the stiffener), allows the stiffener in those areas to remain stable for a longer period. The ability of the stiffener to remain stable at its ends would allow those portions to continue loading until the central portion has completely lost its resistance to rotation and the deflection of the plate in those areas has increased sufficiently to allow a second tripping action to occur. The time of occurrence of this secondary tripping might also be determined from the histories of gauges 9 through 12 (Figures 3.31 and 3.32). From 3.46 msec to 3.72 msec gauges 10 and 11 show small increased in loading because of their retained resistance to

rotation, but at 3.72 msec the loading overcomes this resistance and the central portion of the stiffener drops all of its support for the outer portions. As can be seen in the histories of gauges 9 and 12, the outer portion of the stiffener continues to load as long as the central portion lends some support, enabling those portions to remain stable. At 3.73 msec it appears the stiffener essentially fails along its entire length.

In all of the strain gauges mounted on the plate directly beneath the stiffener (gauges 1, 3, 2 and 8 as shown in Figures 3.27 and 3.28) there was only minor strain action until the primary tripping of the stiffener occurred. In the open area plate mounted gauges (gauges 4, 5, 6 and 7 as shown in Figures 3.29 and 3.30) the strains associated with the loading, unloading, and reloading caused by the incident pressure pulse, resultant cavitation and reimpingement water surge prior to the stiffener tripping are readily evident. The minor strain action of the gauges mentioned previously as located under the stiffener did show some minimal peaks whose occurrence times closely correspond to the peaks present in the open areas prior to tripping. More importantly, the gauges mounted on the stiffener (gauges 9, 10, 11, and 12 shown in Figures 3.31 and 3.32) show peaks of much greater magnitude which also correspond to the peaks of the open areas. The significance of these peaks and their associated magnitudes is that it shows that load being borne by the stiffener

was only affecting the area directly beneath the stiffener, as shown by the relative absence of load in gauges 1, 2, 3, and 8. The open area gauges; however, are clearly undergoing immediate elastic-plastic deformation due to the pressure wave with no support in the transverse and only minimal support in the longitudinal direction. This lack of support transversely can be seen in the larger, more distinct peaks of gauges 6 and 7 (Figure 3.30) prior to tripping. The minimal support in the longitudinal direction is seen in the histories of strain gauges 4 and 5 (Figure 3.29). The initial peaks on these gauges are considerably smaller than those of gauges 6 and 7. It must be noted, hoever, that even the minimal support previously described disappears at the instant tripping occurs.

Upon observation of the failed plate the primary and secondary tripping actions of the stiffener are readily evident. The area of tripping with the largest magnitude of deflection was the primary tripping point in the center of the plate. This was as should be expected because the center portion of the plate experiences the highest compressive stresses during deformation. The outermost points of tripping of the stiffener were determined to be the secondary tripping points because the magnitudes of deflection were less. These smaller deflections required less load in the stiffener. After the primary tripping the outer portions of the stiffener could only build to low levels of strain prior

to loss of stability and the onset of secondary tripping. A schematic of the resultant tripped stiffener configuration is shown in Figure 3.33.

As can be seen, the underwater shock test data and strain histories can provide an insight into the interaction of the test panel and the incident pressure wave by use of arrival times, strain peak values and subsequent cyclic reload times.

2. "Z" Stiffened Panel Shock Test Results

The original test shot for this test misfired at detonation and caused a one day delay in conducting this test. It was found that the cylindrical charges provided were from a stock which was, by this test, nearly depleted and the remaining charges were at or had exceeded their indicated shelf lives. As a result the first charge suffered the failure. Upon receipt of a second charge, which was the youngest of those remaining, the test was again set up for detonation. This time the charge detonated but the resultant explosion was of a smaller magnitude than that experienced in the wide flanged "T" test. This was physically obvious in that the resultant dome and plume from the explosion were on the order of one-half the previous. Analysis of the data obtained from the pressure transducer (Figure 3.34) yields a peak pressure of only 3,039 psi, which at a stand-off distance of 10 feet is the reaction which would be expected of a charge of only 6.2 lb. weight. The trace of the pressure response data

(Figure 3.34) does indeed show a much smaller peak magnitude than the previous test (Figure 3.26), however, it shows additional peaks of a similar magnitude and the characteristic exponential decay appeared delayed in its commencement.

The fact that the charge provided was at the extent of its shelf life holds the key to the explanation of the phenomenon described above. It is common for a charge to experience deterioration as it ages. This deterioration, depending on the charge type, time elapsed and environmental factors, can cause two types of effect. The first effect, and most dangerous, is the loss of chemical stability. Because of this effect's inherent danger, many precautions are taken to prevent its occurrence. The second effect is that portions of the charge become inert. This is undoubtedly what occurred to the charge used for this test. If the detonator were placed in the region of the inert area of the charge, the reaction initiated by the detonator would have to progress around the "dead zone." The delay in time for the reaction to reach all parts of the charge (as shown in Figure 3.35) is the reason for the multiple peaks and the delay in the commencement of the exponential decay. Although the delay in reaction resulted in pressure peaks of lesser magnitude the fact that the same amount of charge was consumed in each test indicates that the impulse of each shot should be equal. The area under the pressure time history trace is proportional to the impulse resulting from the shot. A comparison of the

areas under the pressure traces of the two tests indicates that the areas are equal (within .6%), and hence the impulses resultant from each shot were equal.

When the test chamber was pulled from the water the effect of the lesser peak pressure became clearly evident. The plate remained intact in the panel with the exception of a portion of the longitudinal edges; the circumferential tearing present in the previous test was absent. As in the previous test the pressure pulse arrival times were determined and compared. Table 11 is a summary of these arrival times. Once again the variation in arrival times, at points of the plate at the same level, was less than 1%. Figures 3.36 through 3.41 represent the strain history traces recorded by each stain gauge during the test. It should be noted that strain gauge 10 failed at the onset of the test for unknown reasons. Table 12 is provided as a summary of the noted strain peaks, their occurrence times and magnitudes.

The overall analysis of the elastic-plastic actions of the plate due to a single impulsive load is nearly impossible because of the nature of the actual pressure loading provided by the explosive charge. Essentially the charge provided three "separate" impulsive loads of approximately equal magnitude (about 3000 psi) at about .044 msec intervals. As a result of this loading resultant strain peaks expected from the loading of the pressure wave, unloading from cavitation and reloading were modified. These modifications could

TABLE 11

"Z" STIFFENER
SUMMARY OF SHOCK WAVE ARRIVAL TIMES AND VALUES
OF MAXIMUM STRAIN PEAKS

SENSOR	ARRIVAL TIME (MILLISECONDS)	RECORDED PEAK (MICROSTRAIN)
SG-1	3.40	17.0 K
SG-2	3.39	9.3 K
SG-3	3.39	4.5 K
SG-4	3.39	15.4 K
SG-5	3.39	40.0 K
SG-6	3.40	38.1 K
SG-7	3.39	16.0 K
SG-8	3.39	20.8 K
SG-9	3.33	-20.0 K
SG-10	FAILED	FAILED
SG-11	3.32	-8.5 K
SG-12	3.33	-40.0 K
P-XDCR	3.29	3039 PSI

TABLE 12

"Z" STIFFENER
SUMMARY OF OBSERVED PEAK STRAIN ACTIVITY

SENSOR	PEAK (MICROSTRAIN)	OCCURRENCE TIME (MILLISECONDS)
SG-1	17.0 K *	3.71
	11.8 K	3.73
	12.0 K	3.76
	11.8 K	3.78
	8.0 K	3.81
	12.1 K	3.88
	12.2 K	3.89
	16.0 K	3.92
	40.0 K *	3.93
SG-2	9.3 K *	3.71
	2.0 K	3.73
	3.9 K	3.76
	1.0 K	3.78
SG-3	4.5 *	3.71
	.1 K	3.76
SG-4	15.4 K *	3.68
	12.4 K	3.69
	12.3 K	4.03
SG-5	40.0 K *	3.68
	2.9 K	3.74
	3.0 K	4.03
SG-6	6.7 K	3.48
	10.9 K	3.51
	9.6 K	3.54
	14.8 K	3.60
	38.1 K	3.68
SG-7	2.6 K	3.48
	2.8 K	3.51

TABLE 12 (continued)

SENSOR	PEAK (MICROSTRAIN)	OCCURRENCE TIME (MILLISECONDS)
	10.6 K	3.55
	10.2 K	3.59
	9.6 K	3.63
	16.0 K *	3.68
	13.7 K	3.71
	11.8 K	3.73
	11.8 K	3.76
SG-8	16.8 K	3.71
	20.8 K *	3.73
	13.4 K	3.76
	13.2 K	3.78
	2.1 K	3.81
	2.0 K	3.83
	1.9 K	3.88
SG-9	-16.0 K	3.67
	-14.7 K	3.69
	-20.0 K *+	3.76
SG-11	-1.9 K	3.76
	-0.0 K	3.70
	-7.4 K	3.71
	-8.5 K	3.73
SG-12	-15.0 K	3.63
	-14.4 K	3.67
	-17.2 K	3.69
	-20.0 K	3.70
	-37.1 K *	3.71
	-36.7 K	3.76
	-40.0 K +	3.83

* INDICATES MAXIMUM

+ INDICATES GAUGE FAILED AT THIS POINT

take the form of magnifying, minimizing, or altogether eliminating the strain peaks because of the superposition of the plate response to the secondary and tertiary pressure pulses provided by the charge. A general comparison of the peak magnitudes and occurrence times, however, did indicate that symmetry did exist in most cases for gauges in complementary positions.

In spite of the problems associated with the pressure pulse, analysis of the strain histories was done in the hope that some insight into the tripping of the "Z" stiffener might be obtained. The primary ares of concentration was the stiffener itself and the gauges mounted on it. At a time of 3.67 msec strain gauge 11 (Figure 3.41) attains a relative maximum in compression followed by an unloading, apparently, indicative of the initiation of tripping in the stiffener coincident with the cavitation following the pressure pulse. At this same time strain gauges 9 and 12 (Figure 3.40) appear to undergo some tensile release of their compressive loading. It is noted that after a few moments all of the stiffener gauges continue to load, 9 and 12 until failure and 11 until it attains a maximum constant loading. A possible explanation for the indicated reactions is similar in nature to that proposed in the wide flanged "T" shock test discussion. After the initial rotation from the vertical plane associated with tripping the tripped portion of the stiffener retains a certain amount of resistance to rotation owing to the basic

rigidity of the web and flange material. This resistance to rotation lends support to the outer portions of the stiffener. The additional support allows the ends of the stiffener to remain stable and accept additional load until the applied load overcomes the center portion's resistance. At that point the outer portions would lose their support, hence they become unstable and tripping would occur in those portions.

In the free plate gauges (4, 5, 6 and 7 as shown in Figures 3.38 and 3.39) the effect of the tripping becomes clearly evident. At 3.68 msec all four gauges exhibited the maximum peak strain represented over all of their individual histories. This corresponds directly to the instant of tripping as determined from the stiffener mounted strain gauge and is indicative of the load being redistributed throughout the plate. Those strain gauges mounted directly beneath the stiffener (1, 3, 2 and 8 as shown in Figures 3.36 and 3.37) had slightly slower reactions which can be accounted for by the plate's larger flexural rigidity and effective mass (produced by the location of the base flange of the "Z" stiffener) in that area. In those positions the reaction of the strain corresponding to the redistribution of load after tripping started at the instant of tripping, but the maximum strains were not reached until about .03 msec after the tripping (at a time of 3.71 msec). The peak exhibited by strain gauge 8 (Figure 3.37) spans a time period of about .05 msec from 3.71 msec to 3.76 msec and is probably the result of the continued rotation of the stiffener above it.

The total deflection of the plate was 1.50 inches or the equivalent of eight plate thicknesses. The stiffener itself showed a tripping configuration as shown in Figure 3.42, with a maximum deflection from vertical of .06 inches at the center of the stiffener. The primary tripping of the stiffener occurred at 3.46 msec or an elapsed time of .27 msec after the incidence of the shock wave. Even with the difficulties resulting from the inconsistency of the pressure pulse certain trends in the plate response can be noted. As in the previous test the stiffener provided essentially no support in the transverse direction and some support in the longitudinal direction. The support provided longitudinally is greater in magnitude than that provided by the wide flanged "T" in the previous test as the peaks of gauges 4 and 5 prior to tripping are barely discernible and the final large peak exhibited by gauges 6 and 7 prior to tripping and the redistribution of the load does not exist at all. As a final note, a comparison of gauges 6 and 7 (Figure 3.39) shows that the strain level on the side of the base flange of the stiffener is considerably smaller than that of the opposite side. From the discussion presented in the results of the hydrostatic "Z" stiffener test it would seem that this indicates that the stiffener trips toward strain gauge 6. Physically viewing the tripped stiffener verifies this fact.

The test data and strain histories presented for the shock test of the "Z" stiffened panel provided the opportunity

to verify various plate reactions noted in the previous wide flanged "T" test and to determine the applicability of the results of the hydrostatic "Z" test. The analysis of this data was fairly successful in both of these areas. The only detrimental effect noted, which could be attributed to the poor shot performance, was that of the early failure of the stiffener mounted strain gauges. These failures are probably due to the additional, excessive movement of the wiring caused by the multiple pressure peaks.

3. Narrow Flanged "T" Stiffened Panel Shock Test Results

As was done in the discussion of the hydrostatic test, the results and data previous presented in reference 16, page 35 will be reviewed in this section. This review will provide a basis for comparison of the responses of the three test cases. Tables 13 and 14 as well as Figures 3.43 through 3.47 are provided for the purpose of continuity.

The analysis of the arrival times of the shock wave at the different gauges indicated that the test chamber was suspended such that the panel was at an angle of 22 degrees to the shock wave vice being parallel. Although the different strain gauge positions had different shock wave arrival times the symmetry of complementary positions was maintained. Across the stiffener mounted strain gauges the tripping action was still observable. The only surviving innermost gauge (strain gauge 10) increased its load to a point less

TABLE 13

NARROW FLANGED "T" STIFFENER
SUMMARY OF SHOCK WAVE ARRIVAL TIMES AND VALUES
OF MAXIMUM STRAIN PEAKS

SENSOR	ARRIVAL TIME (MILLISECONDS)	RECORDED PEAK (MICROSTRAIN)
SG-1	2.85	20.2 K
SG-2	2.82	30.0 K
SG-3	2.88	44.0 K
SG-4	2.50	17.0 K
SG-5	2.76	23.0 K
SG-6	2.82	25.2 K
SG-7	2.50	40.0 K
SG-8	2.88	35.0 K
SG-9	2.56	-36.0 K
SG-10	2.56	-16.0 K
SG-11	----------FAILED --------	
SG-12	2.56	-36.0 K
P-XDCR-1	2.42	3780 PSI
P-XDCR-2	2.40	3500 PSI

TABLE 14

NARROW FLANGED "T" STIFFENER
SUMMARY OF SHOCK WAVE ARRIVAL TIMES, PEAK TIMES,
TIME TO CAVITATION, AND RELOAD TIMES

SENSOR	ARRIVAL TIME (milliseconds)	*PEAK TIMES (milliseconds)	ELAPSED TIME PRIOR TO CAVITATION (milliseconds)	RELOAD TIME (milliseconds)
SG-1	2.85	3.35/3.39/3.41	.56	3.45
SG-2	2.82	3.30/3.31/3.39 3.41	.59	3.44
SG-3	2.88	3.39/3.42	.54	3.44
SG-4	2.50	2.64/2.74	.24	2.75
SG-5	2.76	3.08	.32	3.09
SG-6	2.82	3.09/3.13	.31	3.16
SG-7	2.55	2.67	.12	2.70
SG-8	2.88	3.32/3.40/3.44 3.46	.58	3.49
SG-9	2.56	2.65/2.85/2.97 3.05/3.27	.71	3.49
SG-10	2.56	2.77/2.92/3.11	.55	3.18
SG-11	----------	----------FAILED----------	----------	----------
SG-12	2.56	2.68/2.75/2.91 3.07/3.39	.83	3.49

*UNDERLINED PEAK TIME INDICATES TIME OF
MAXIMUM STRAIN VALUE.

than the outer edges and experienced cyclic unloading and reloading as the stiffener underwent its successive deformations. Consideration of the schematic of the tripped stiffener (Figure 3.48) in conjunction with these gauge histories would indicate that the tripping first occurred near strain gauge 20 in the center of the stiffener followed by the portion in the vicinity of strain gauge 9 and lastly near gauge 12.

4. Comparisons of the Wide Flanged "T", "Z" and Narrow Flanged "T" Stiffened Panel Underwater Shock Test Results

For comparisons between these test cases many choices come to mind: the differences in elapsed time from shock wave incidence to stiffener tripping, magnitudes of strain in the area of tripping at its onset, differences in general plate reaction resulting from the pressure pulse and tripping, magnitudes of the resultant plastic deformation of the plate, and the configuration of the plastically tripped stiffeners. These are the areas of comparison which will be addressed in this section.

The baseline for a comparison of the elapsed time prior to the onset of tripping was that of the arrival time of the shock wave at the center stiffener mounted strain gauges. Because of the constancy of the standoff distance maintained throughout the three tests this assured a comparison relative to the load history. The center portion was chosen because, in all cases, it was the first area to lose stability. For the wide flanged "T" stiffener the shock

front arrived at about 3.085 msec after detonation and the loss of stability occurred at 3.46 msec for an elapsed time prior to tripping of .375 msec. The "Z" stiffener had an arrival time of 3.32 msec with tripping occurring at about 3.67 msec for an elapsed time of .350 msec. Last of all, the narrow flanged "T" stiffener had an arrival time of 2.56 msec and a tripping time of about 2.92 msec for an elapsed time of .36 msec. From these elapsed times it appears that the wide flange "T" offered a somewhat longer period of stability with the "Z" stiffener offering a lesser period.

The comparison of the magnitudes of strain present at the center of each stiffener at tripping provides more significant insight into the relative superiority of these cross sections. The wide flanged "T" stiffener was withstanding in excess of 40 thousand microstrain at the moment of tripping where the narrow flanged "T" was supporting 16 thousand microstrain and the "Z" only withstood 1.9 thousand microstrain. Combined with the previous comparison this shows that wide flanged "T" retained its stability for a longer period with a higher amount of strain than either of the other two test cases. Conversely, it should also be noted that the "Z" stiffeners not only lost its stability earliest, but also at the lowest strain. This may appear fairly straight forward and indicate that the "Z" configuration is not as efficient as either the wide or narrow flanged "T" stiffeners in the pressence of dynamic loading; however,

in view of the pressure pulse inconsistency as previously discussed, this may not be the case. For example, the initial pressure peak may have started to load the plate and stiffener causing deformation of the plate and changing the angle of incidence between the stiffener, the plate and the succeeding pressure pulses. These successive changed in the orientation of the stiffener and plate might have resulted in reflected waves from later pulses impinging directly upon the stiffener triggering the tripping at deceptively low values of strain and earlier than might have otherwise occurred. In addition, because of the inclination of the test chamber during the narrow flanged "T" stiffener test the entire plate was not uniformly nor instantaneously loaded. This "incremental" loading of the plate stiffener system is no doubt the cause of the tripping going from the position of strain gauge 10 to gauge 12 and then to gauge 9 as opposed to progressing from 10 to both 9 and 12 simultaneously as did the wide flanged "T". This delay in the full loading of the plate may have contributed to higher values of elapsed time to tripping than actually would be expected under a uniformly applied impulsive load.

Although the previous comparisons were somewhat complicated by problems which put those comparisons into perspective, it is possible to determine some common trends as well as differences in plate response to impulsive loading in all three tests. First, in all three tests it was found that

all free area plate mounted gauges (strain gauges 4 through 7) essentially behaved as if they had minimal stiffening support upon incidence of loading. During that same period of time the gauges mounted below the stiffener (gauges 1, 2, 3 and 8) showed little activity as the stiffener took the majority of the strain. At the point of stiffener tripping and load redistribution, differences begin to show. The "Z" stiffener, with its base flange mounted directly on the plate lends some transverse support to the surrounding plate while both of the "T" stiffeners redistribute larger amounts of stress longitudinally. This is well illustrated by noting the redistribution peak strain for all three cases at gauge 6 and 7. For the wide flanged "T" the peaks were at 33 k microstrain each, for the narrow flanged "T" the only surviving transverse gauge at that time (gauge 6) had its peak at 25 k microstrain and gauge 7 recorded 2.6 k microstrain. The transverse values of strain in the "Z" stiffened plate were 10 to 20 percent of those of the other two tests.

A comparison of the actual deformed plates after the tests shows that the two "T" stiffened plates underwent a total central deflection equivalent to 7 plate thicknesses, the "Z" plate had a maximum defleciton of 8 plate thicknesses. Neither of the "T" stiffeners left the vertical plane except at the points of instability whereas the "Z" stiffener, as shown in Figure 3.45 moved almost completely out of the vertical plane in the direction of strain gauge 6. The asymmetry

of tripped areas on the narrow flanged "T" stiffener is attributable to its profression of tripping as previously described. That is, because of the continuous loading along the stiffener the tripped center portion no longer provides equal resistance to rotation to both ends of the stiffener so succeeding points of instability may occur nearer to or farther from the center.

Over all these tests provided an excellent opportunity to gain a greater understanding of the reactions of stiffened panels udner impulsive loading. It also provided information concerning the effect of varying stiffener geometry on those reactions.

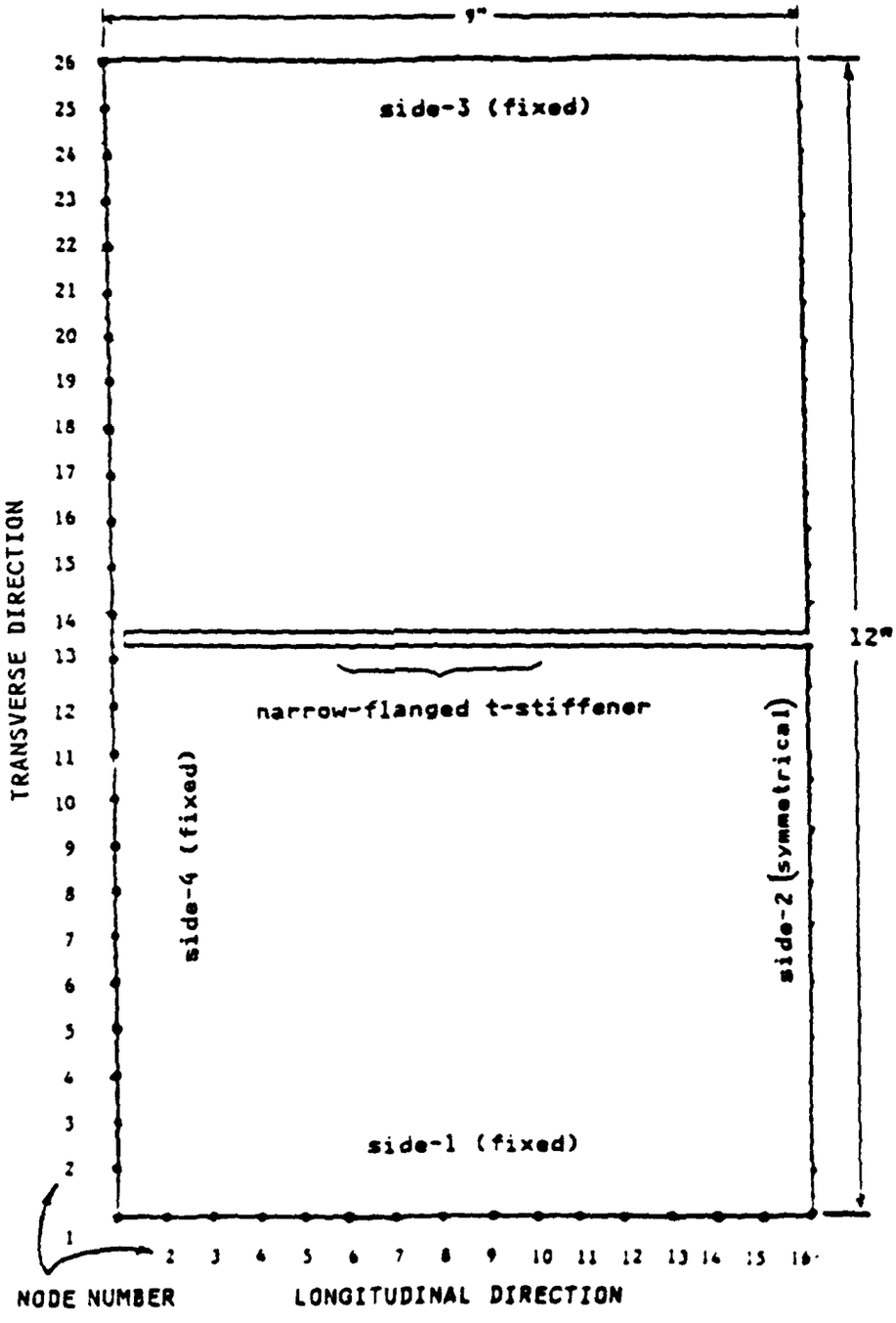

Figure 3.1 Segmentation of Half-plate

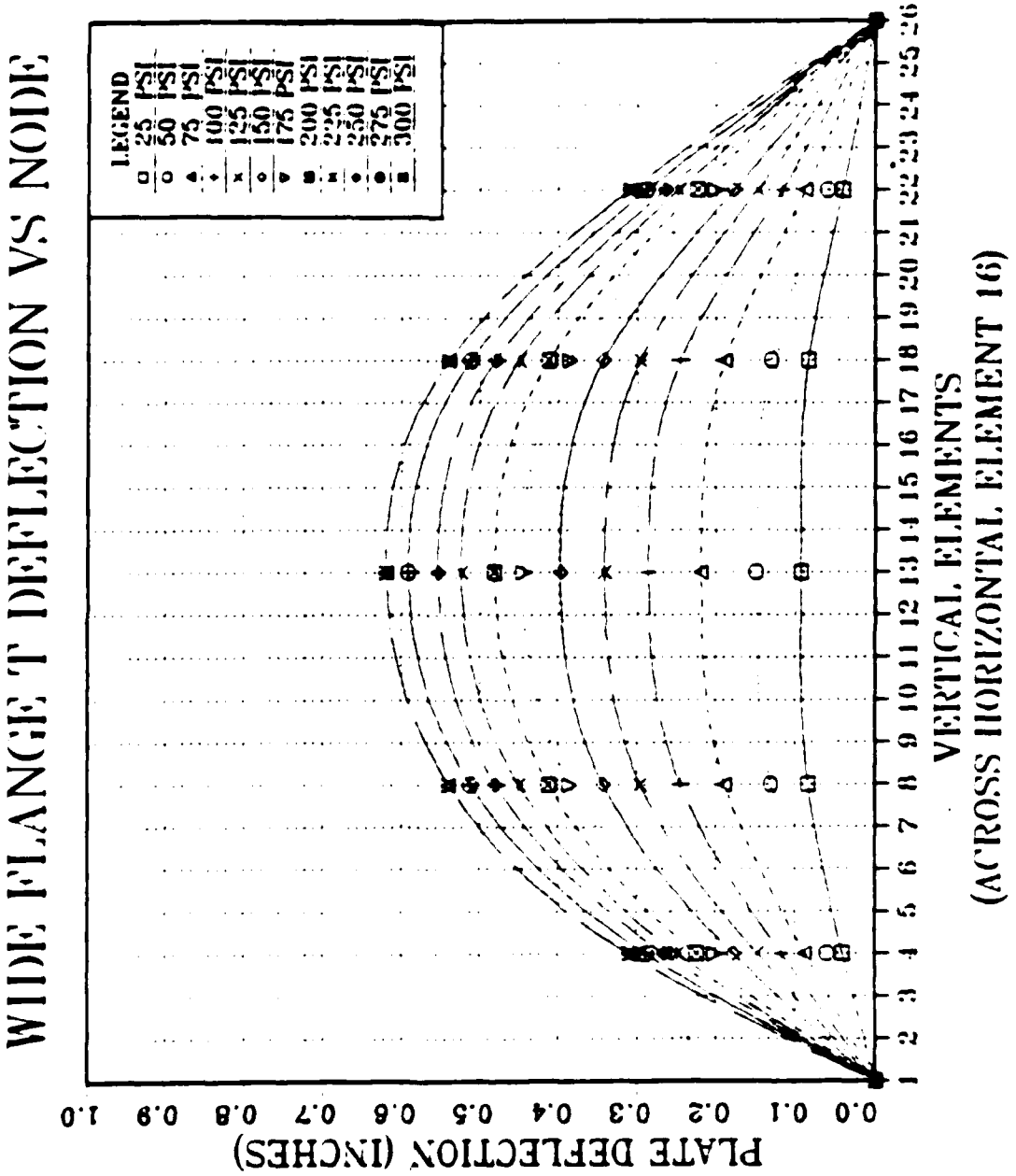

Figure 3.2 Plot of Wide Flanged "T" Static Test Deflection Results

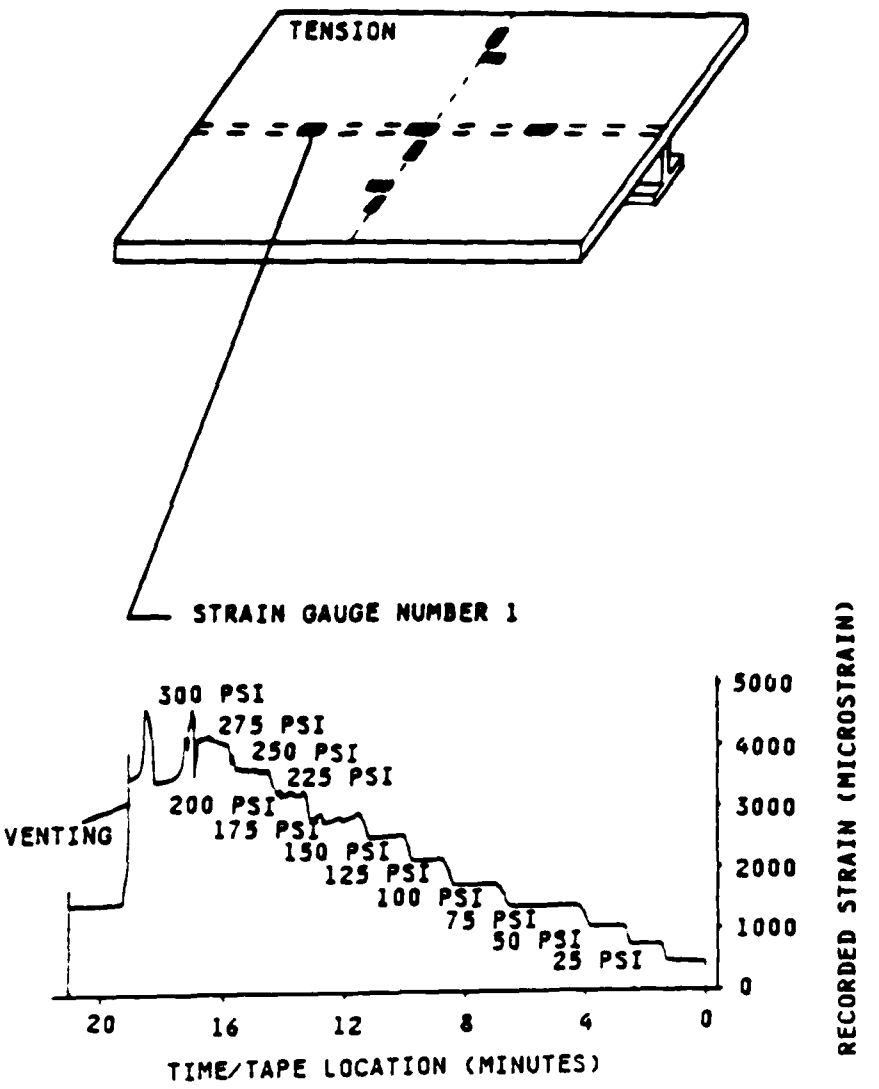

Figure 3.3 Strain Gauge No. 1 Strain History, Wide Flanged "T" Hydrostatic Test

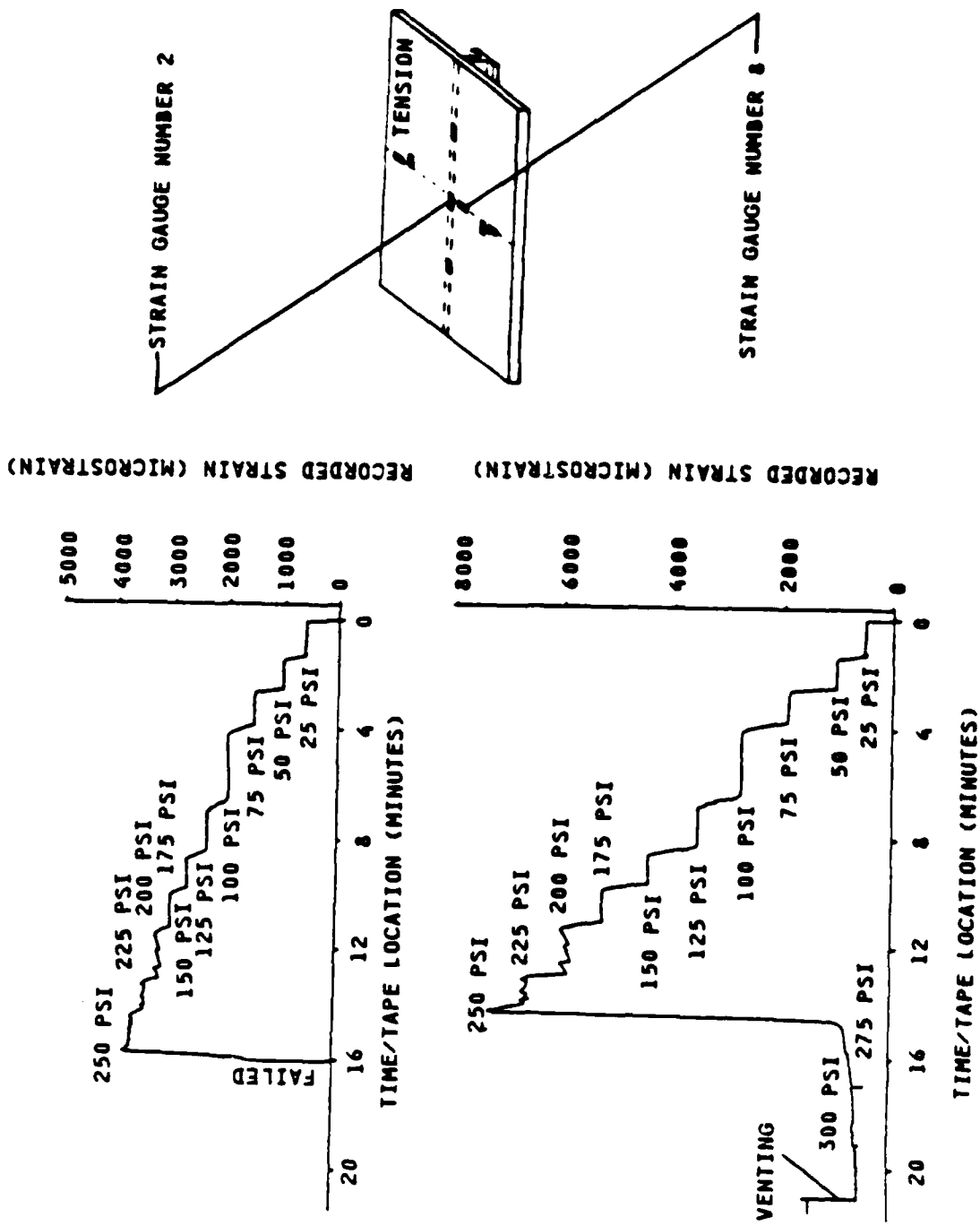

Figure 3.4 Strain Gauge Nos. 2 and 8 Strain Histories, Wide Flanged "T" Hydrostatic Test

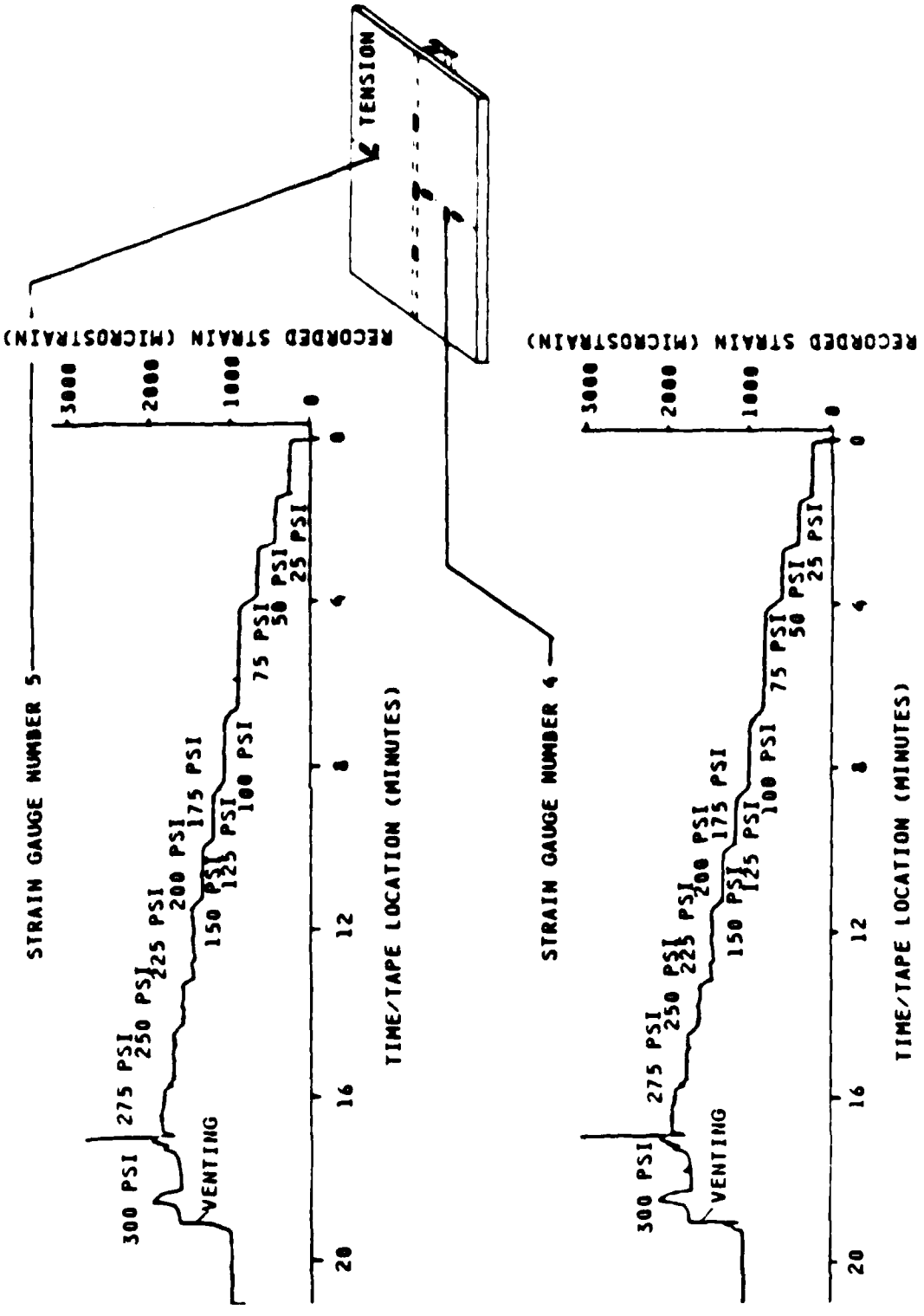

Figure 3.5 Strain Gauge Nos. 4 and 5 Strain Histories, Wide Flanged "T" Hydrostatic Test

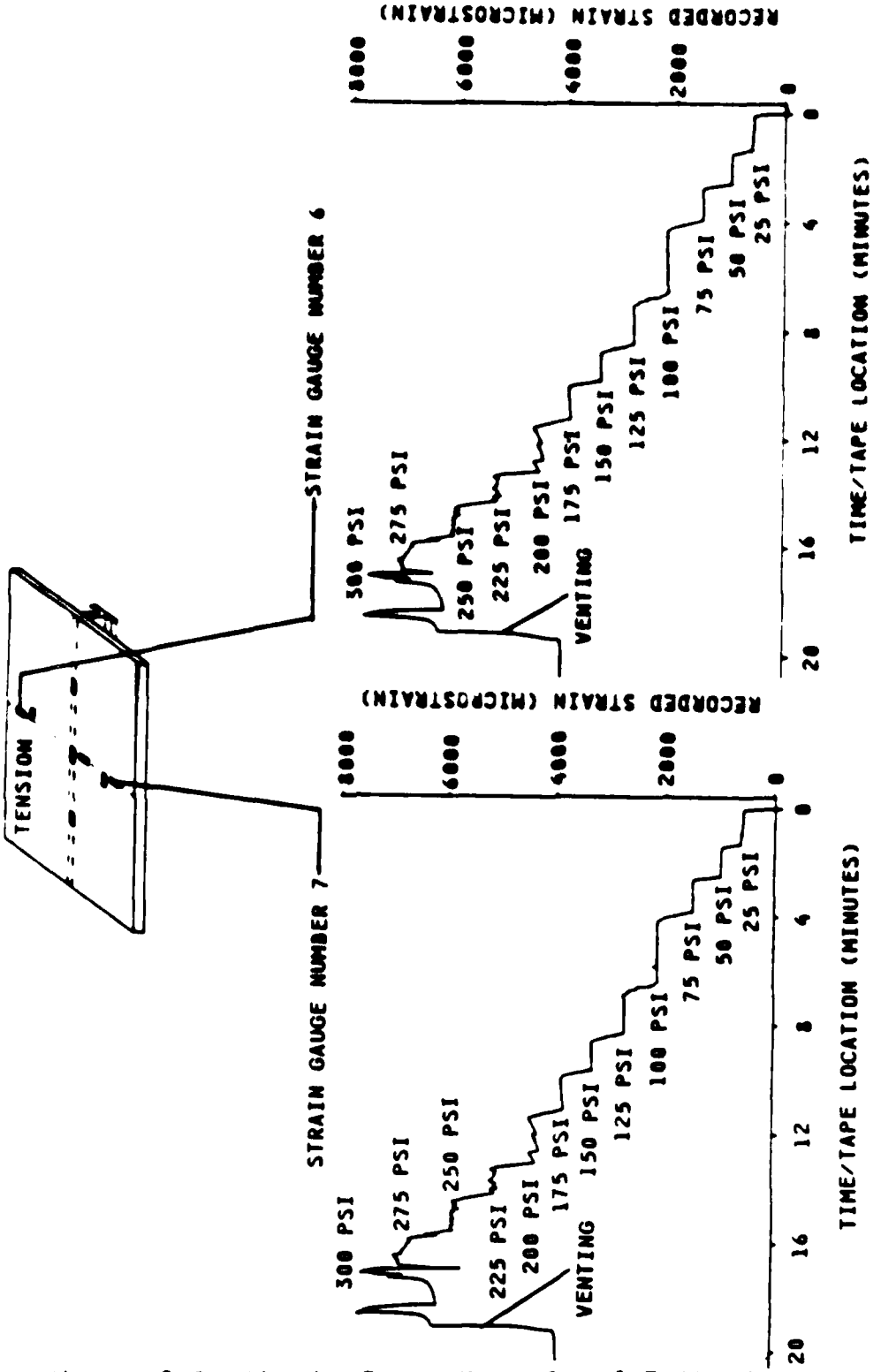

Figure 3.6 Strain Gauge Nos. 6 and 7 Strain Histories, Wide Flanged "T" Hydrostatic Test

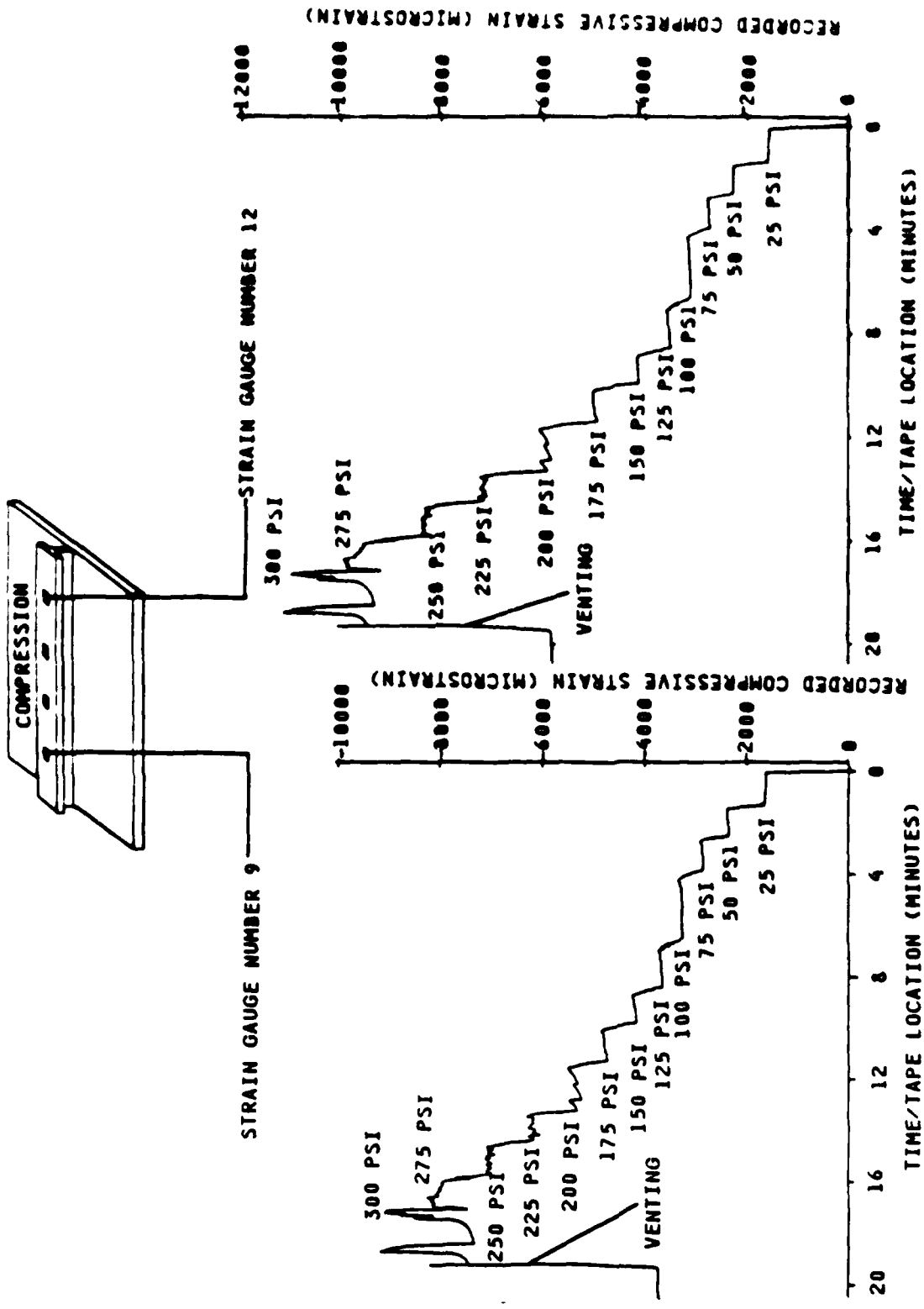

Figure 3.7 Strain Gauge Nos. 9 and 12 Strain Histories, Wide Flanged "T" Hydrostatic Test

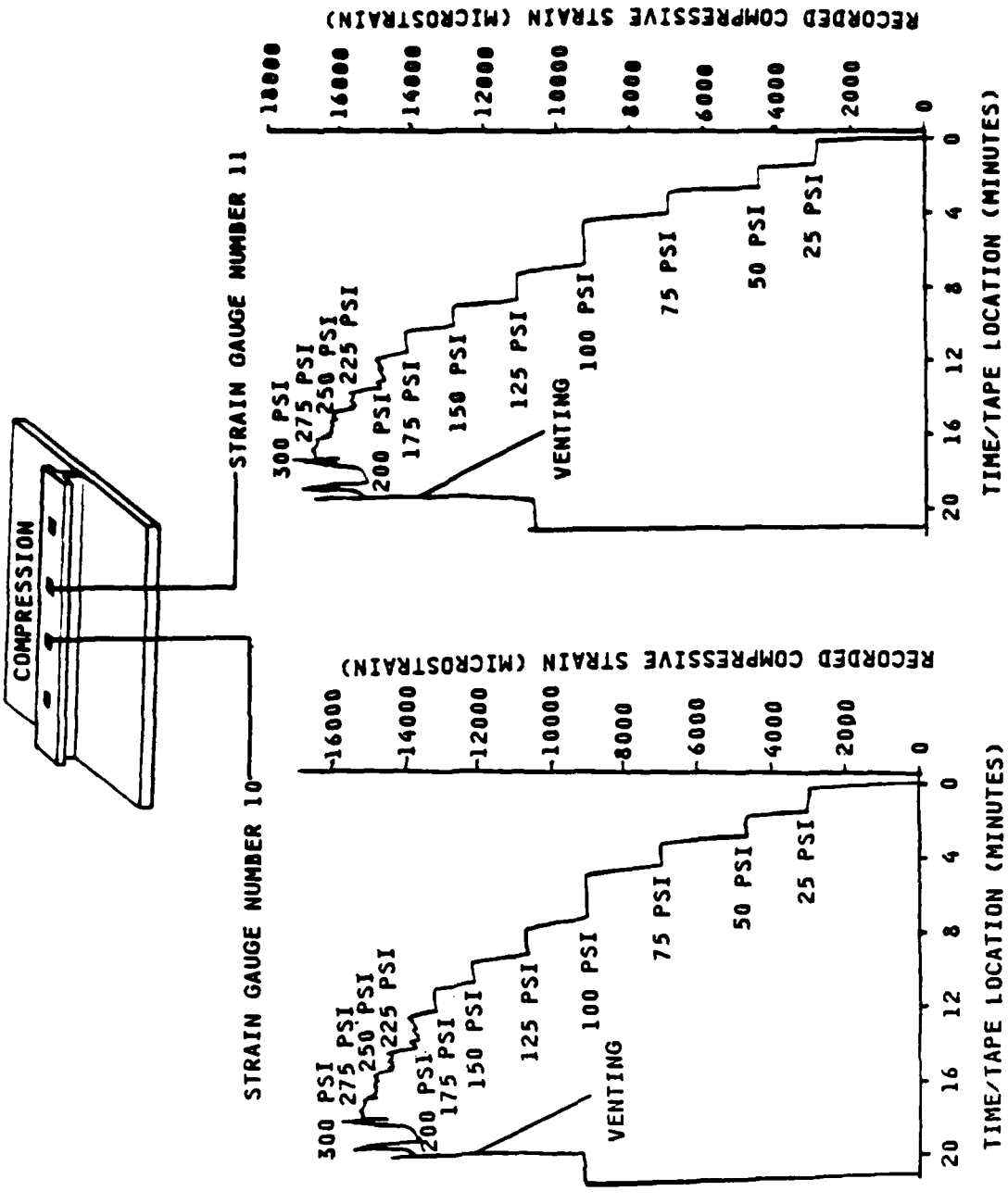

Figure 3.8 Strain Gauge Nos. 10 and 11 Strain Histories, Wide Flanged "T" Hydrostatic Test

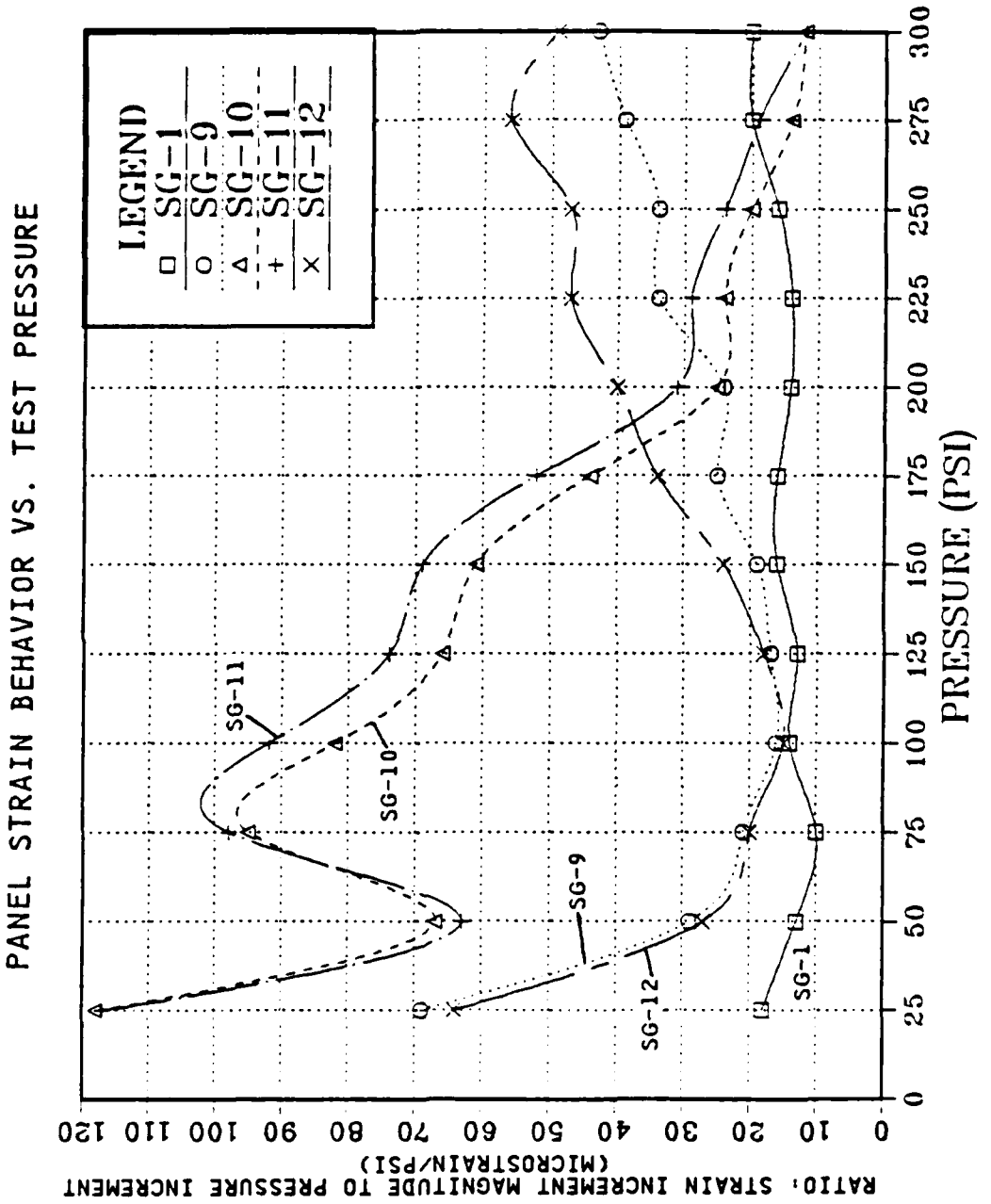

Figure 3.9 Plot of Wide Flanged "T" Static Test Ratio of Strain Increment to Pressure Increment vs. Test Pressure

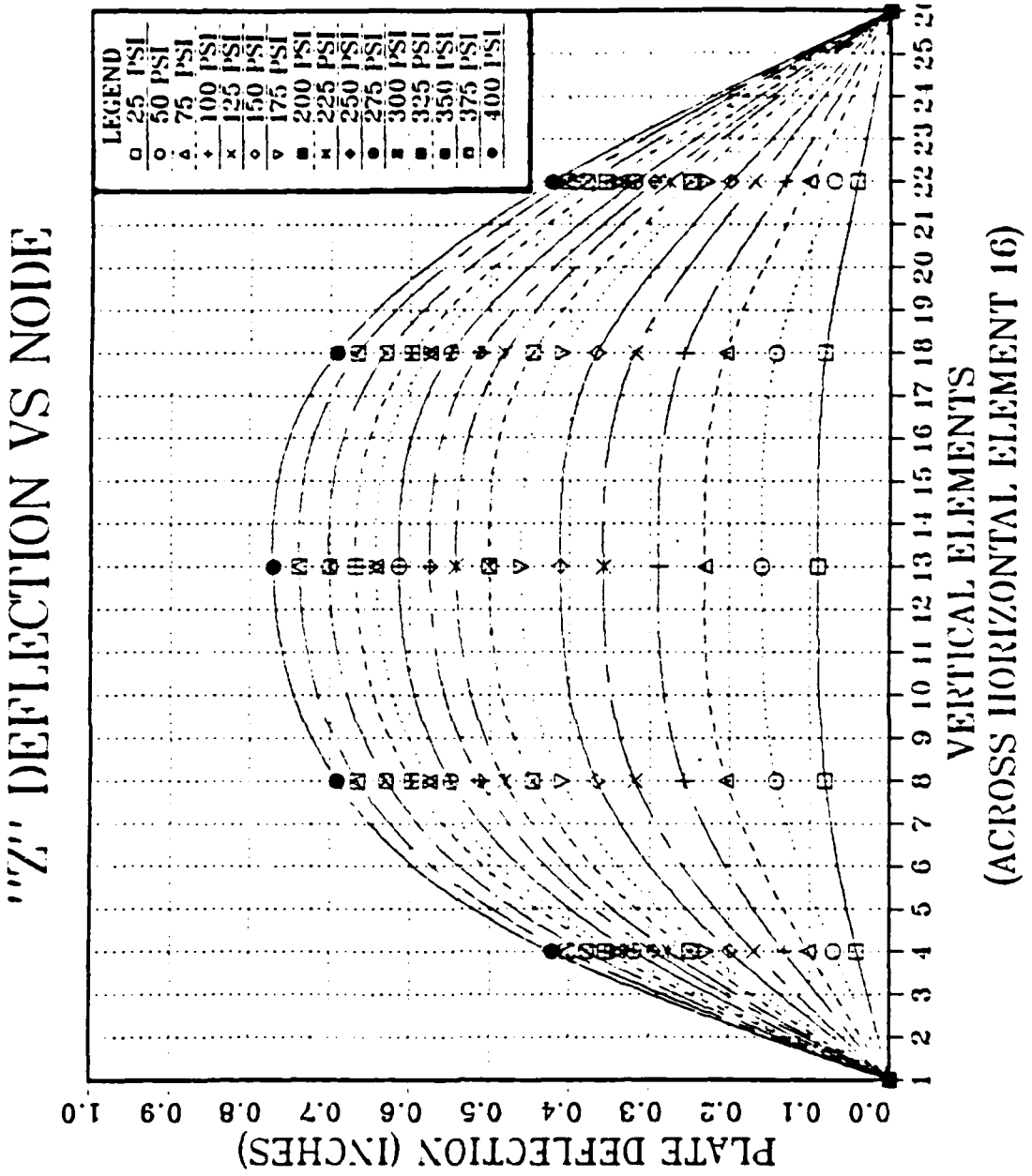

Figure 3.10 Plot of "Z" Stiffener Static Test Deflection Results

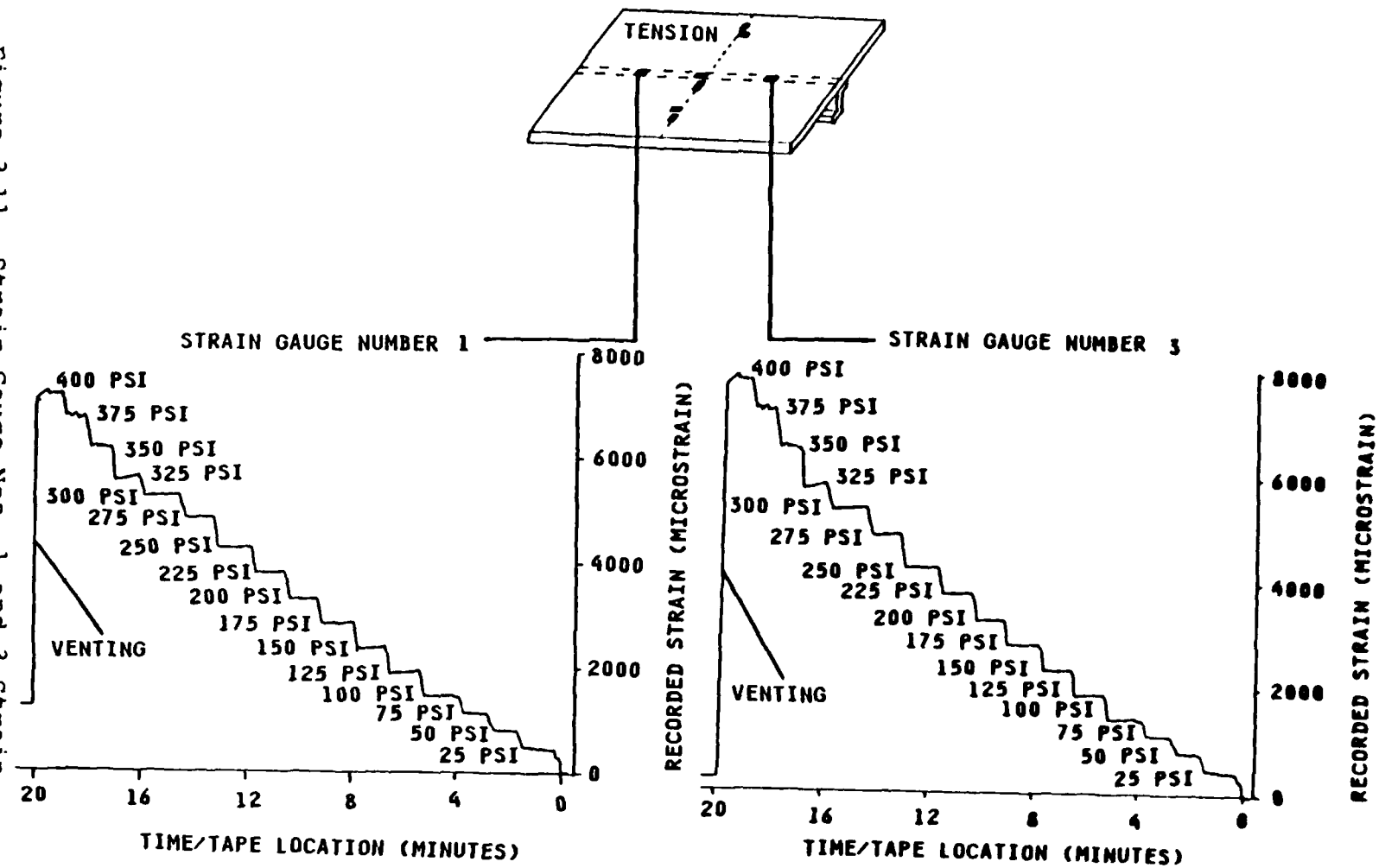

Figure 3.11 Strain Gauge Nos. 1 and 3 Strain Histories, "Z" Stiffener Hydrostatic Test

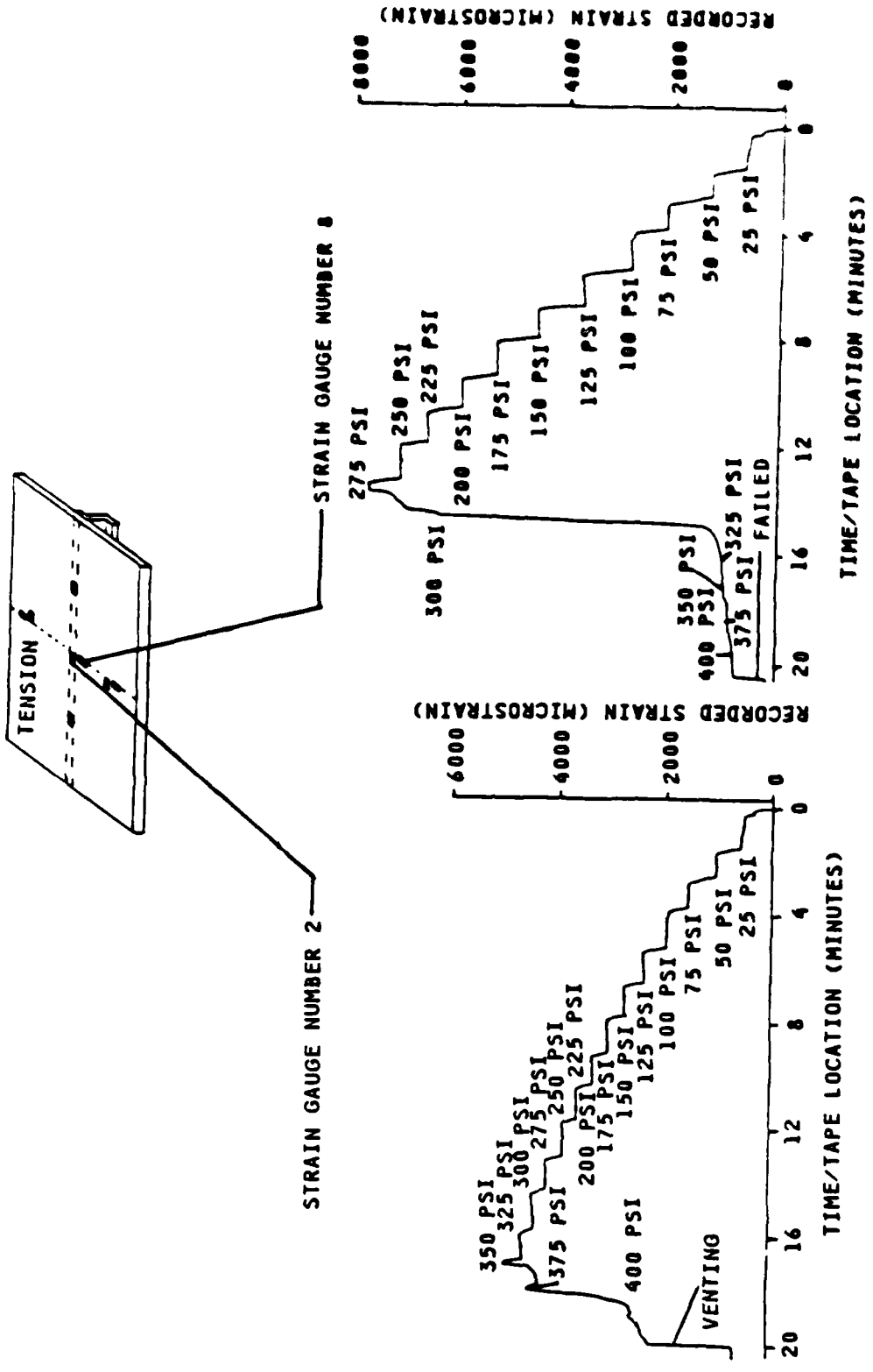

Figure 3.12 Strain Gauge Nos. 2 and 8 Strain Histories, "Z" Stiffener Hydrostatic Test

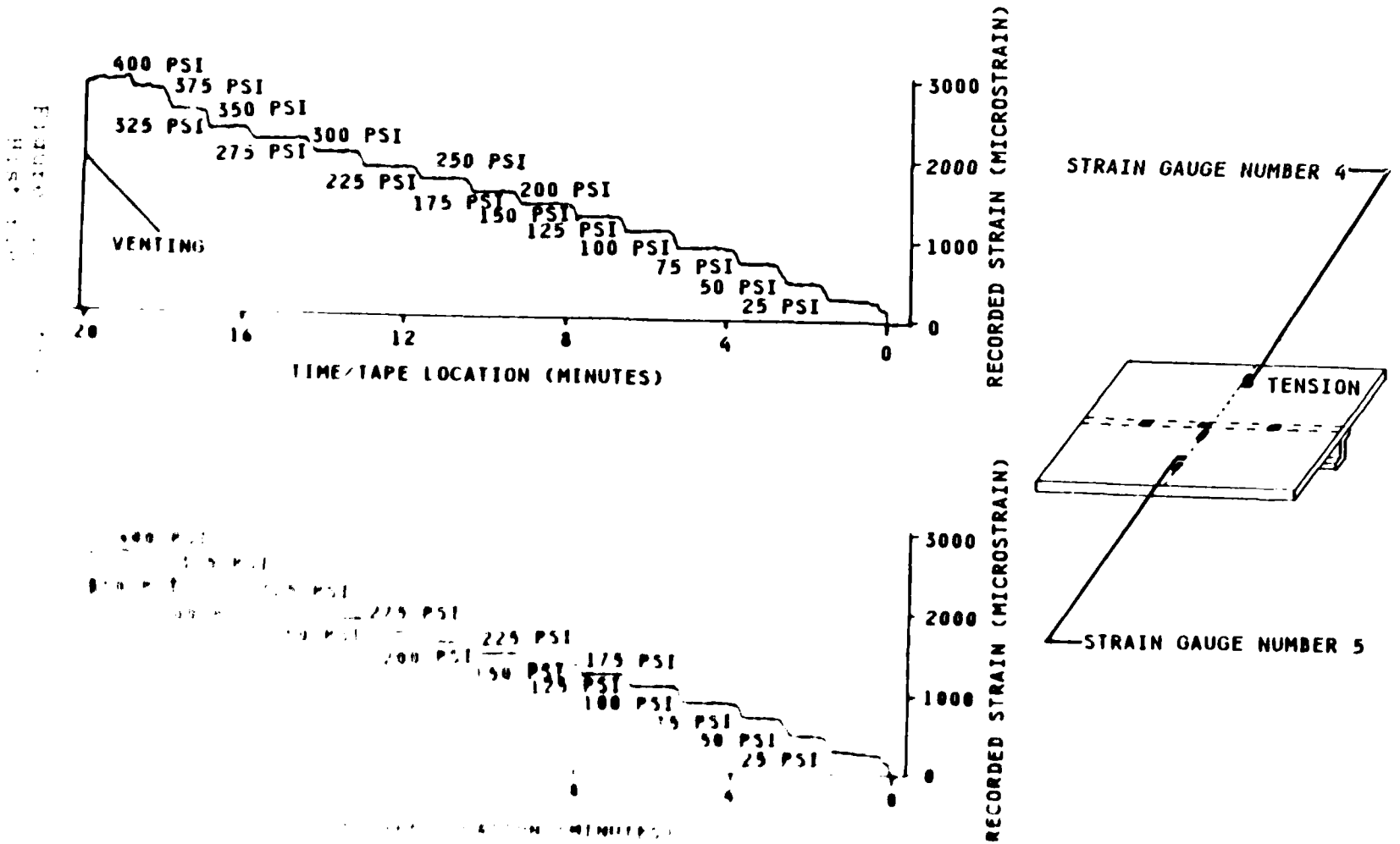
400 PSI
375 PSI
350 PSI
325 PSI
300 PSI
275 PSI
250 PSI
225 PSI
200 PSI
175 PSI
150 PSI
125 PSI
100 PSI
75 PSI
50 PSI
25 PSI
VENTING
20
16
12
8
4
0
TIME/TAPE LOCATION (MINUTES)
3000
2000
1000
0
RECORDED STRAIN (MICROSTRAIN)
STRAIN GAUGE NUMBER 4
TENSION
STRAIN GAUGE NUMBER 5

AD-A181 890 A COMPARISON OF TRIPPING BEHAVIOR OF WIDE AND NARROW 2/2
FLANGED 'T' AND 'Z' STIFFENED PANELS(U) NAVAL
POSTGRADUATE SCHOOL MONTEREY CA R B MILLER MAR 87
UNCLASSIFIED F/G 13/10 1 NL

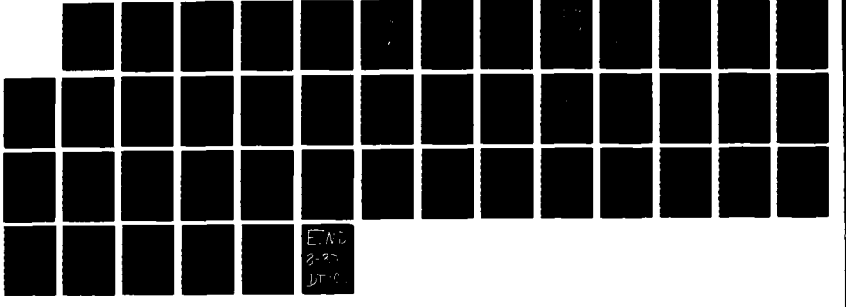

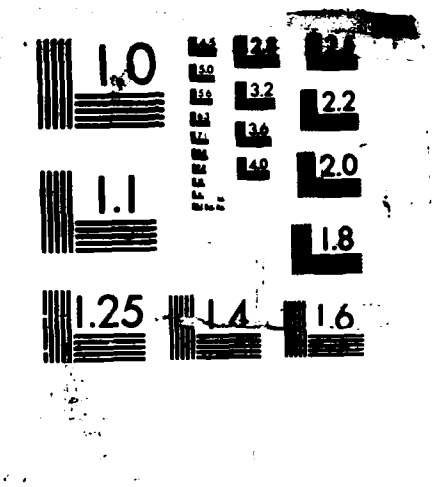

MICROCOPY RESOLUTION TEST CHART

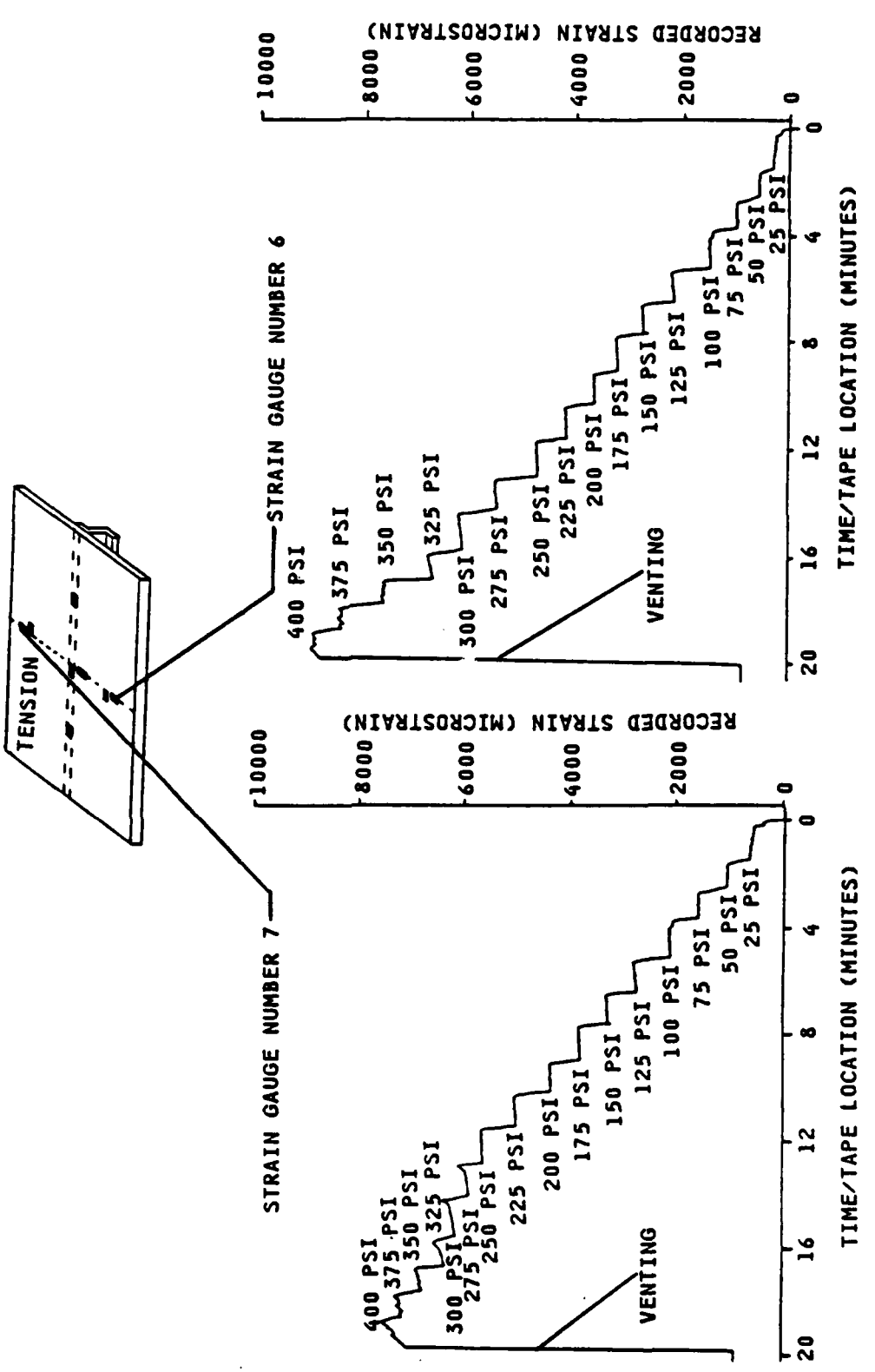

Figure 3.14 Strain Gauge Nos. 6 and 7 Strain Histories, "Z" Stiffener Hydrostatic Test

Figure 3.15 Strain Gauge Nos. 9 and 12 Strain Histories, "Z" Stiffener Hydrostatic Test

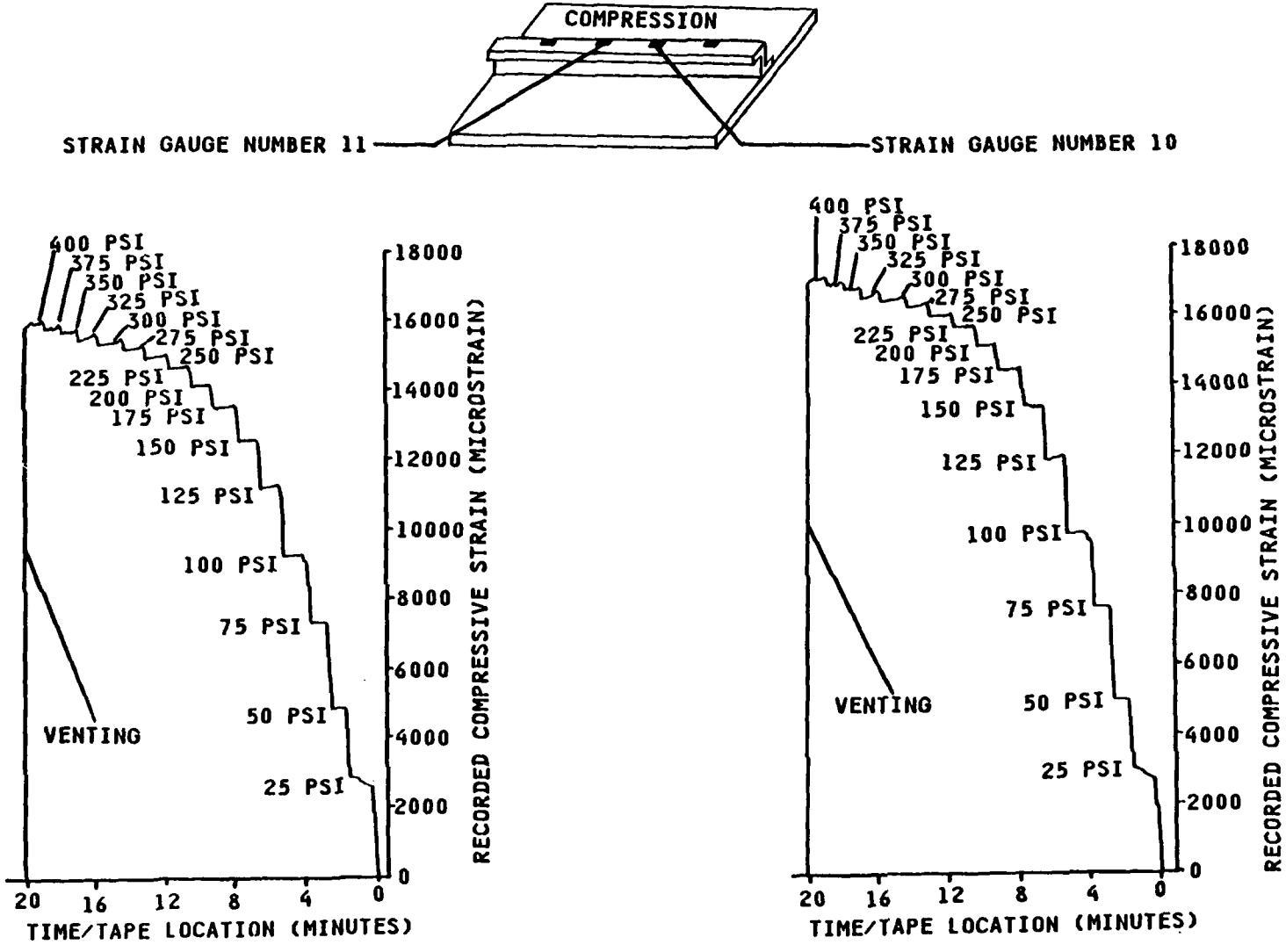

Figure 3.16 Strain Gauge Nos. 10 and 11 Strain Histories, "Z" Stiffener Hydrostatic Test

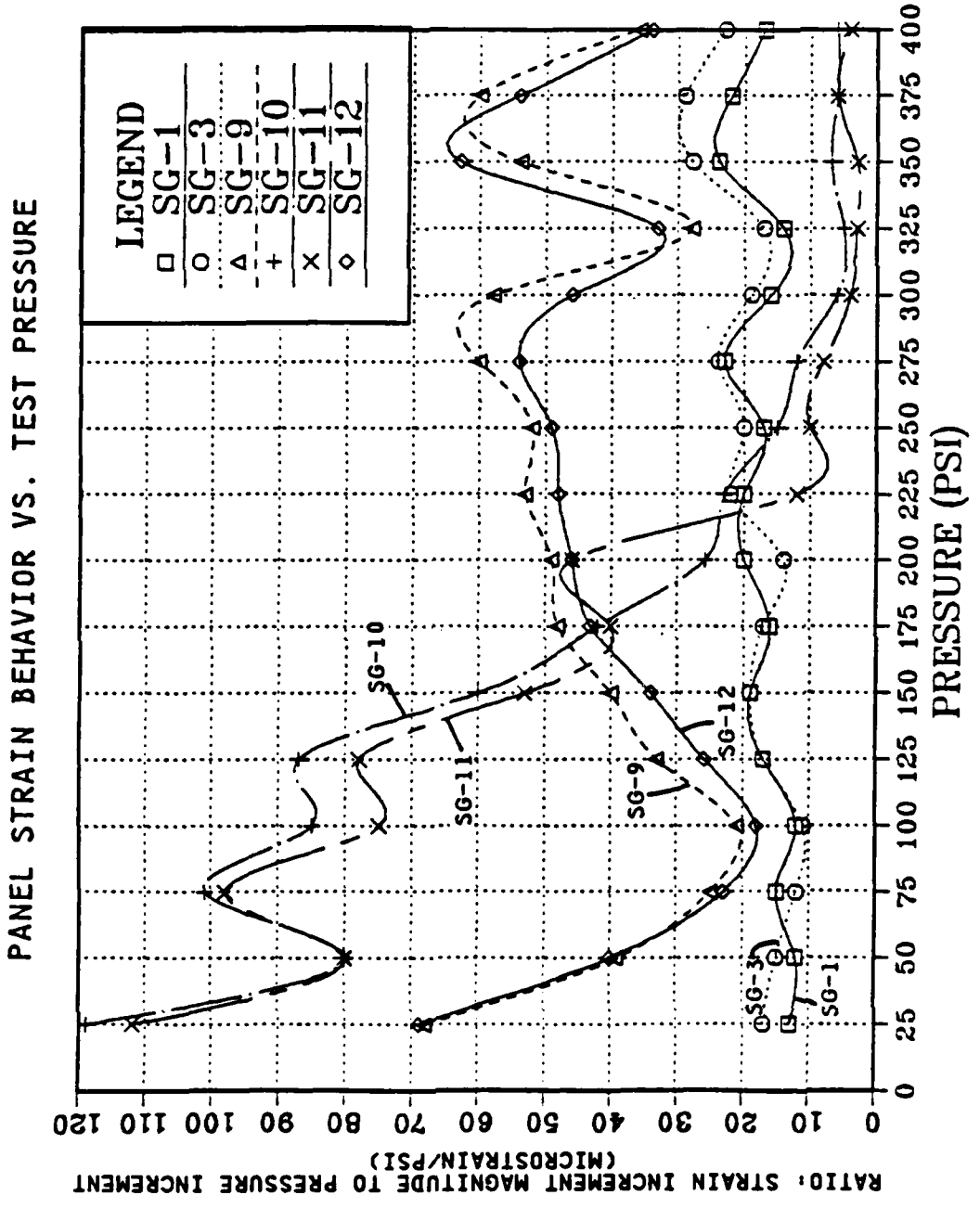

Figure 3.17 Plot of "Z" Stiffener Static Test Ratio of Strain Increment to Pressure Increment vs. Test Pressure

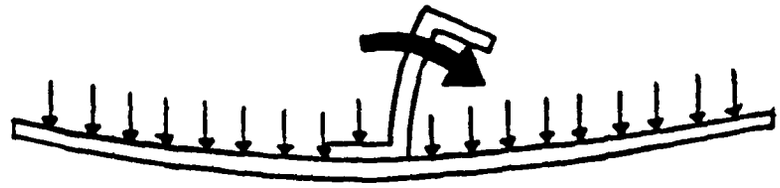

INITIAL TRIPPING BY WEB BUCKLING AND
THE UPPER FLANGE ROLLING OVER.

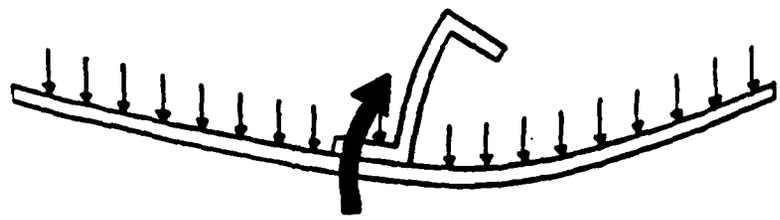

CONTINUATION OF TRIPPING BY A ROTATION OF THE STIFFENER
AND A PORTION OF THE PLATE ABOUT THE BASE OF THE STIFFENER.

Figure 3.18 Schematic Diagram of the "Z"
Stiffener Tripping Mechanism

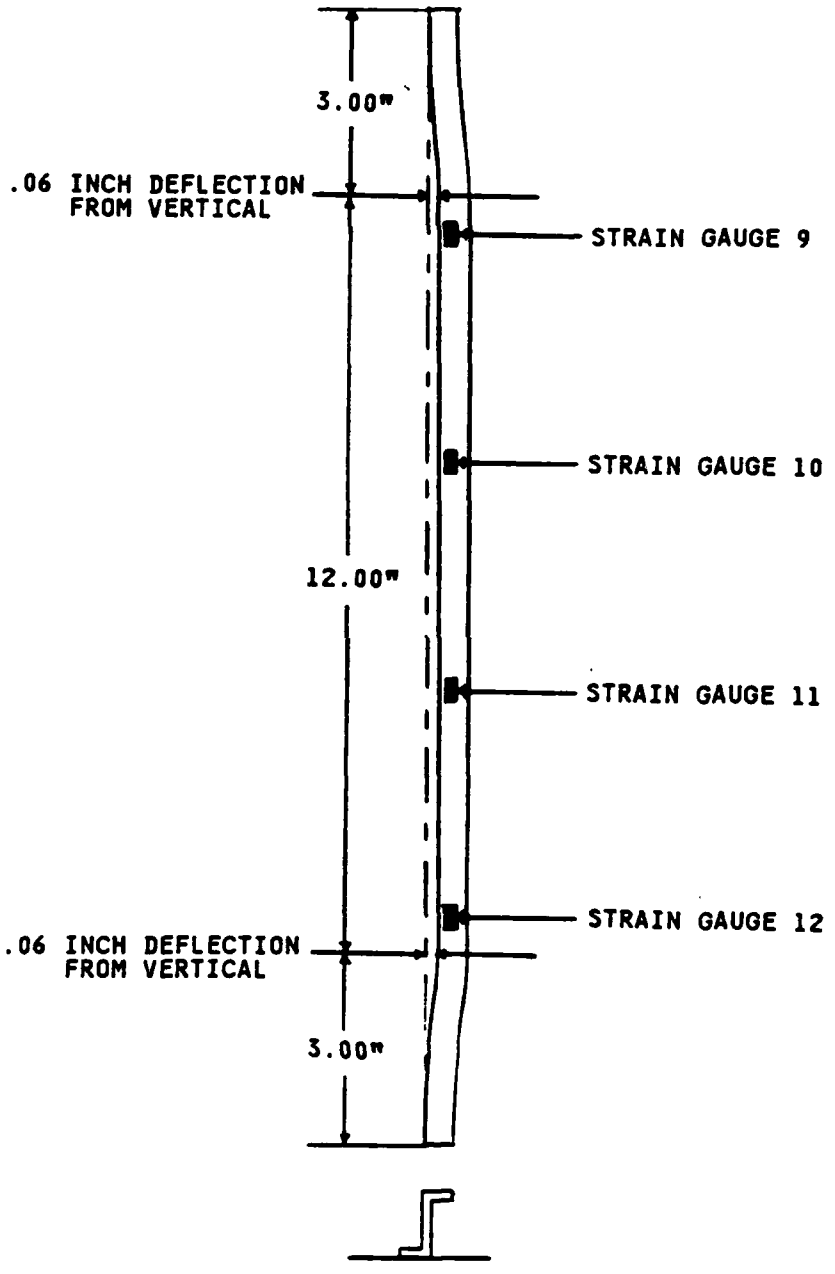

Figure 3.19 Schematic of the Resultant Plastic Tripping of the "Z" Stiffener

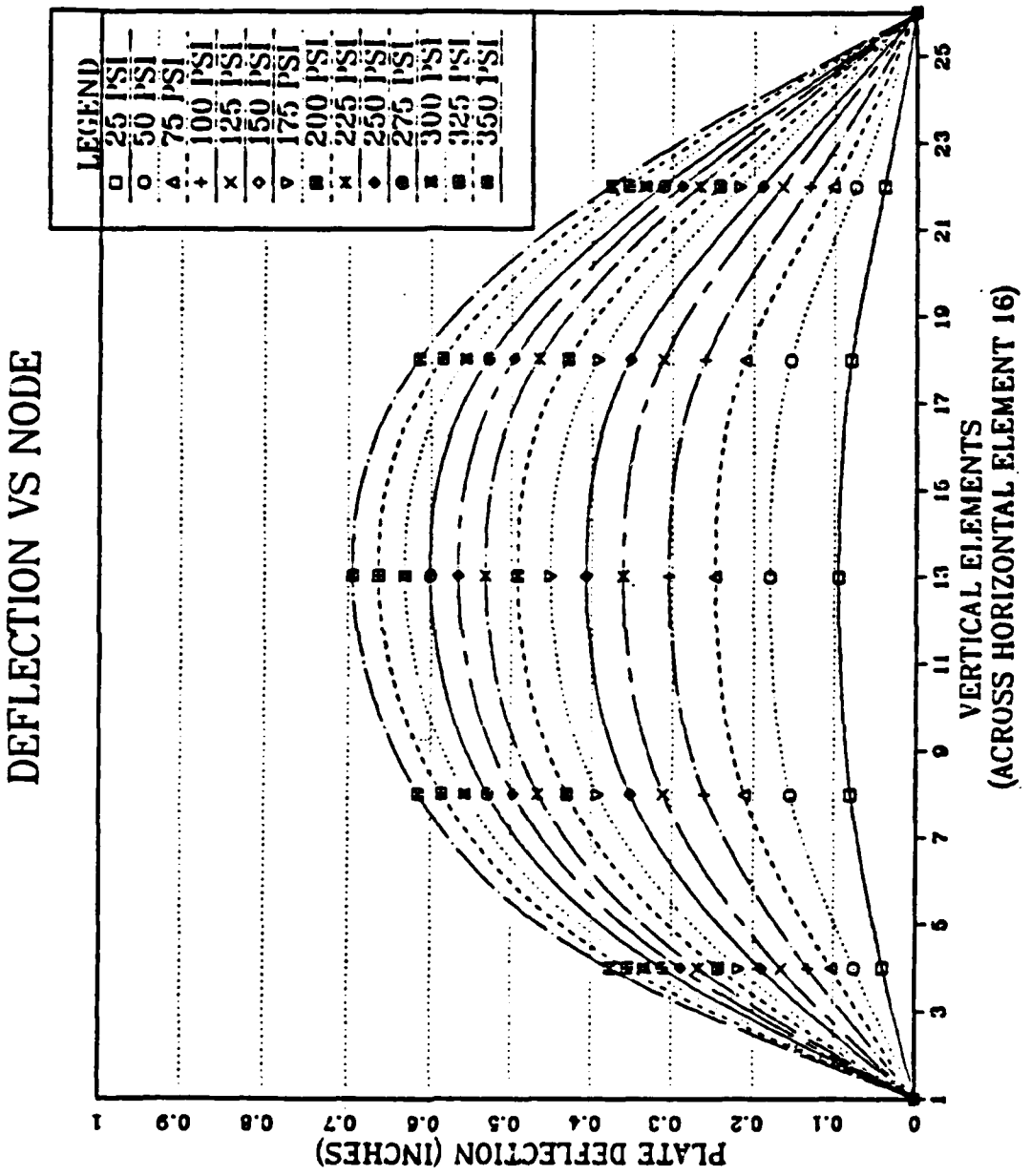

Figure 3.20 Plot of Narrow Flanged "T" Static Test Deflection Results

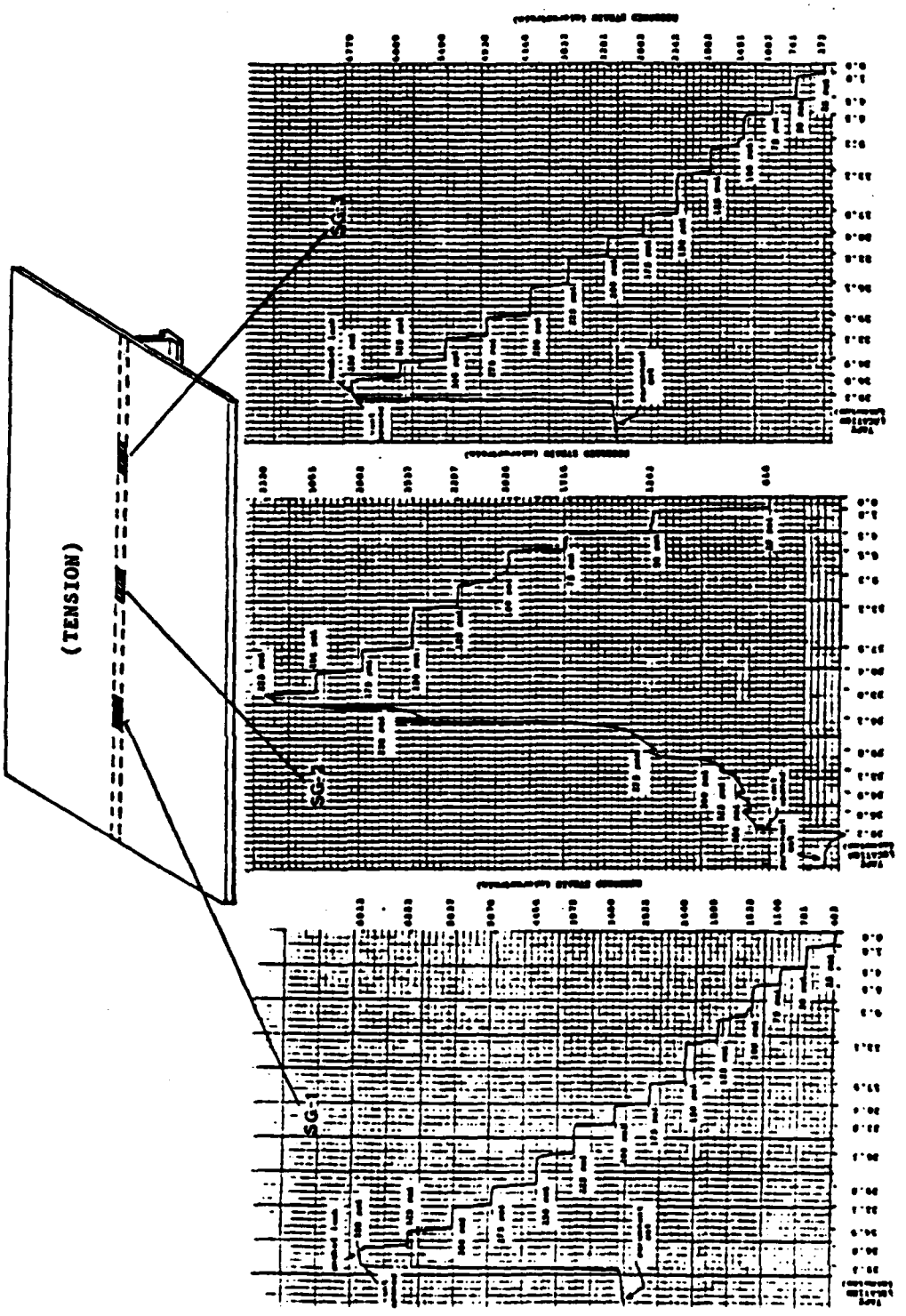

Figure 3.21 Strain Gauge Nos. 1, 2 and 3 Strain Histories, Narrow Flanged "T" Hydrostatic Test

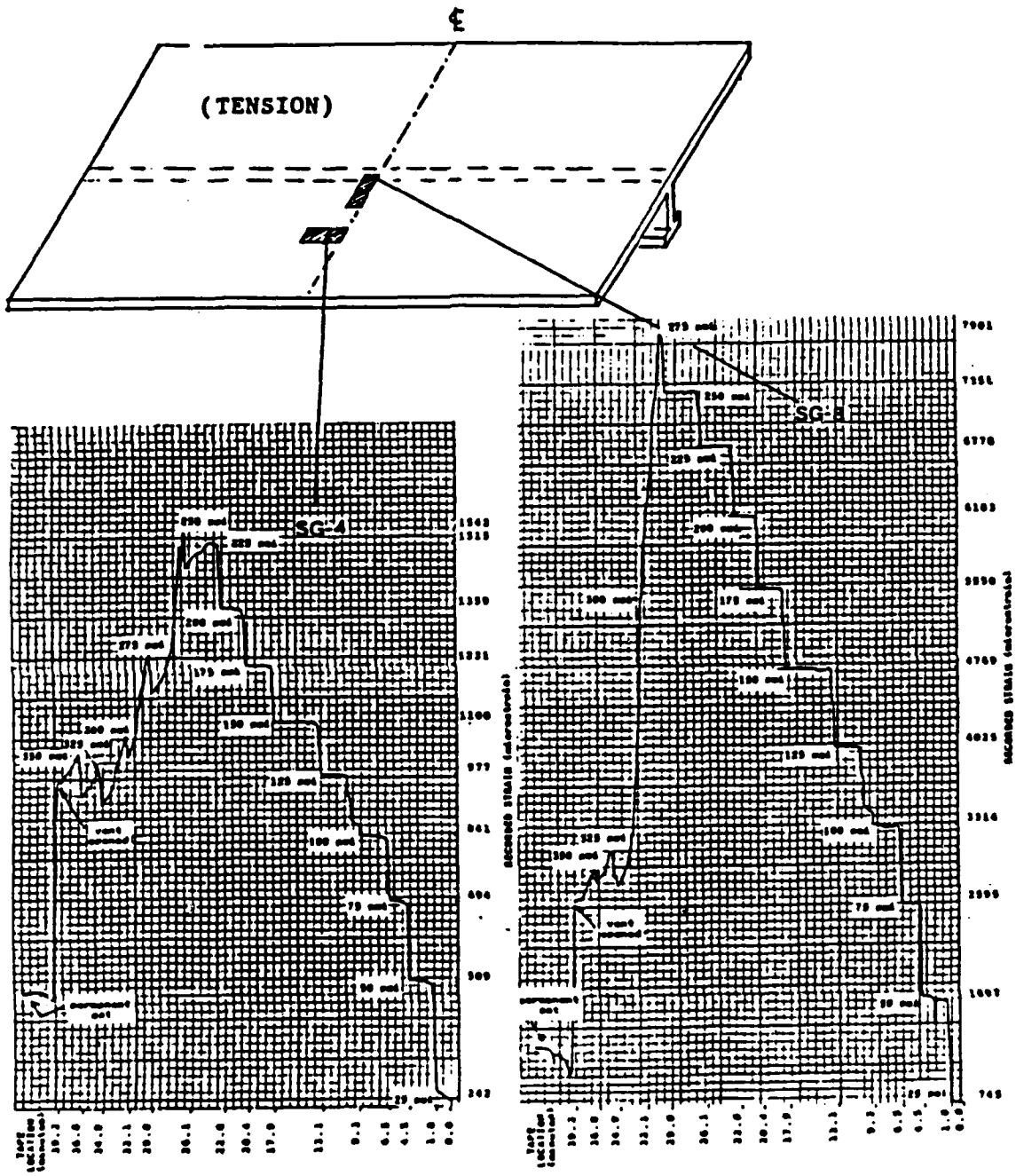

Figure 3.22 Strain Gauge Nos. 4 and 8 Strain Histories, Narrow Flanged "T" Hydrostatic Test

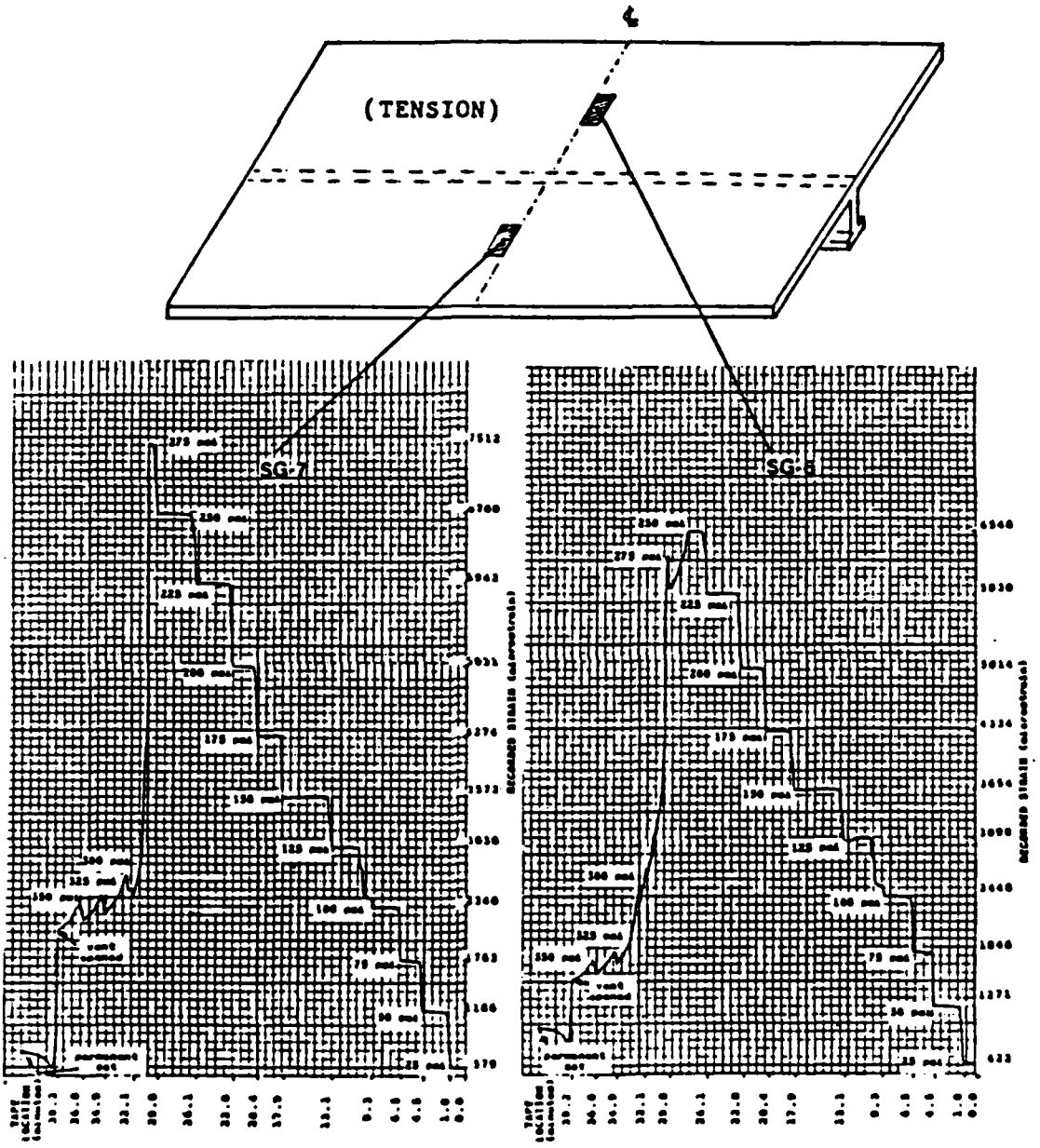

Figure 3.23 Strain Gauge Nos. 6 and 7 Strain Histories, Narrow Flanged "T" Hydrostatic Test

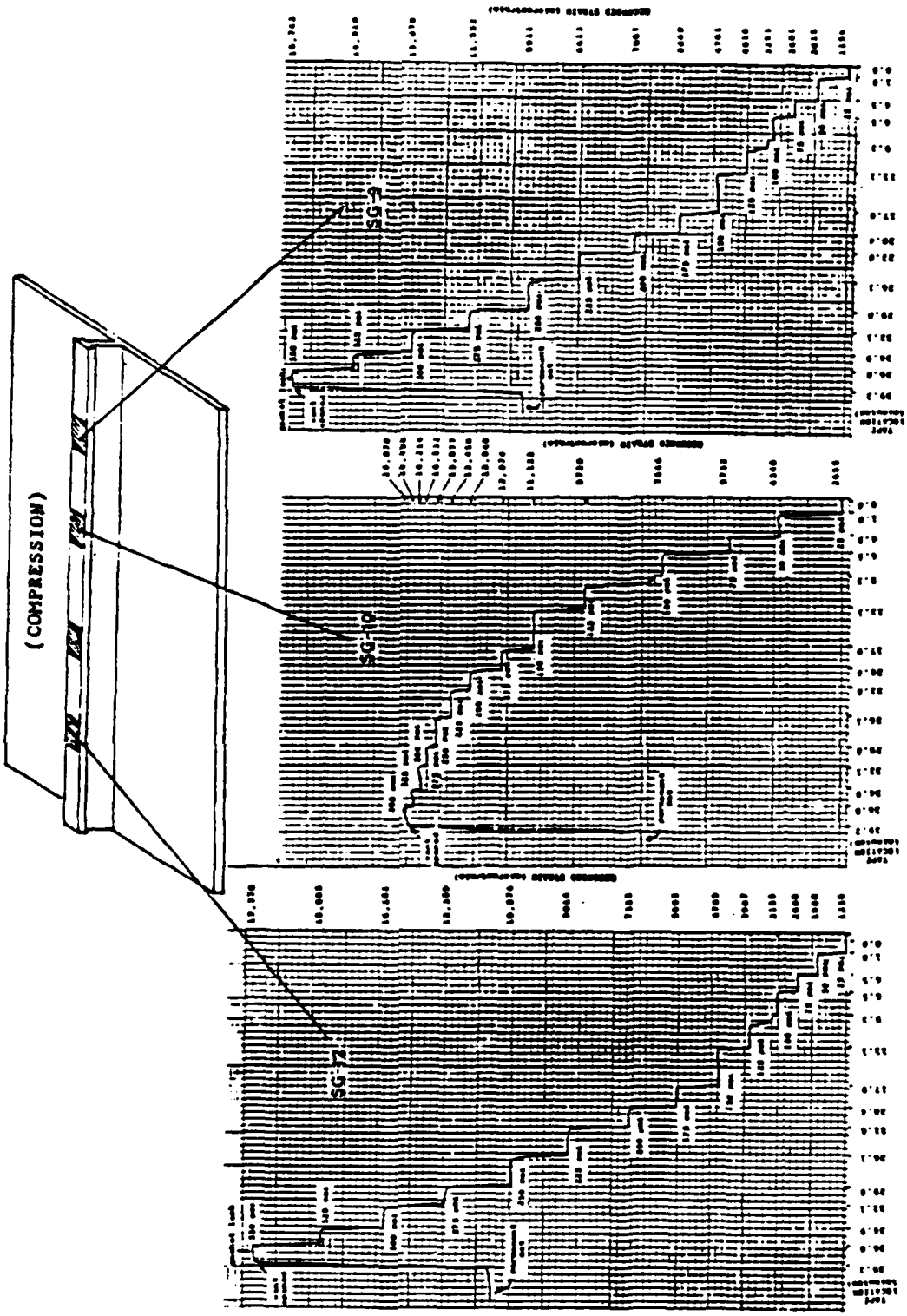

Figure 3.24 Strain Gauge Nos. 9, 10 and 12 Strain Histories, Narrow Flanged "T" Hydrostatic Test

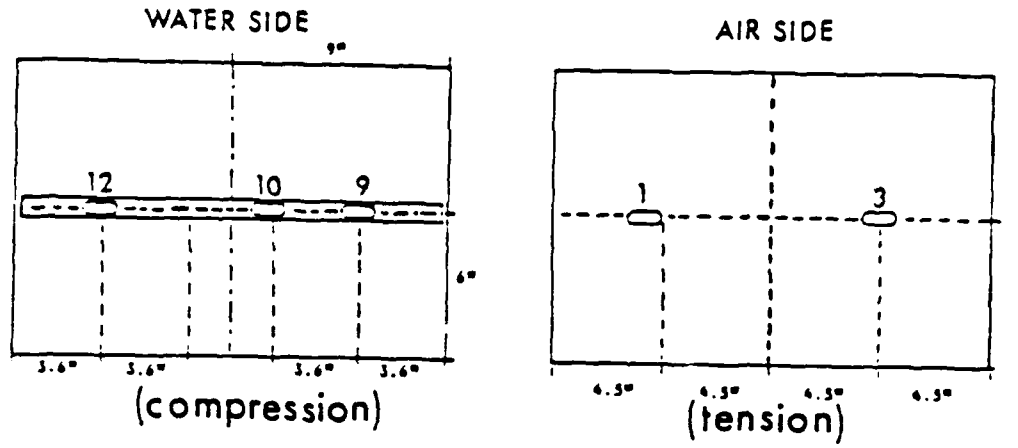

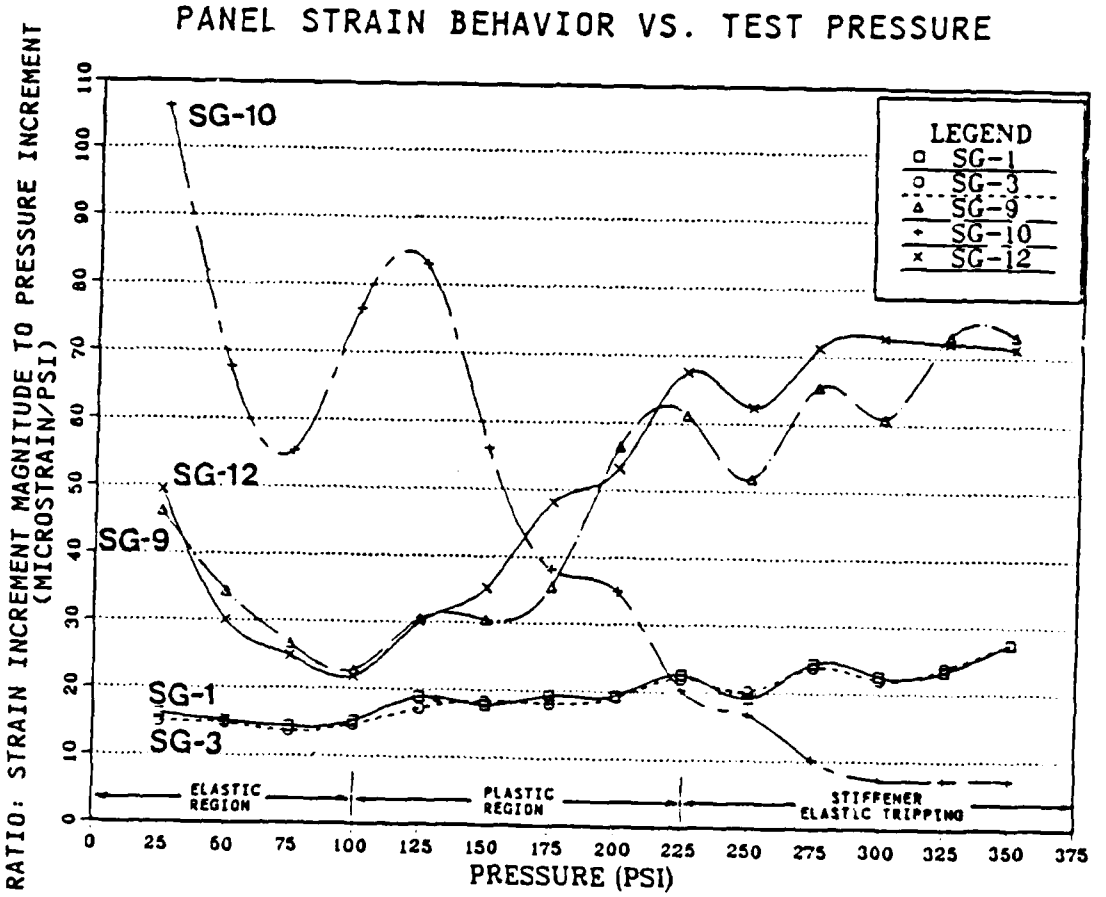

Figure 3.25 Plot of Narrow Flanged "T" Static Test Ratio of Strain Increment to Pressure Increment vs. Test Pressure

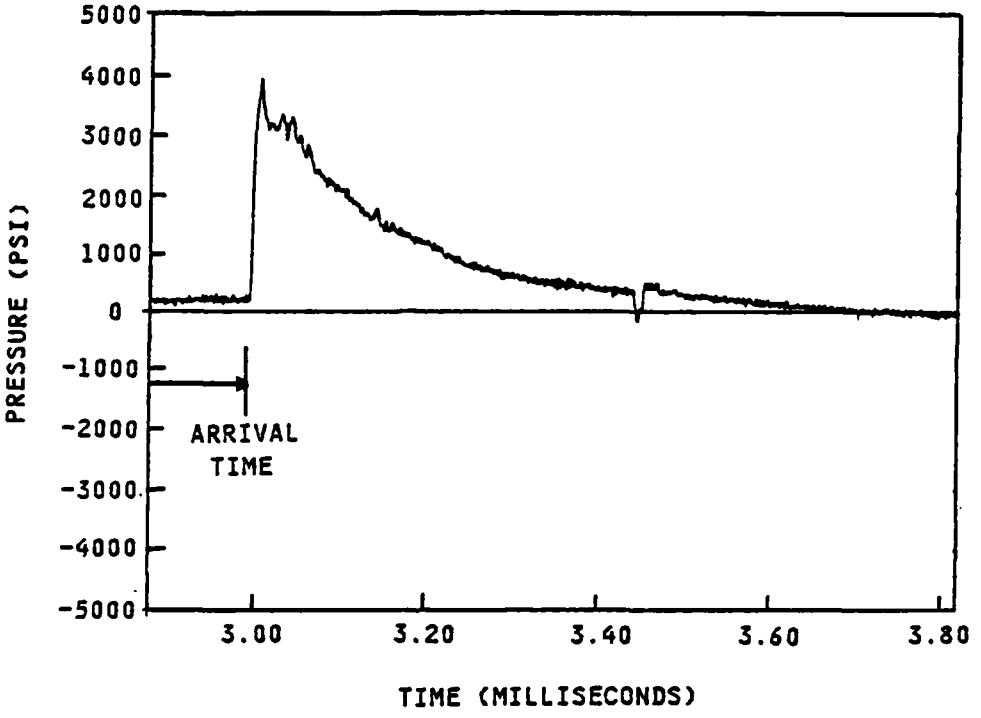

Figure 3.26 Wide Flanged "T" Dynamic Test
Incident Pressure Pulse

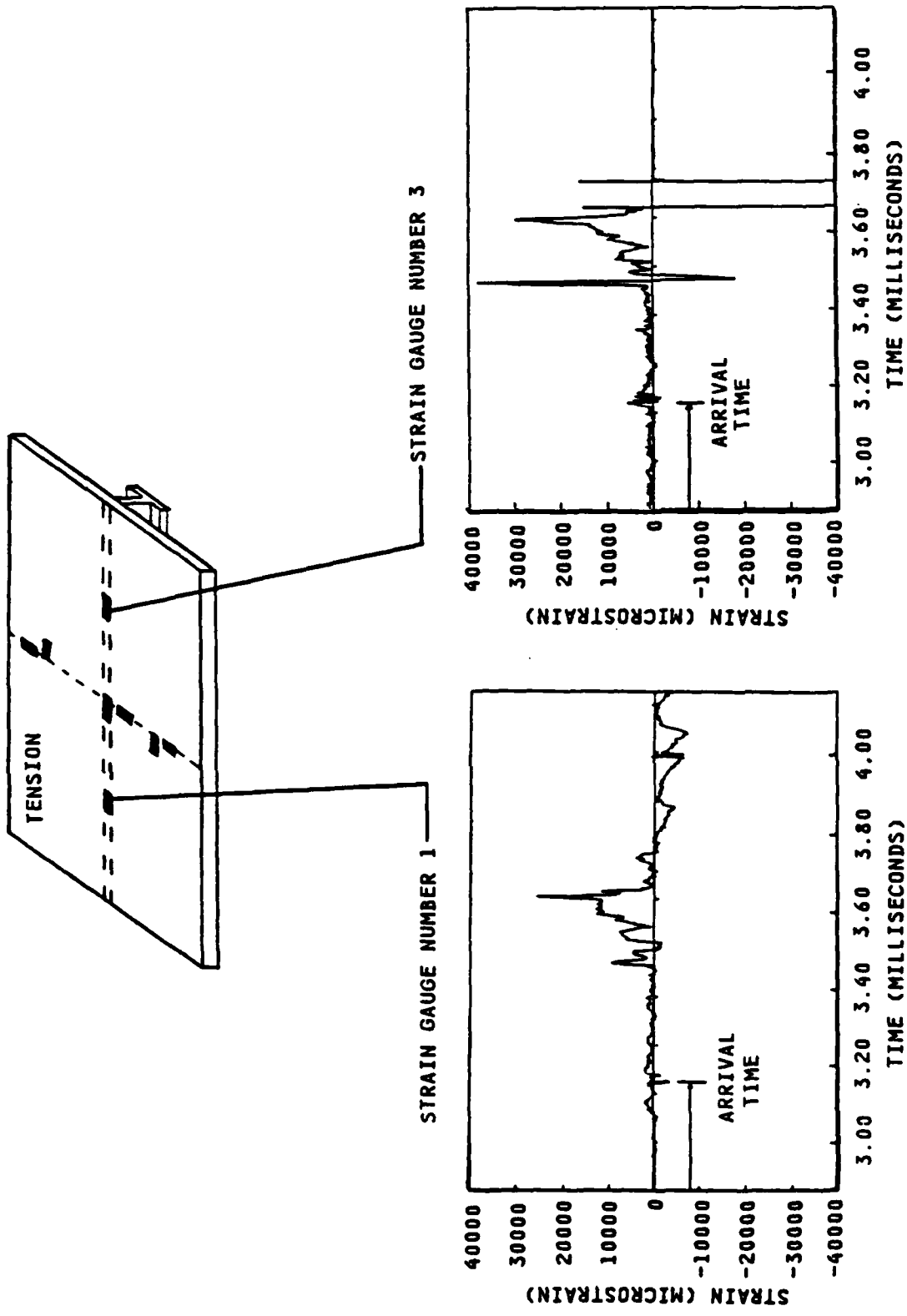

Figure 3.27 Strain Gauge Nos. 1 and 3 Strain Histories, Wide Flanged "T" Dynamic Test

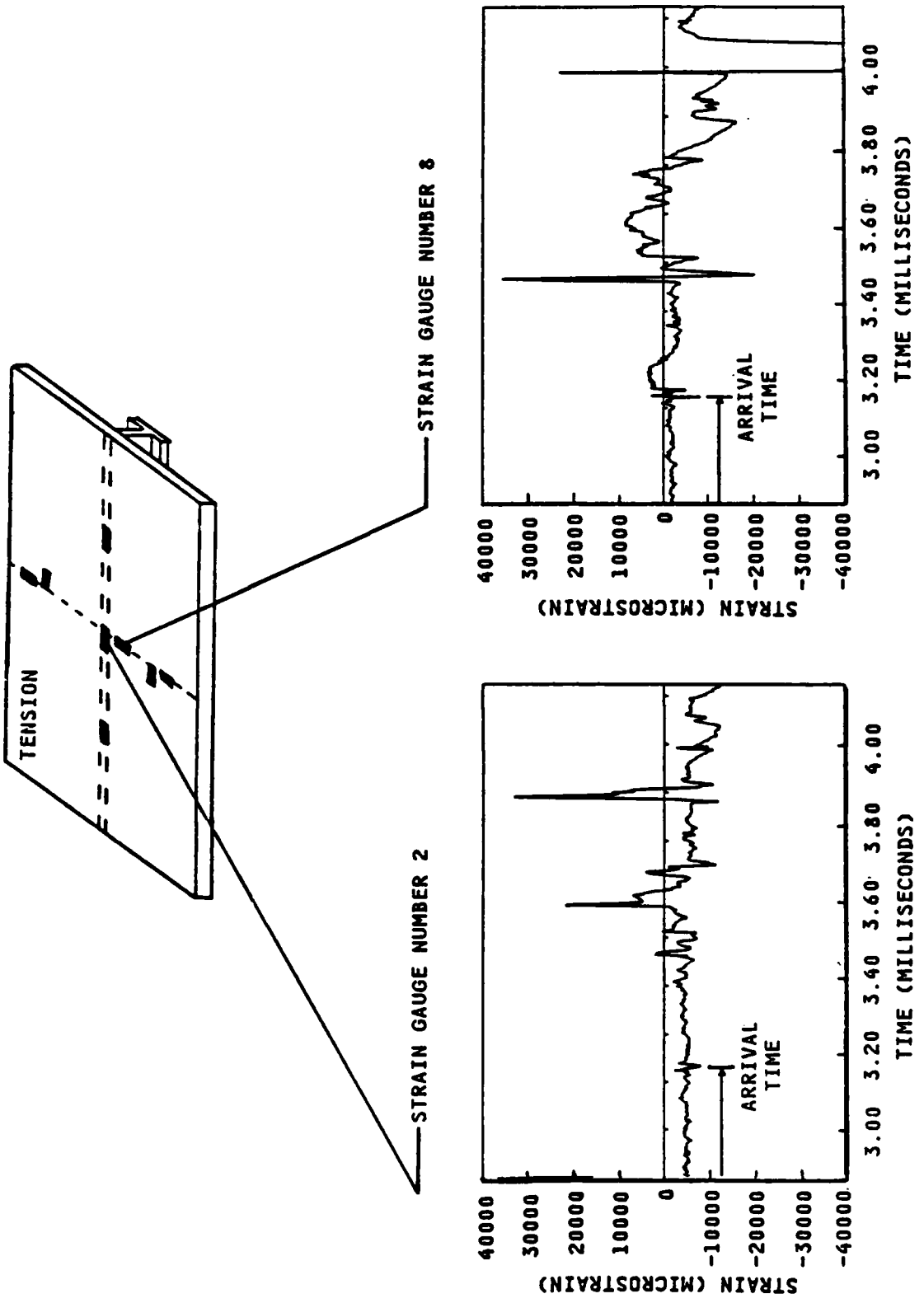

Figure 3.28 Strain Gauge Nos. 2 and 8 Strain Histories, Wide Flanged "T" Dynamic Test

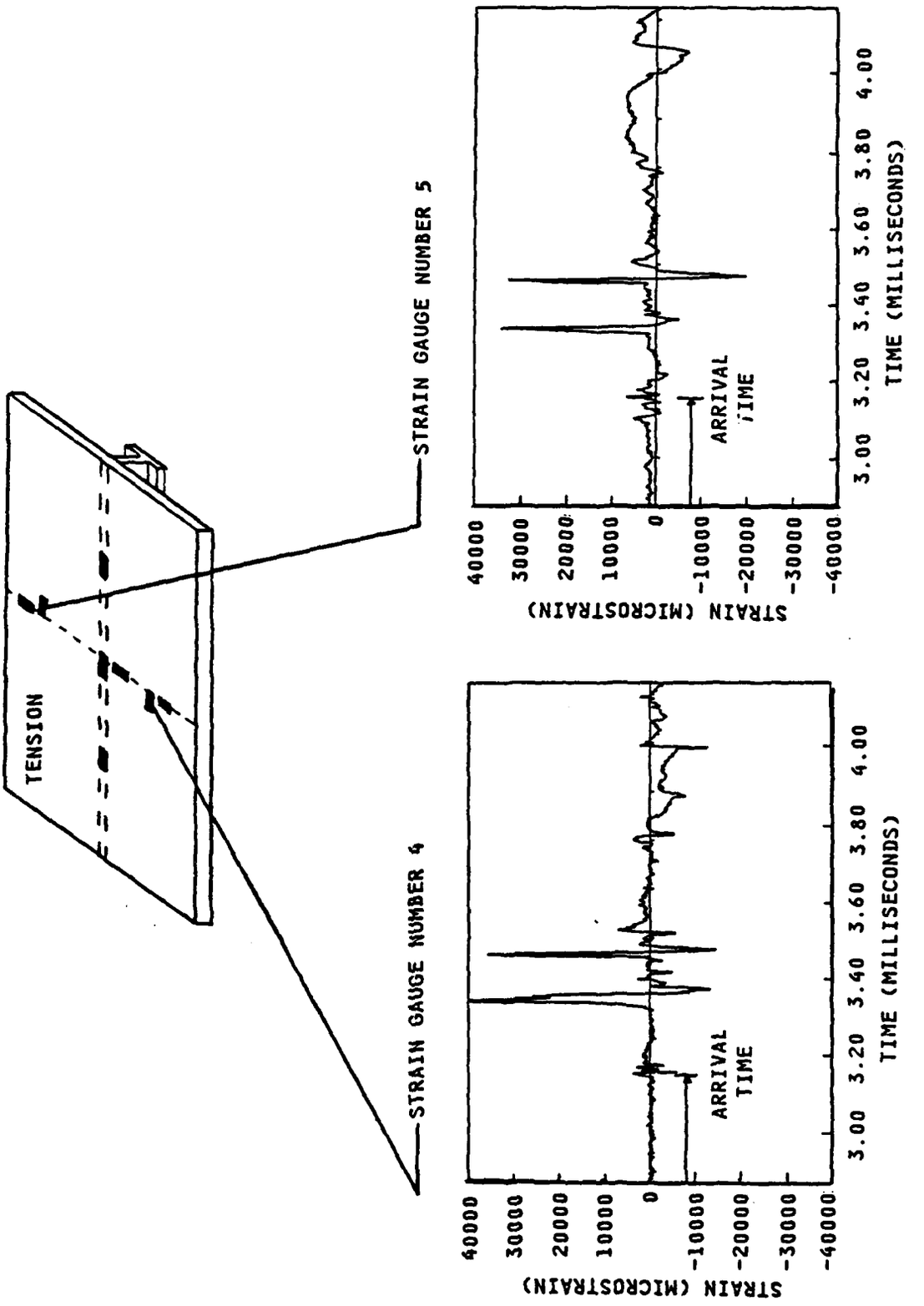

Figure 3.29 Strain Gauge Nos. 4 and 5 Strain Histories, Wide Flanged "T" Dynamic Test

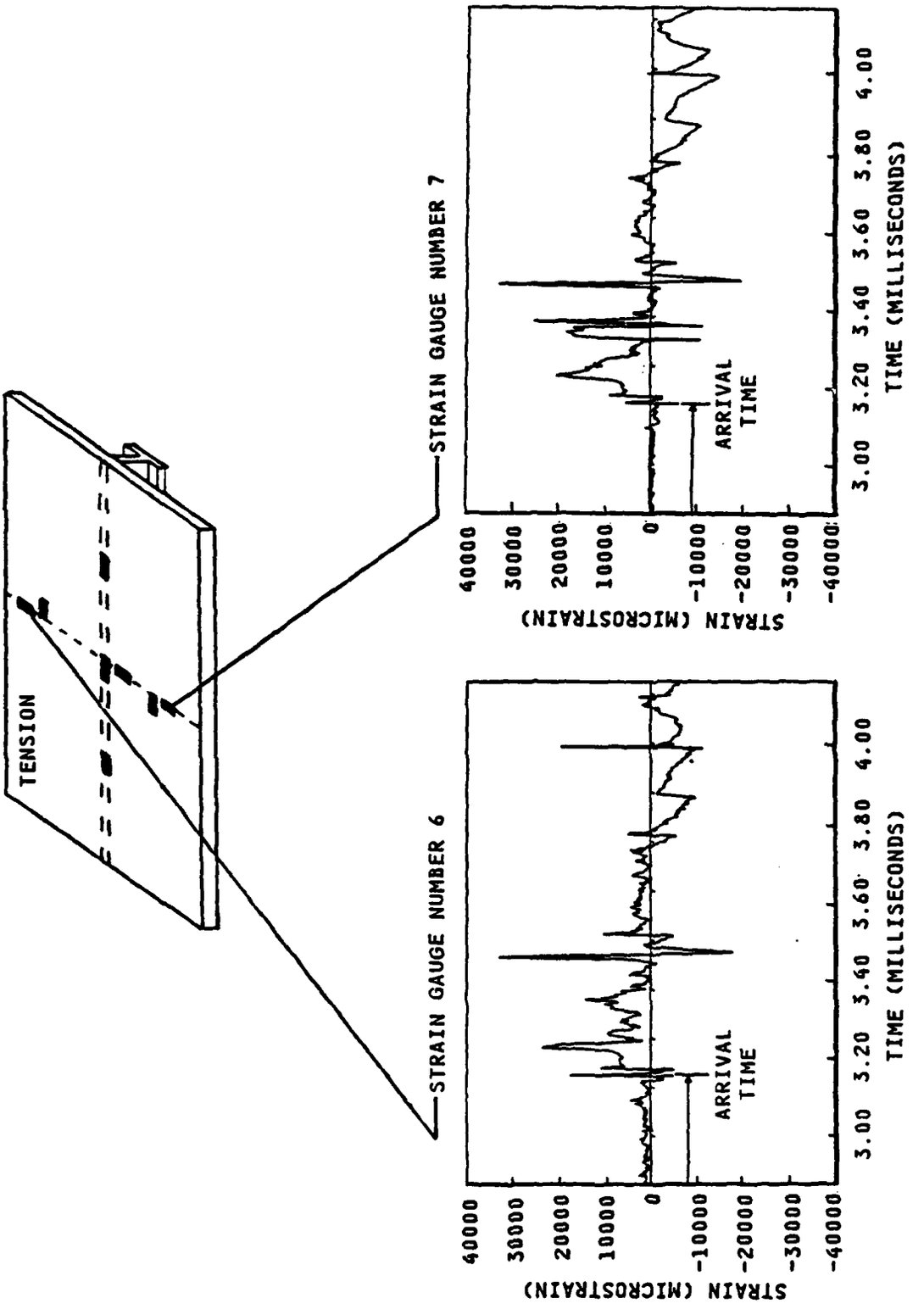

Figure 3.30 Strain Gauge Nos. 6 and 7 Strain Histories, Wide Flanged "T" Dynamic Test

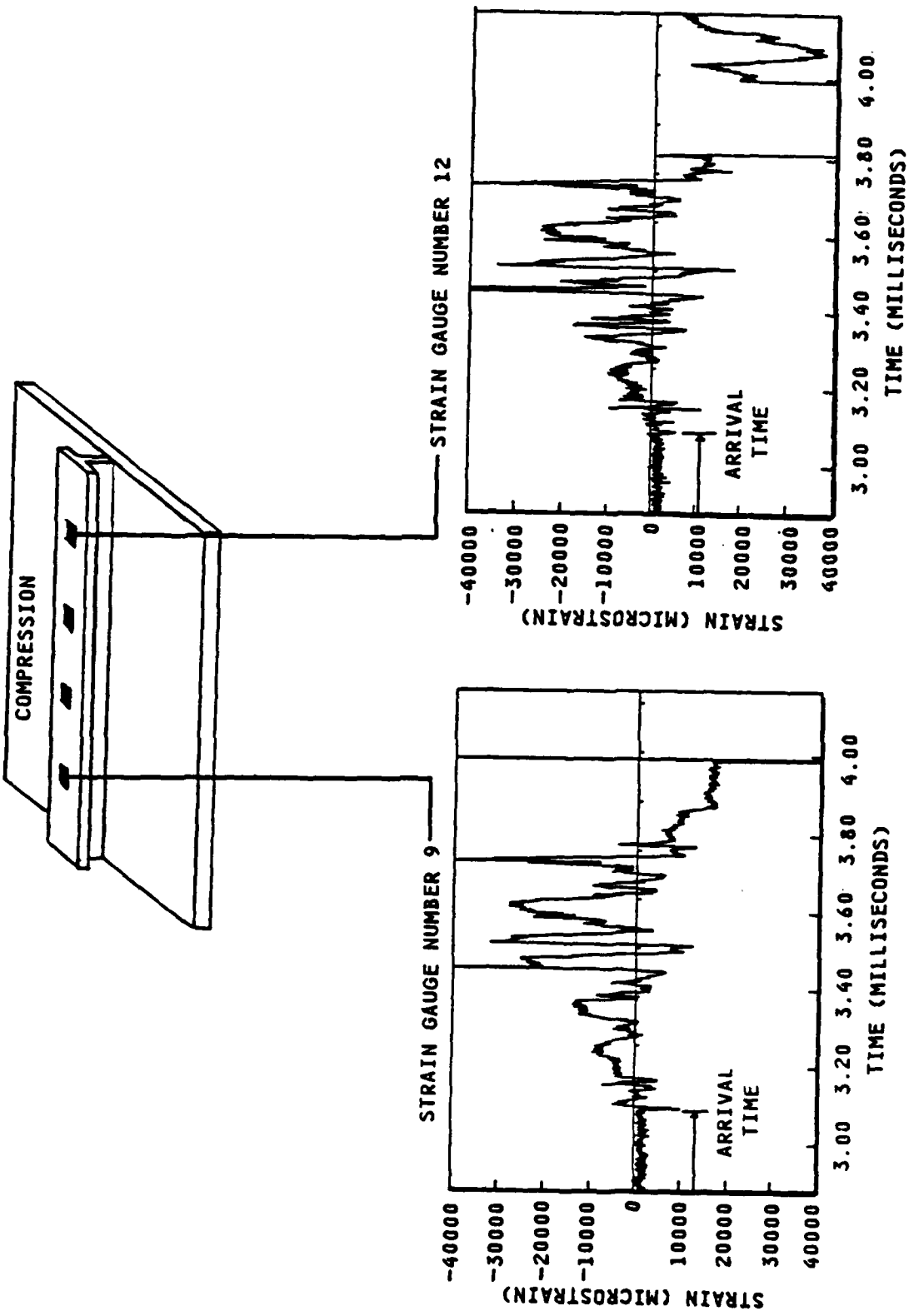

Figure 3.31 Strain Gauge Nos. 9 and 12 Strain Histories, Wide Flanged "T" Dynamic Test

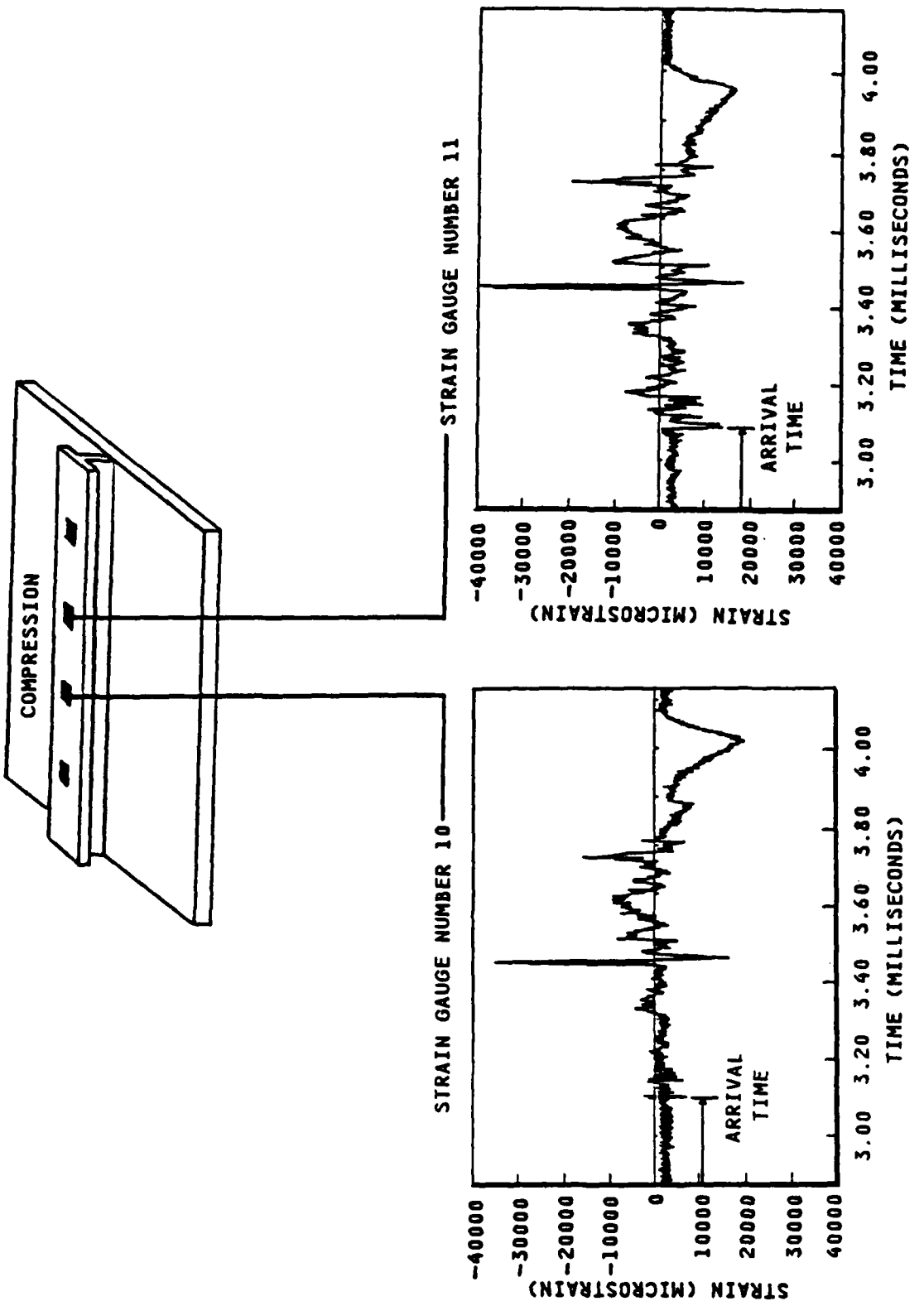

Figure 3.32 Strain Gauge Nos. 10 and 11 Strain Histories, Wide Flanged "T" Dynamic Test

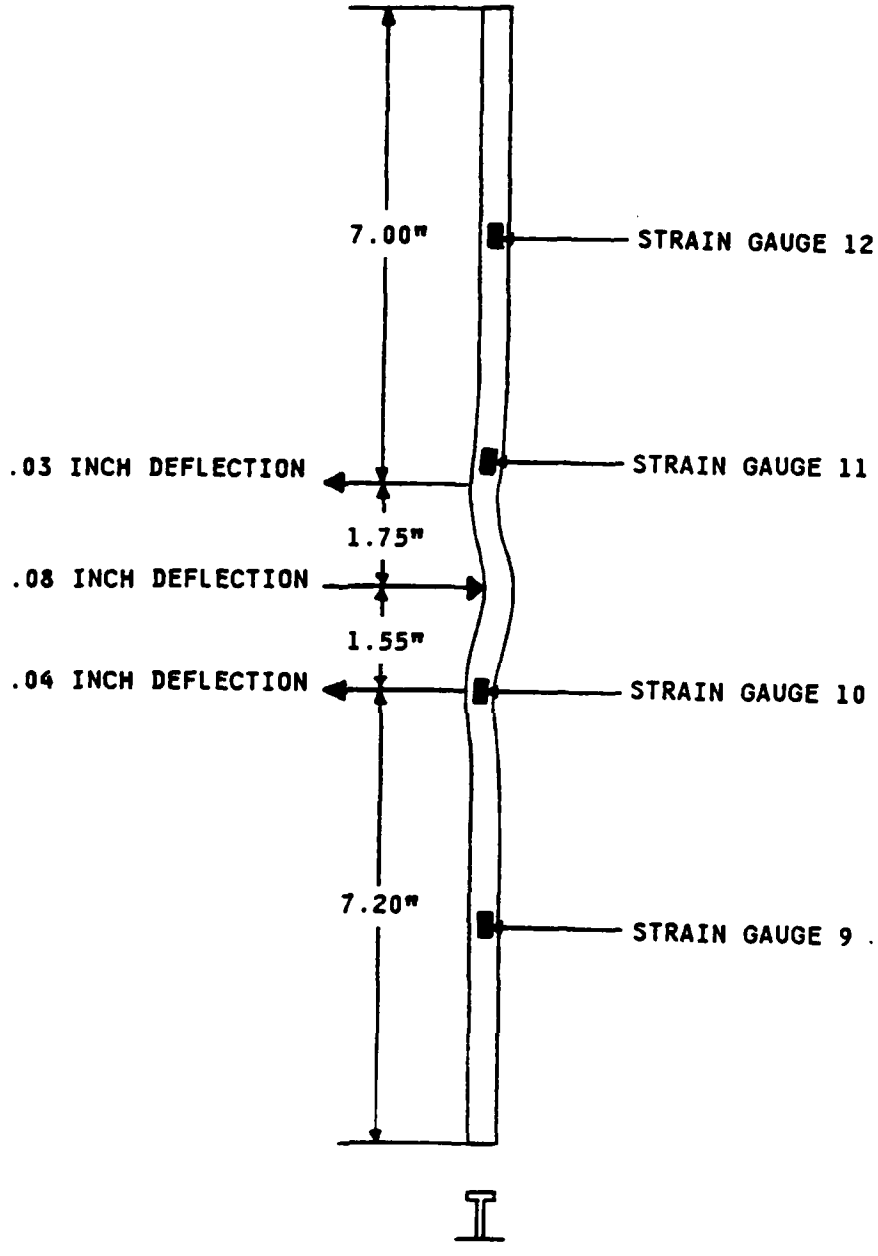

Figure 3.33 Schematic of the Wide Flanged "T" Stiffener Tripping Resultant from Dynamic Testing

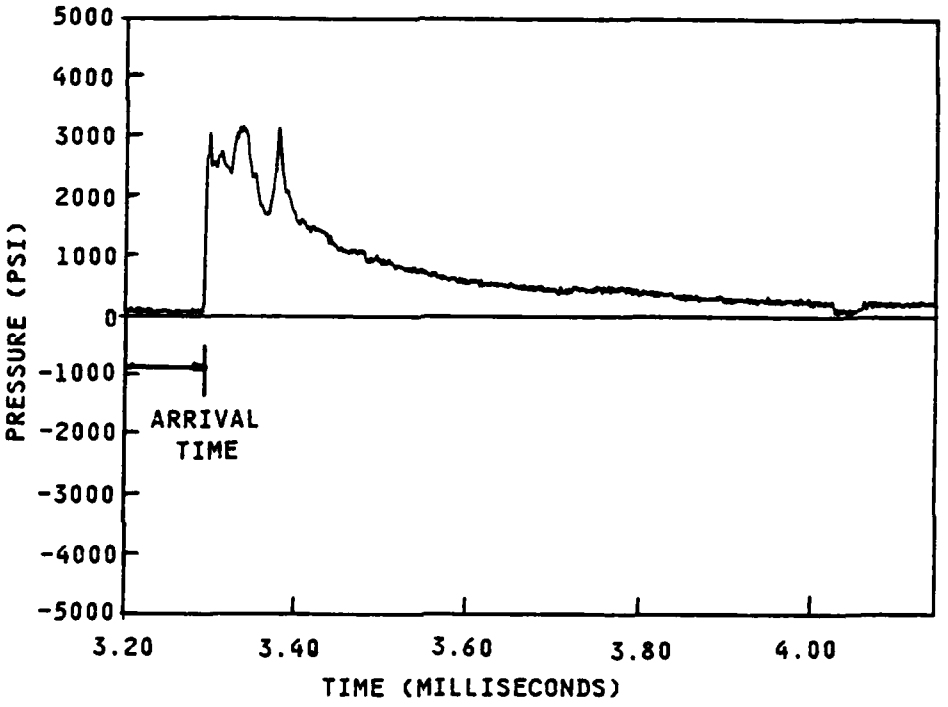

Figure 3.34 "Z" Stiffener Dynamic Test
Incident Pressure Pulse

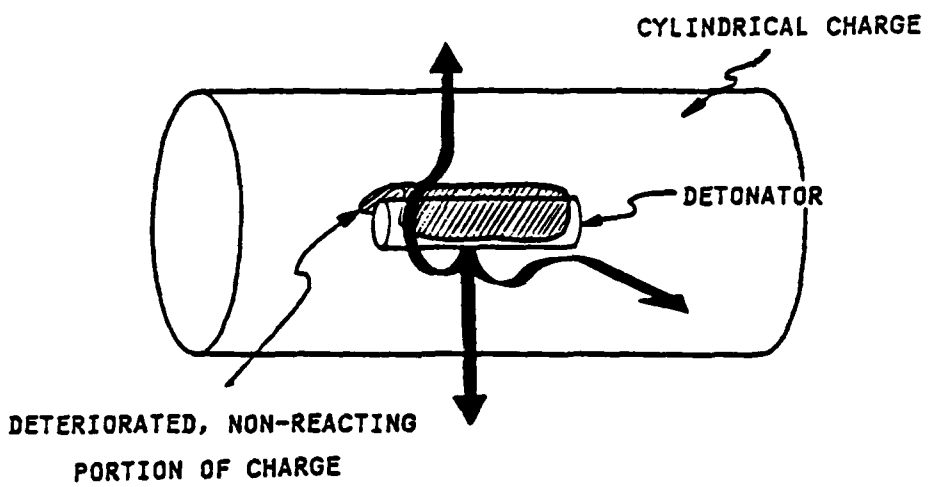

Figure 3.35 Explosive Charge Detonation Reaction Propagation

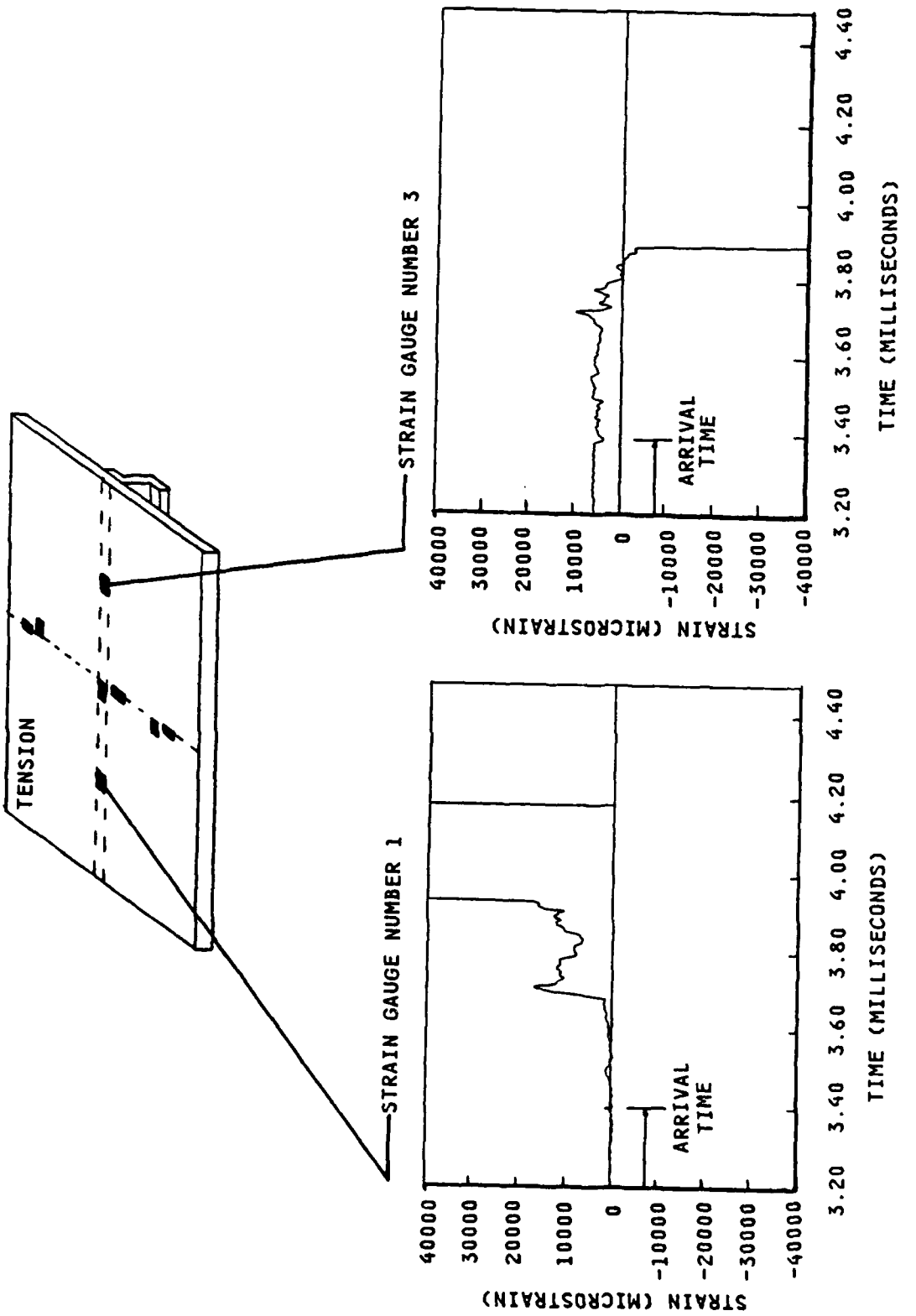

Figure 3.36 Strain Gauge Nos. 1 and 3 Strain Histories, "Z" Stiffener Dynamic Test

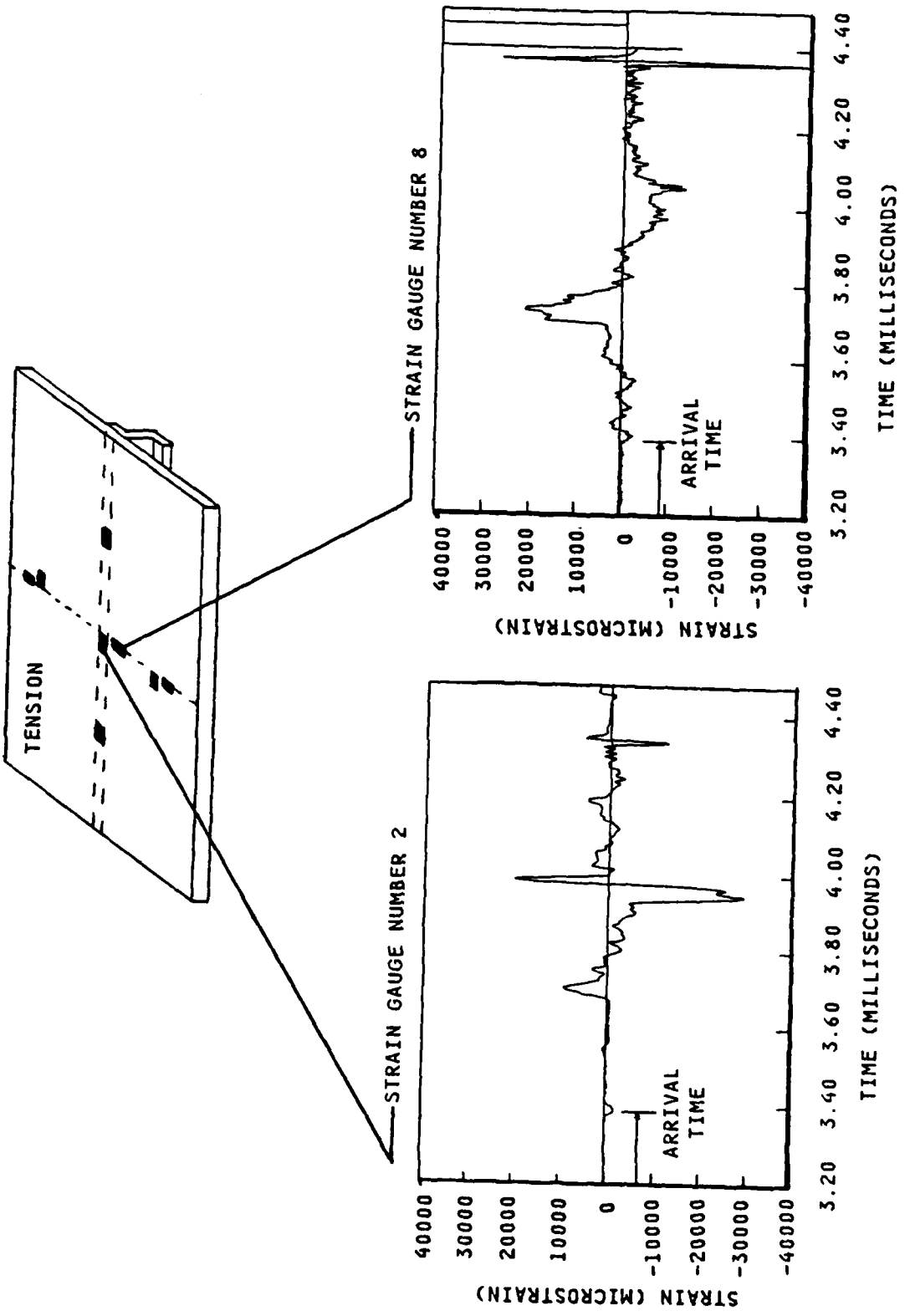

Figure 3.37 Strain Gauge Nos. 2 and 8 Strain Histories, "Z" Stiffener Dynamic Test

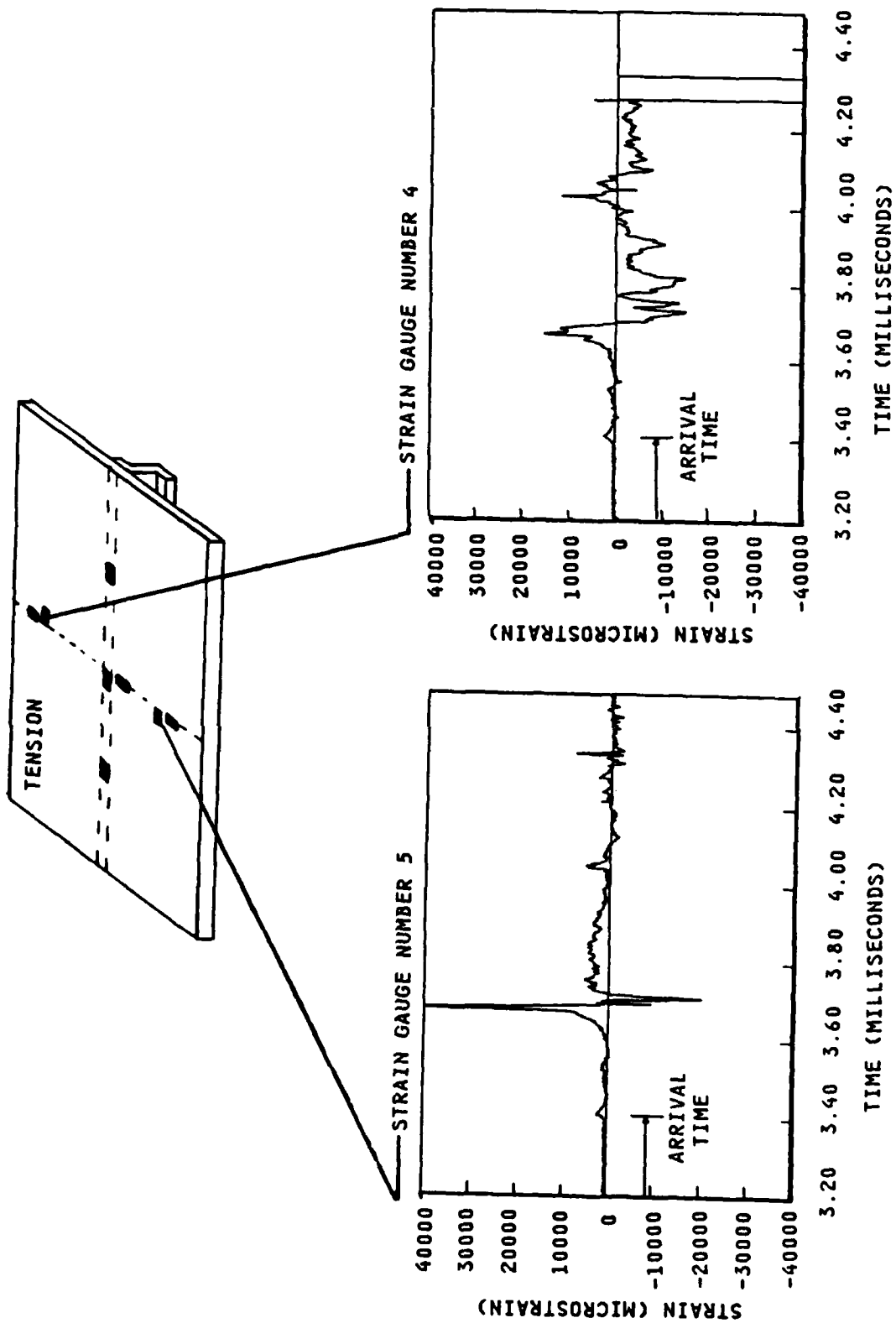

Figure 3.38 Strain Gauge Nos. 4 and 5 Strain Histories, "Z" Stiffener Dynamic Test

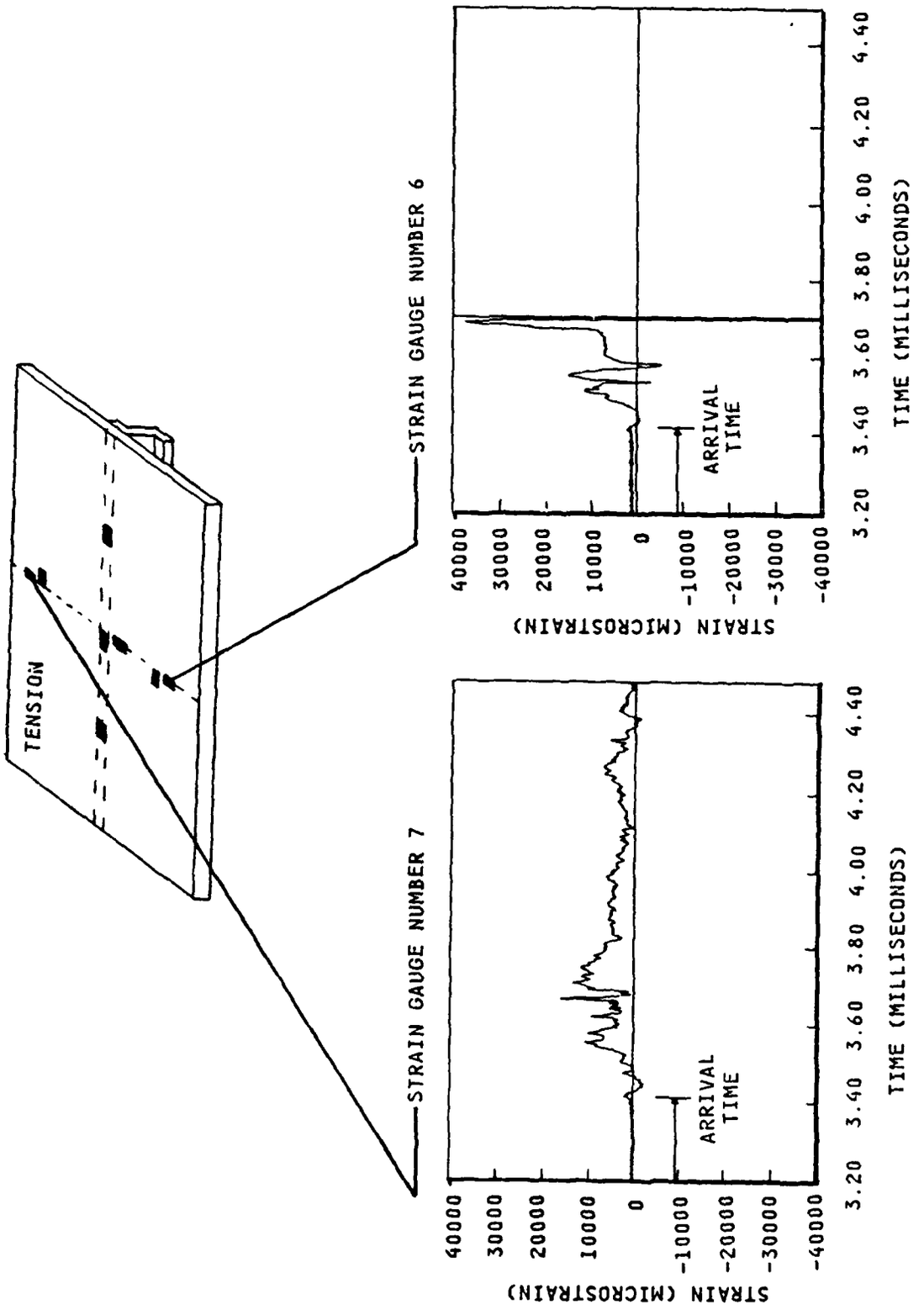

Figure 3.39 Strain Gauge Nos. 6 and 7 Strain Histories, "Z" Stiffener Dynamic Test

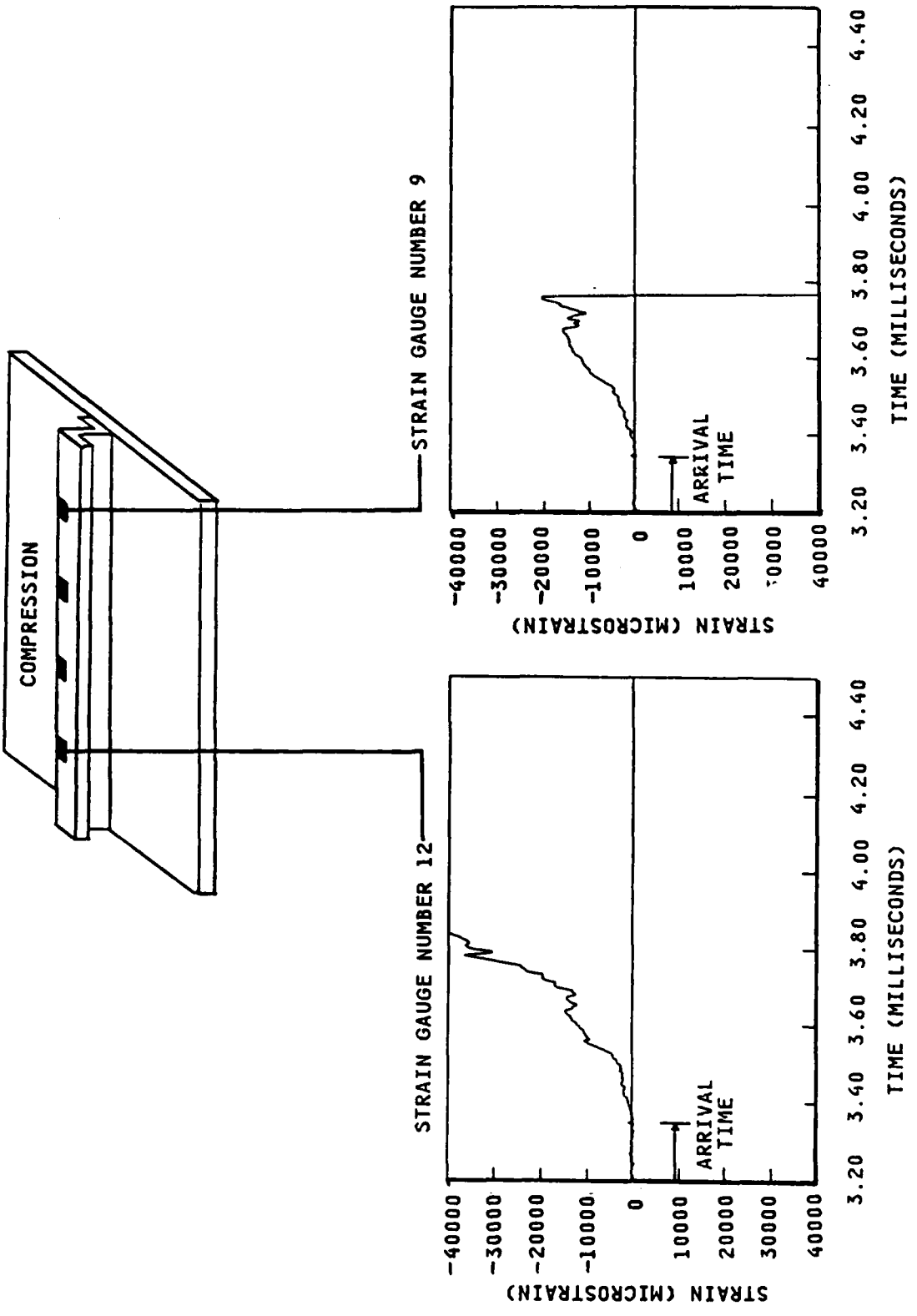

Figure 3.40 Strain Gauge Nos. 9 and 12 Strain Histories, "Z" Stiffener Dynamic Test

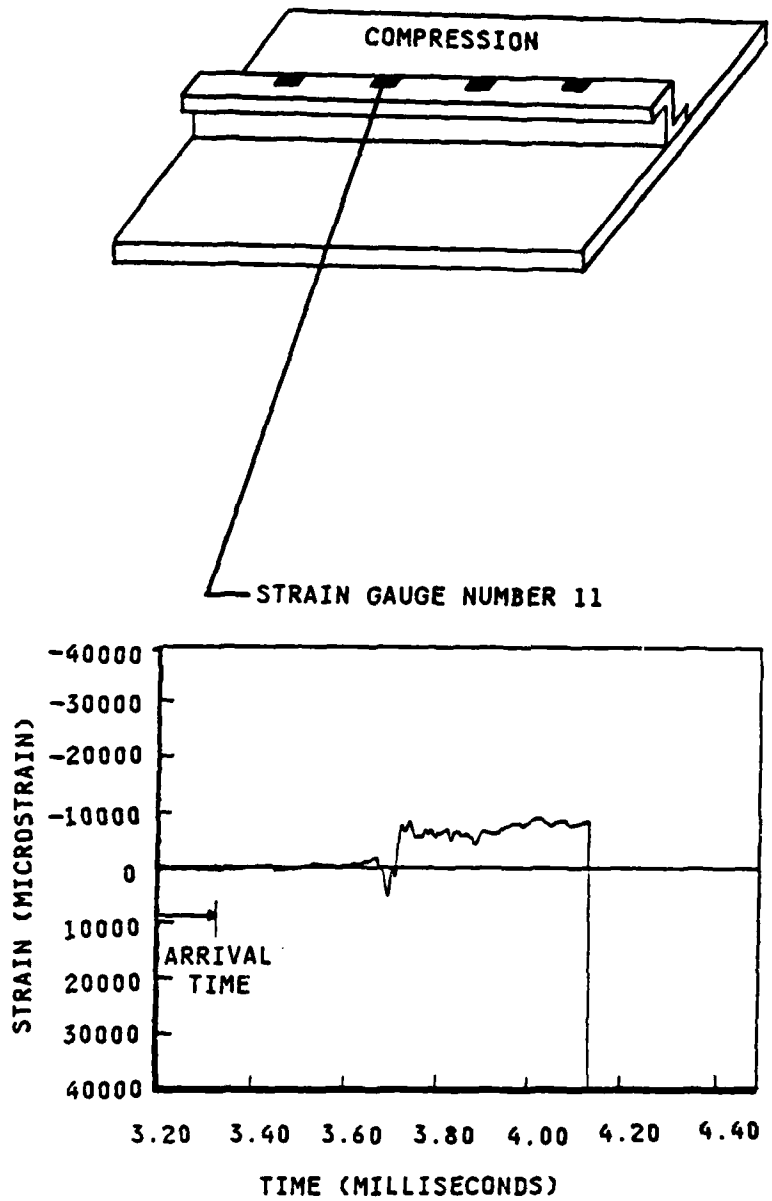

Figure 3.41 Strain Gauge Number 11 Strain History, "Z" Stiffener Dynamic Test

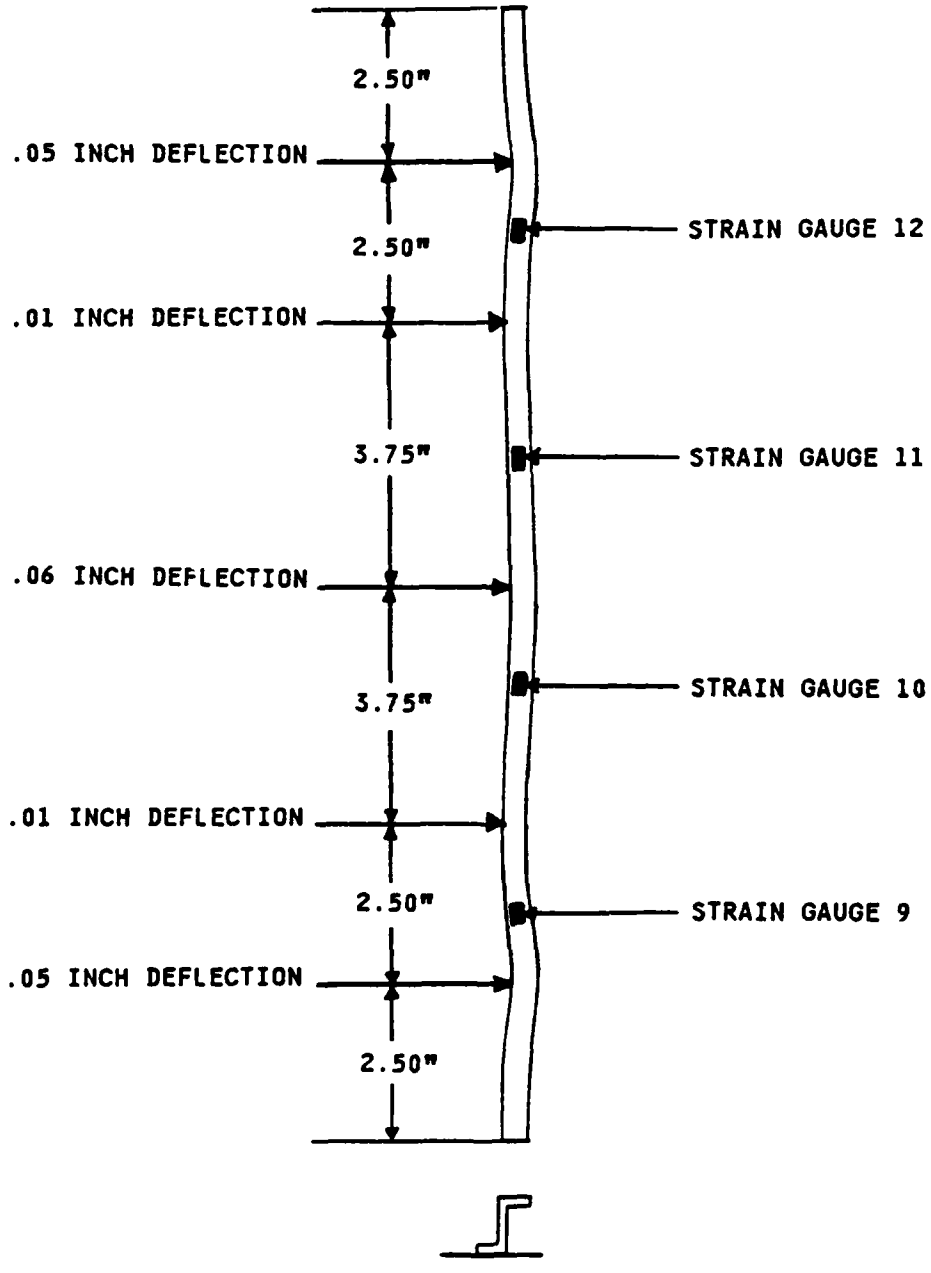

Figure 3.42 Schematic of the "Z" Stiffener Tripping Resulting from Dynamic Testing

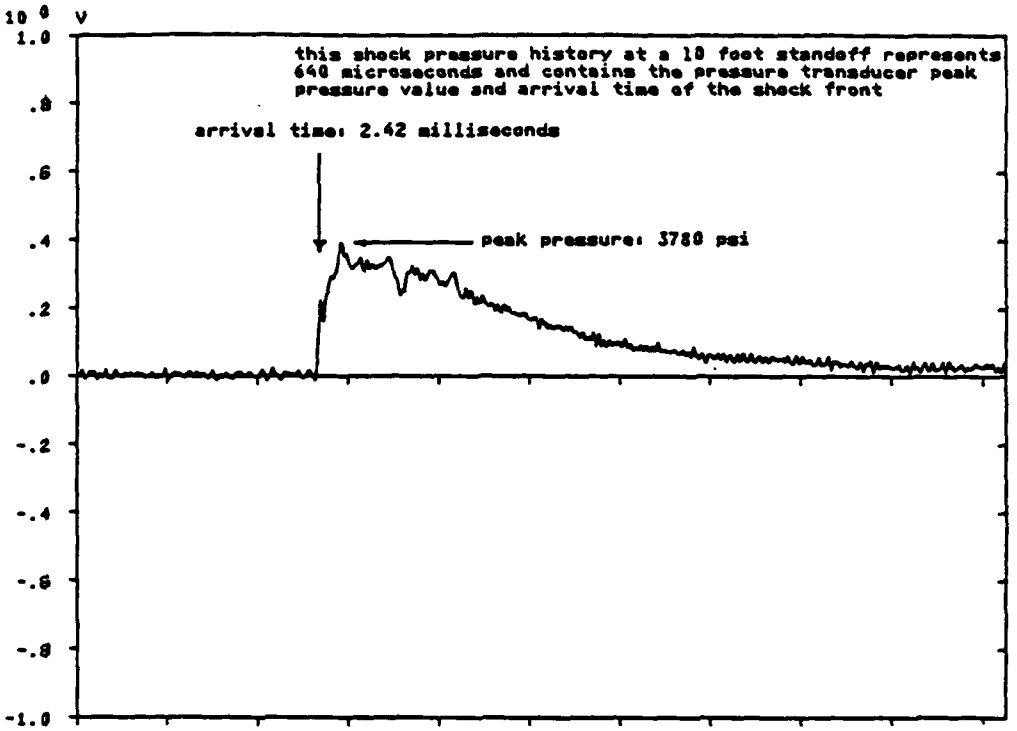

Figure 3.43 Narrow Flanged "T" Stiffener Dynamic Test Incident Pressure Pulse

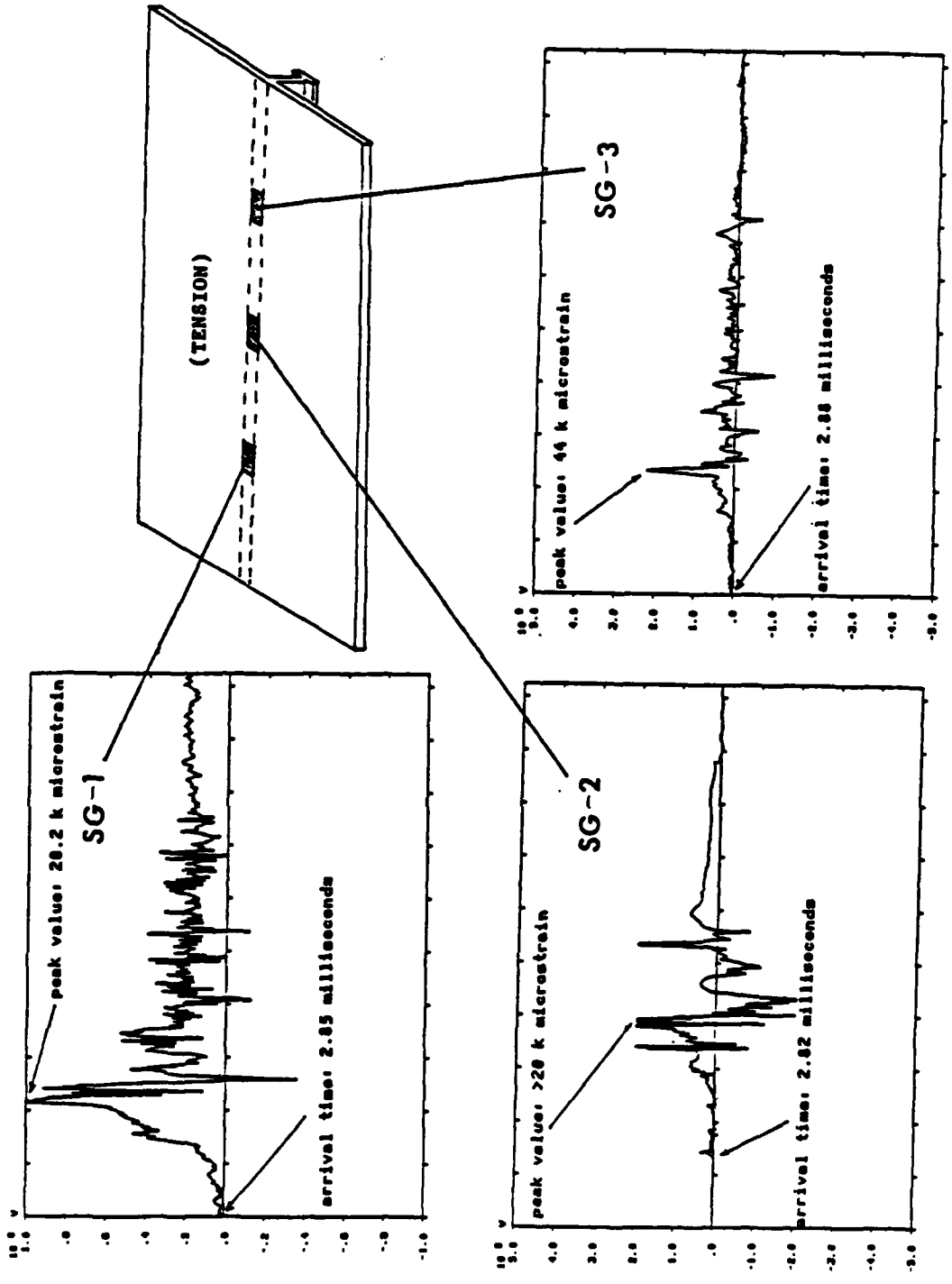

Figure 3.44 Strain Gauge Nos. 1, 2 and 3 Strain Histories, Narrow Flanged "T" Stiffener Dynamic Test

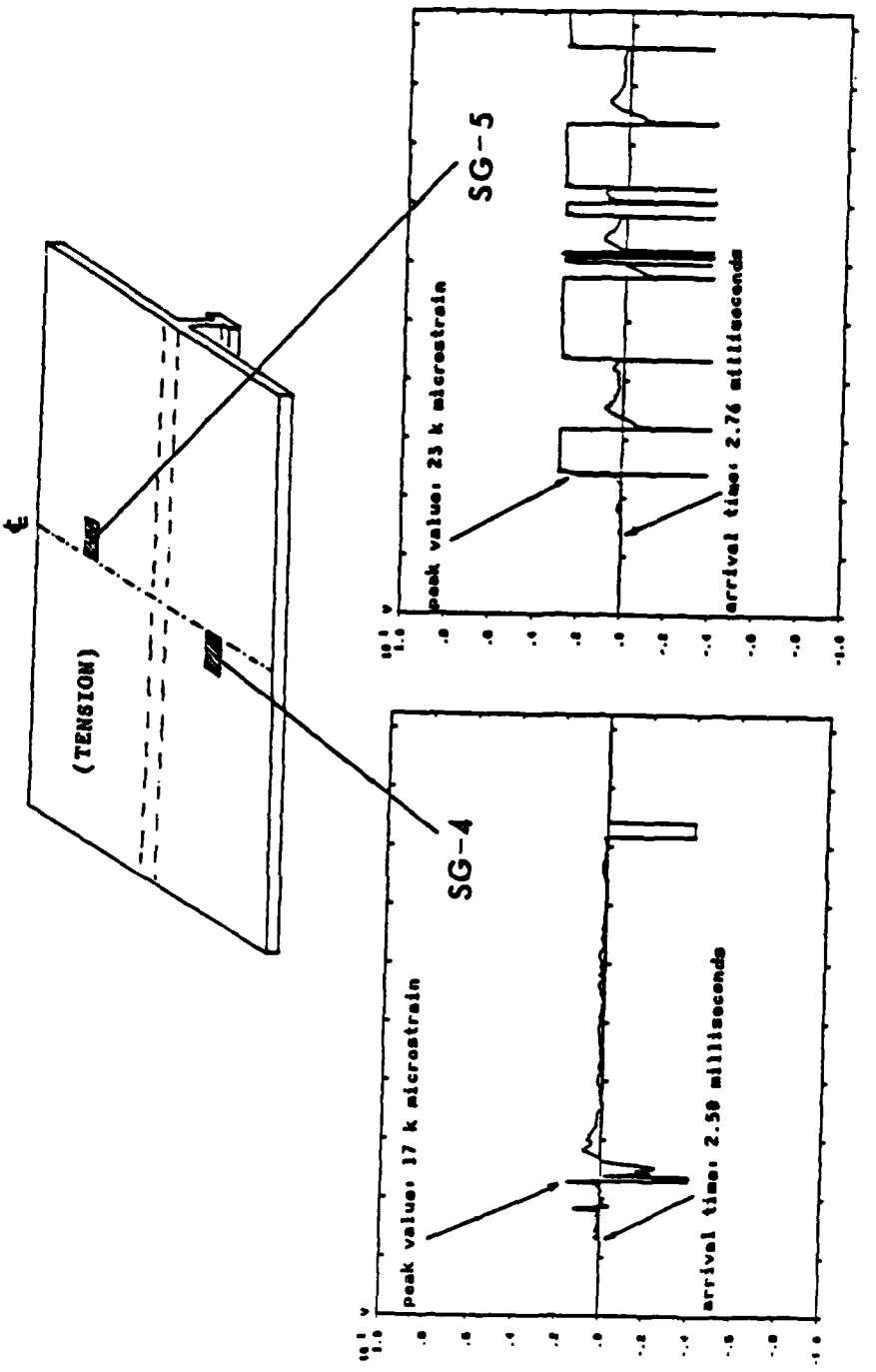

Figure 3.45 Strain Gauge Nos. 4 and 5 Strain Histories, Narrow Flanged "T" Stiffener Dynamic Test

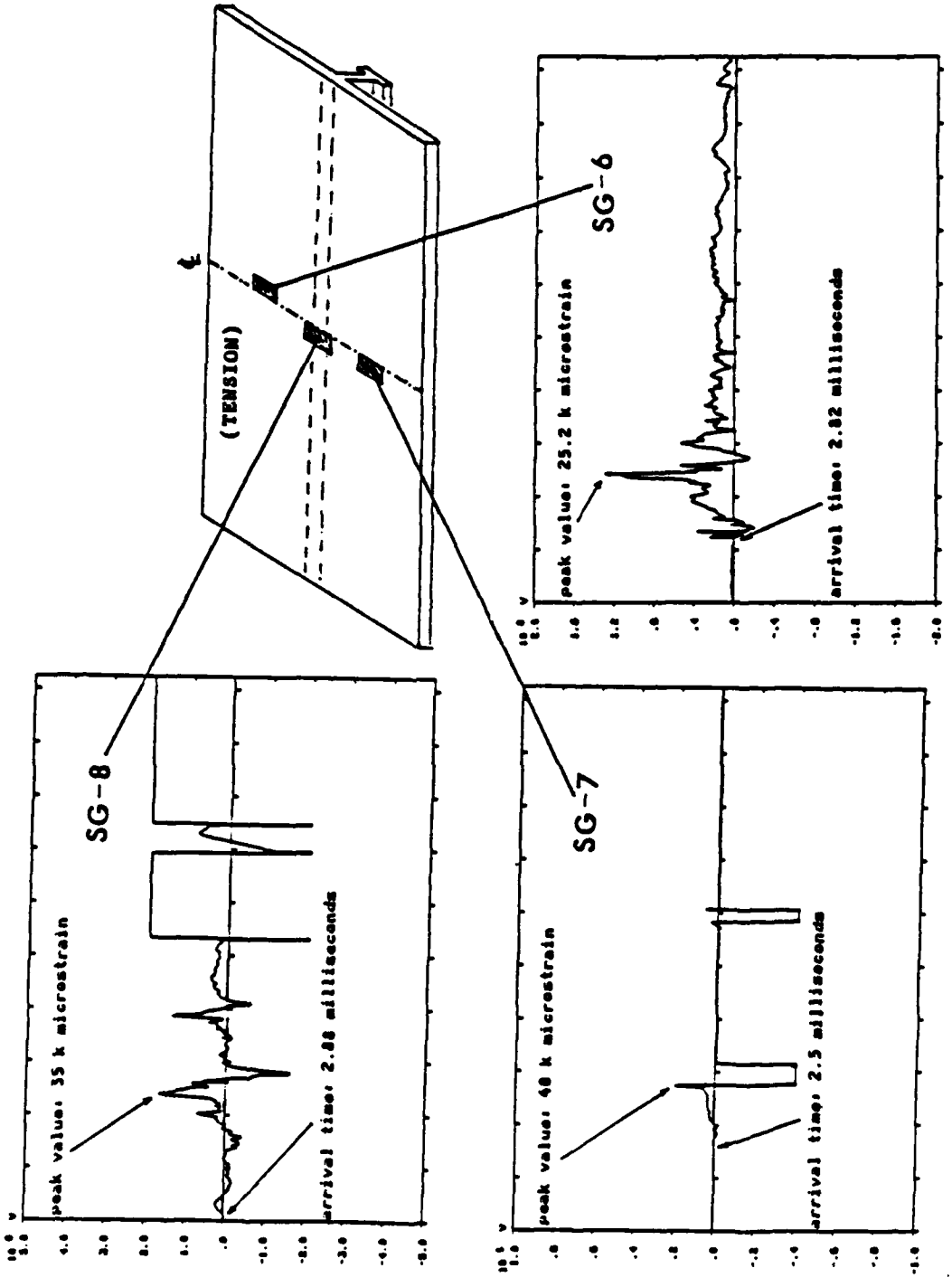

Figure 3.46 Strain Gauge Nos. 6, 7 and 8 Strain Histories, Narrow Flanged "T" Stiffener Dynamic Test

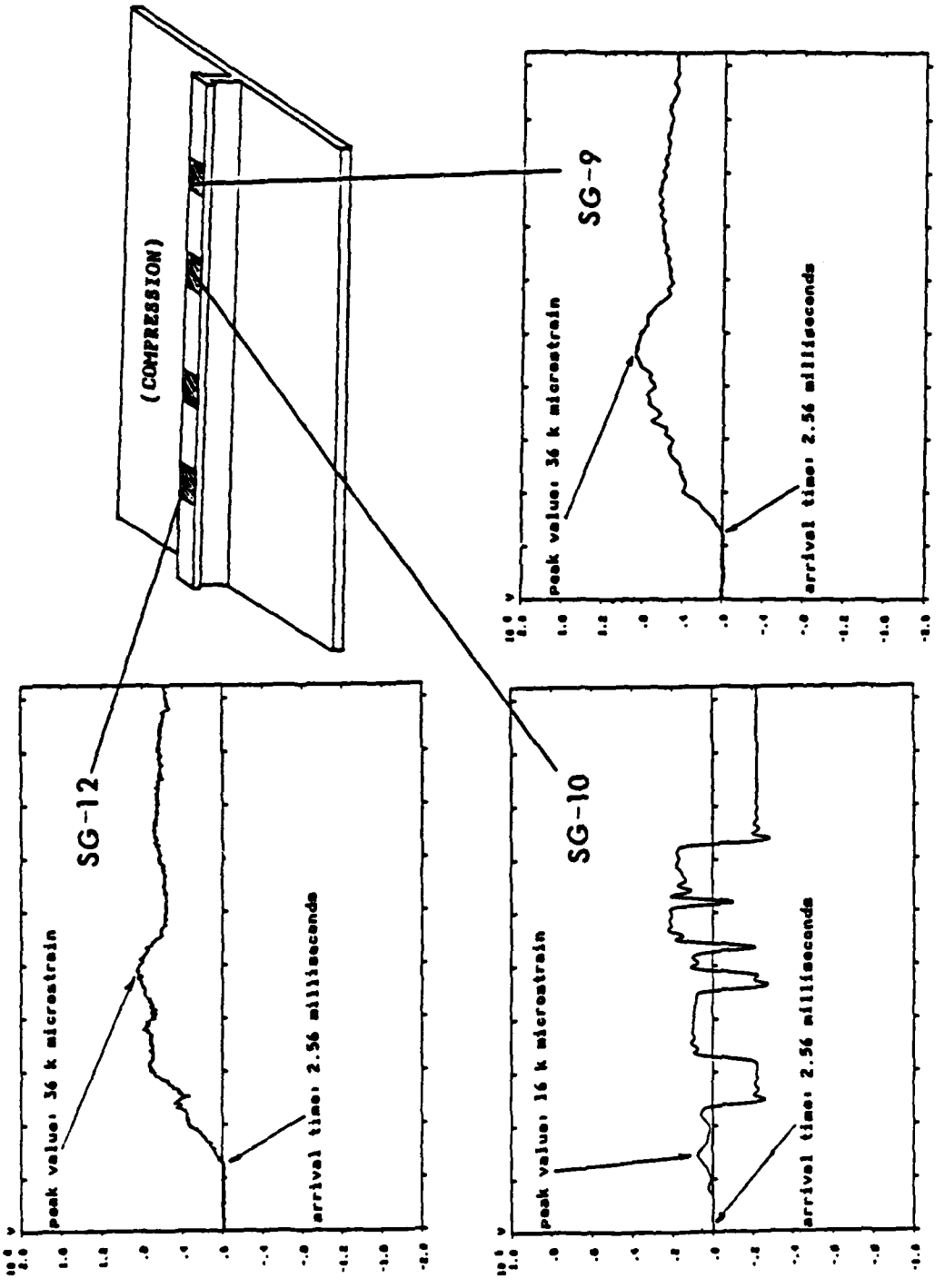

Figure 3.47 Strain Gauge Nos. 9, 10 and 12 Strain Histories, Narrow Flanged "T" Stiffener Dynamic Test

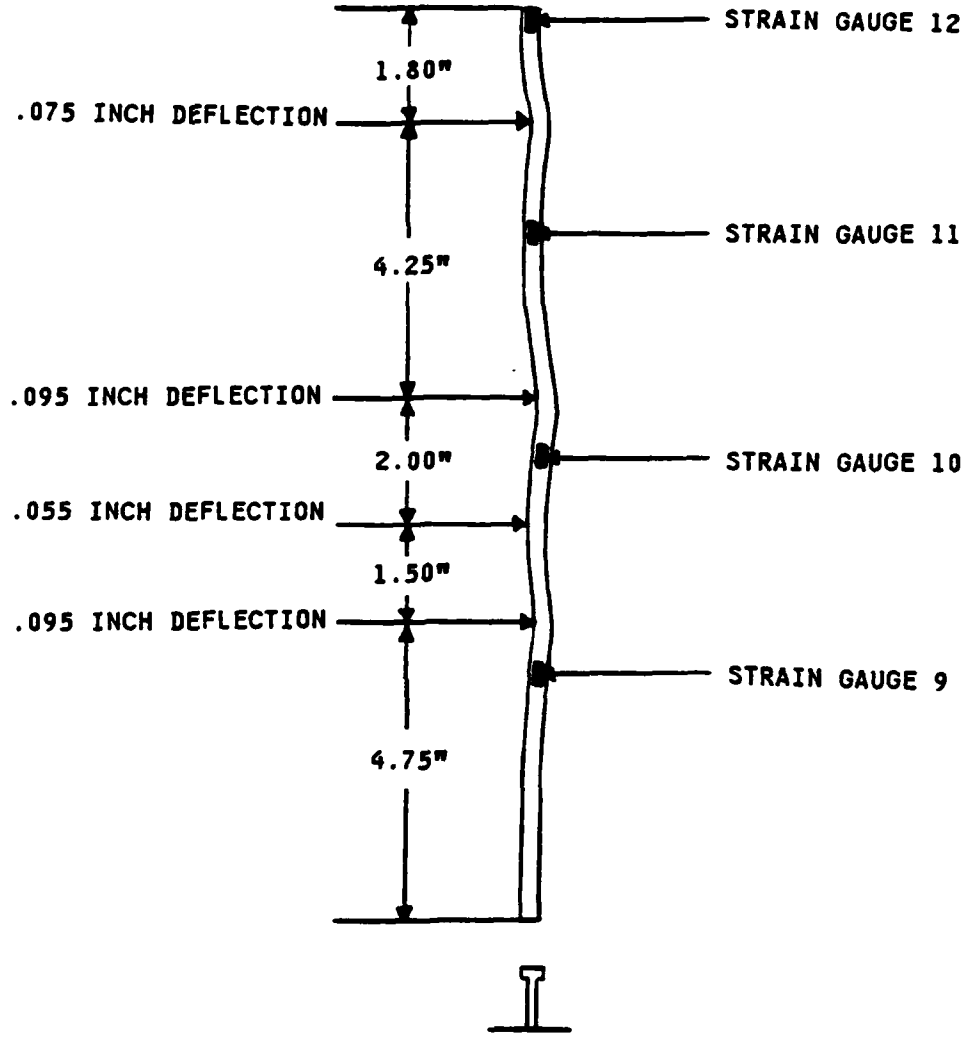

Figure 3.48 Schematic of the Narrow Flanged "T" Stiffener Tripping Resulting from Dynamic Testing

IV. CONCLUSIONS AND RECOMMENDATIONS

The data obtained from the hydrostatic tests of all three stiffener configurations considered provided excellent quantitative information concerning the plate/stiffener system reaction under increasing load. The review and analysis of this data enabled a qualitative description of the plate behavior to be made and used for comparison between the test cases. From the comparisons of the test cases it was determined that for a common plate geometry and stiffener orientation the ranges of hydrostatic pressure over which elastic plate behavior, plastic plate behavior, and elastic stiffener tripping behavior occur appears to remain the same in spite of varying the stiffener cross-section and varying the plastic section modulus by as much as 29%. It was determined, however, that the variation of the stiffener cross-section did significantly affect the relative magnitude of strain experienced in the plate during these ranges. In addition, one of the tests was conducted such that the plastic stiffener tripping range was attained. This resulted in data from which the stiffener tripping progression from center to extreme edge could be verified as well as a physically deformed stiffener specimen which itself verified the direction of tripping as deduced from transverse plate mounted strain gauges. Finally, these tests proved the conclusion reached by LT Budweg [Ref.

16:p. 92] that it would require a static deflection in excess of 4 plate thicknesses to result in the plastic tripping of the stiffener under load.

The results of the underwater shock tests were quite sufficient to assess qualitatively the plate and stiffener behavior upon incidence of the shock front generated by the test charge. It was determined, in view of the difficulties experienced with the chamber orientation in one case and with the charge's pressure pulse integrity in another case, that a numerical comparison of strain withstood by the stiffeners at tripping would yield an improper conclusion about which configuration was more resistant to dynamic loading. It was noted, however, that the process of stiffener tripping, as determined by analysis of the shock test data, parallels the process deduced in the static test. It was also found that for the wide and narrow flanged "T" stiffened panels, the open areas of plate on either side of the stiffener showed no apparent transverse support by the stiffener throughout the test whereas the "Z" stiffened panel showed some support. This support was due to the presence of the large base flange of the "Z" as opposed to the significantly smaller base section of the "T" stiffeners. Lastly, the conclusion concerning the failure of the test panel as a result of cavity corner amplification [Ref. 16:p. 93] was disproved by the similar panel failure experienced by the wide flanged "T" plate under the same loading conditions with no cavity present.

If further underwater shock testing is to be done then several recommendations should be considered. First, the age of the compound, of which the charge is composed, is critical. If possible, the test shot charge should be well under its shelf life. Secondly, in order to provide a more complete picture of the actual tripping progression, three additional strain gauges should be mounted on the stiffener: one on the flange at its midpoint and one on either side of the web, also at the center, in a vertical orientation. The placement of these gauges would more directly show the maximum strain in the stiffener at tripping as well as provide an indication of the onset of any web buckling as the stiffener rotates out of the vertical plane. Finally, the range of recorded strain should be increased to 60 k microstrain to ensure all peaks are properly recorded, especially during the redistribution of load after tripping.

If additional hydrostatic testing is to be done, the following four recommendations should be considered. First, to avoid the high pressure seal leakage problem a two row bolted attachment configuration should be made use of with a seal provided by an "O" ring supplemented by internally applied silicone seal. Secondly, a pneumatically operated hydropump should be used, this would provide more constant increases in pressure during the test, allow better incremental pressure level control as well as extend the pressure range available over the manual pump used in this test. Third, for asymmetric stiffener

test cases (e.g., "Z" stiffeners) dial indicators should be used across the entire transverse section to verify strain data suggesting asymmetric deflections. Lastly, the plastic tripping range should be more fully investigated by increasing the test pressure range to about 500 psi.

In view of the positive effects of the presence of the base flange on the "Z" stiffener as compared to the linear attachment of the wide flanged and narrow flanged "T" stiffeners and the apparent superiority of the wide flanged "T" in other areas, one additional stiffener cross-section might be considered for testing and comparison. This cross-section would be a wide flanged "T" with a base flange or a wide flanged "I" stiffener.

LIST OF REFERENCES

1. Busby, F. R., Manned Submersibles, Office of the Oceanographer of the Navy, 1976.

2. Faulkner, D., The Collapse Strength and Design of Submarines, paper presented at the Symposium on Naval Submarines, London, May 1983.

3. Myers, J. J., Holm, C. H., and McAllister, R. F., Handbook of Ocean and Underwater Engineering, McGraw-Hill, 1969.

4. David W. Taylor Naval Ship Research Center Report 79/064, Design Equations for Tripping of Stiffeners Under Inplane and Lateral Loads, by J. C. Adamchak, October 1979.

5. Evans, J. H., Ship Structural Design Concepts, Cornell Maritime Press, 1975.

6. Thompson, J. M. T., and Hunt, G. W., Collapse, Cambridge University Press, 1982.

7. Evans, J. H., and Adamchak, J. C., Ocean Engineering Structures, vol. 1, The MIT Press, 1969.

8. Gerard, G., Introduction to Structural Stability Theory, McGraw-Hill Book Company, 1962.

9. Bleich, F., Buckling Strength of Metal Structures, Mc-Graw-Hill Book Company, 1952.

10. Kennard, E. H., Tripping of T-shaped Stiffening Rings on Cylinders Under External Pressure, Report 1079, NS 731-038, 1959.

11. Jones, N., Dumas, J. W., Giannotti, J. G., and Grossit, K. E., "The Dynamic Plastic Behavior of Shells," Dynamic Response of Structures, Pergamon Press, 1972.

12. Rinehart, J. S., and Pearson, J., Explosive Working of Metals, Pergamon Press, 1963.

13. Weertman, J., "Dislocation Mechanics at High Strain Rates," Metallurgical Effects at High Strain Rates, Pelnum Press, 1973.

14. Department of the Navy, Naval Ship Engineering Center, Project SR-225, Gross Panel Strength Under Combined Loading, by A. E. Mansour, 1977.

15. Flax, A. H., "Aero and Hydro-Elasticity," Structural Mechanics, Pergamon Press, 1960.

16. Budweg, H. L., An Investigation into the Tripping Behavior of Longitudinally T-Stiffened Rectangular Flat Plates Loaded Statically and Impulsively, Master's Thesis, Naval Postgraduate School, Monterey, California, March 1986.

17. Rentz, T. R., An Experimental Investigation into the Dynamic Response of a Stiffened Flat Plate Loaded Impulsively by an Underwater Shockwave, Master's Thesis, Naval Postgraduate School, Monterey, Calfironia, June 1984.

18. King, N. R., Underwater Shock-Induced Responses of Stiffened Flat Plates: An Investigation into the Predictive Capabilities of the USA-STAGS Code, Master's Thesis, Naval Postgraduate School, Monterey, California, December 1984.

19. Langan, J. R., An Investigation into the Comparisons of the Underwater Shock Effects on a Stiffened Flat Plate to the Predictive Nature of a Computer Model, Master's Thesis, Naval Postgraduate School, Monterey, California, March 1985.

20. Cole, R. H., Underwater Explosions, Princeton University, Princeton, New Jersey, 1948.

BIBLIOGRAPHY

American Society of Tool and Manufacturing Engineeers, High-Velocity Forming of Metals, Prentice-Hall, 1964.

Carden, A. E., Williams, P. E., and Karpp, R. R., "Comparison of the Flow Curves of 6061 Aluminum Alloy," Shock Waves and High-Strain-Rate Phenomena in Metal, Plenum Press, 1981.

Cottrell, A. H., "Deformation of Solids at High Rates of Strain," The Properties of Materials at High Rates of Strain, Institution of Mechanical Engineers, pp. 1-12, 1957.

Gilot, A., and Clifton, R. J., "Pressure-Shear Waves in 6061-T6 Aluminum and Alpha-Titanium," J. Mech. Phys. Solids, no. 3, pp. 263-284, 1985.

Johnson, J. N. and Barker, L. M., "Dislocation Dynamics and Steady Plastic Wave Profiles in 6061-T6 Aluminum," J. of Applied Physics, vol. 40, no. 11, pp. 4321-4334, October 1969.

Kirkwood, J. G., Shock and Detonation Waves, Gordon and Breach Science Publishers, New York, NY, 1967.

Muckle, W., The Design of Aluminum Alloy Ship Structures, Cornell Maritime Press, Cambridge, Maryland, 1963.

Naval Construction Research Establishment, Great Britain, R/611, Compressive Strength of Welded Steel Ship Grillages, by C. S. Smith, May 1975.

Nicholas, T., "Tensile Testing of Materials at High Rates of Strain," Experimental Mechanics, pp. 177-185, May 1981.

Richardson, J. M., and Kirkwood, J. G., "Buckling Instability of Thin Cylindrical Shells," Underwater Explosion Research, Volume III, Office of Naval Research, Department of the Navy, pp. 423-459, February 28, 1950.

Rinehart, J. S., and Pearson, J., Behavior of Metals Under Impulsive Loads, The American Society for Metals, 1954.

Smith, C. S., "Bending, Buckling and Vibration of Orthotropic Plate-Beam Structures," J. of Ship Research, vol. 12, no. 5, pp. 249-268, December 1968.

Smith, C. S., and Dow, R. S., "Effects of Localized Imperfections on Compressive Strength of Long Rectangular Plates," J. of Construction Steel Research, pp. 51-76, 1984.

Wittrick, W. H., "General Sinusoidal Stiffness Matrices for Buckling and Vibration Analyses of Thin Flat-Walled Structures," International Journal of Mechanical Sciences, vol. 10, no. 12, pp. 949-966, December 1968.

INITIAL DISTRIBUTION LIST

		No. Copies
1.	Defense Technical Information Center Cameron Station Alexandria, Virginia 22304-6145	2
2.	Library, Code 0142 Naval Postgraduate School Monterey, California 93943-5002	2
3.	Professor Y. S. Shin, Code 69Sg Department of Mechanical Engineering Naval Postgraduate School Monterey, California 93943-5000	5
4.	Department Chairman, Code 69 Department of Mechanical Engineering Naval Postgraduate School Monterey, California 93943-5000	1
5.	Professor R. E. Newton, Code 69Ne Department of Mechanical Engineering Naval Postgraduate School Monterey, California 93943-5000	1
6.	Dr. N. T. Tsai Defense Nuclear Agency SPSS Washington, D. C. 20305-1000	3
7.	Dr. M. L. Baron Weidlinger Associates 333 Seventh Avenue New York, New York 10001	1
8.	Dr. R. Daddazio Weidlinger Associates 3333 Seventh Avenue New York, New York 10001	1
9.	Dr. Andrew P. Misovec Weidlinger Associates 333 Seventh Avenue New York, New York 10001	1

10. Dr. B. Whang, Code 1750.2 — 1
Hull Group Head, Submarine Protection Division
David Taylor Naval Ship Research
and Development Center
Bethesda, Maryland 20084

11. Dr. H. Huang, Code R14 — 1
Naval Surface Weapon Center
White Oaks
Silver Spring, Maryland 20910

12. Professor T. L. Geers — 1
Campus Box 427
Department of Mechanical Engineering
University of Colorado
Boulder, Colorado 80309

13. Dr. J. A. DeRuntz — 1
Lockheed Research Laboratory
3251 Hanover Street
Palo Alto, CA 94304

14. LCDR. H. L. Budweg, USN — 1
620 Cedar Lane
Mare Island, California 94592

15. Mr. R. R. Miller — 1
3937 COL. Ellis
Alexandria, Virginia 22304

16. Mr. M. R. Miller — 1
9006 Triple Ridge Road
Fairfax Station, Virginia 22039

17. LT. B. S. L. Miller, USN — 1
3937 COL. Ellis
Alexandria, Virginia 22304

18. Mr. John F. Kirchhoff — 1
12700 Hoven Lane
Bowie, Maryland 20715

19. LT. Robert B. Miller — 2
3937 COL. Ellis
Alexandria, Virginia 22304

END

8-87

DTIC